Naval Research Reviews

Office of Naval Research
One / 1987
Vol XXXIX

NAVAL POSTGRADUATE SCHOOL ISSUE

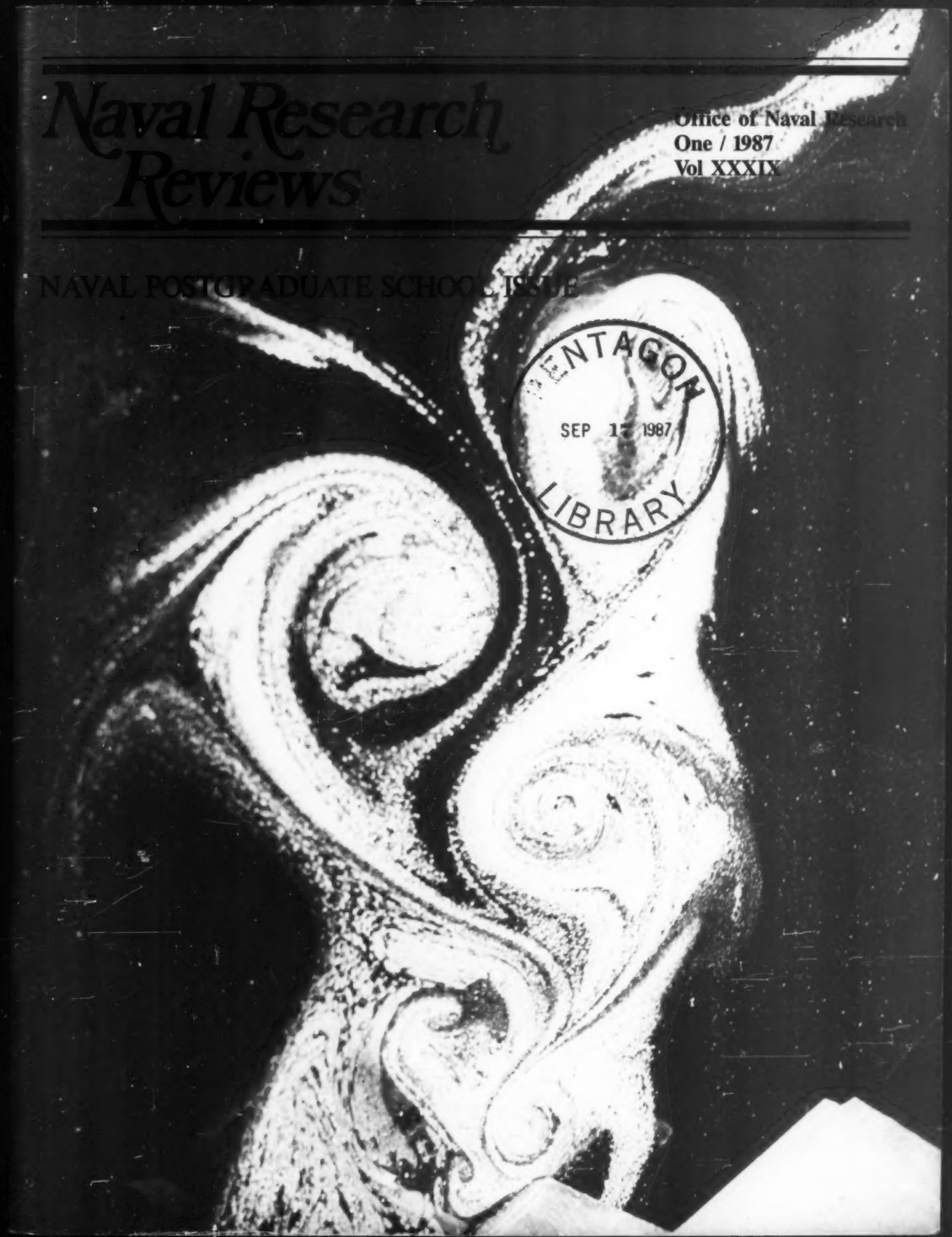

PENTAGON
SEP 17 1987
LIBRARY

LTJG Harry Nicholson at the console of the Control Data Corporation computer in 1960. This 1604 computer was the first commercial computer built and sold by CDC. It was also the first computer used by what is now the Fleet Numerical Oceanography Center, Monterey, California. CAPT Harry Nicholson later became Commanding Officer of FLENUMOCEANCEN in 1982.

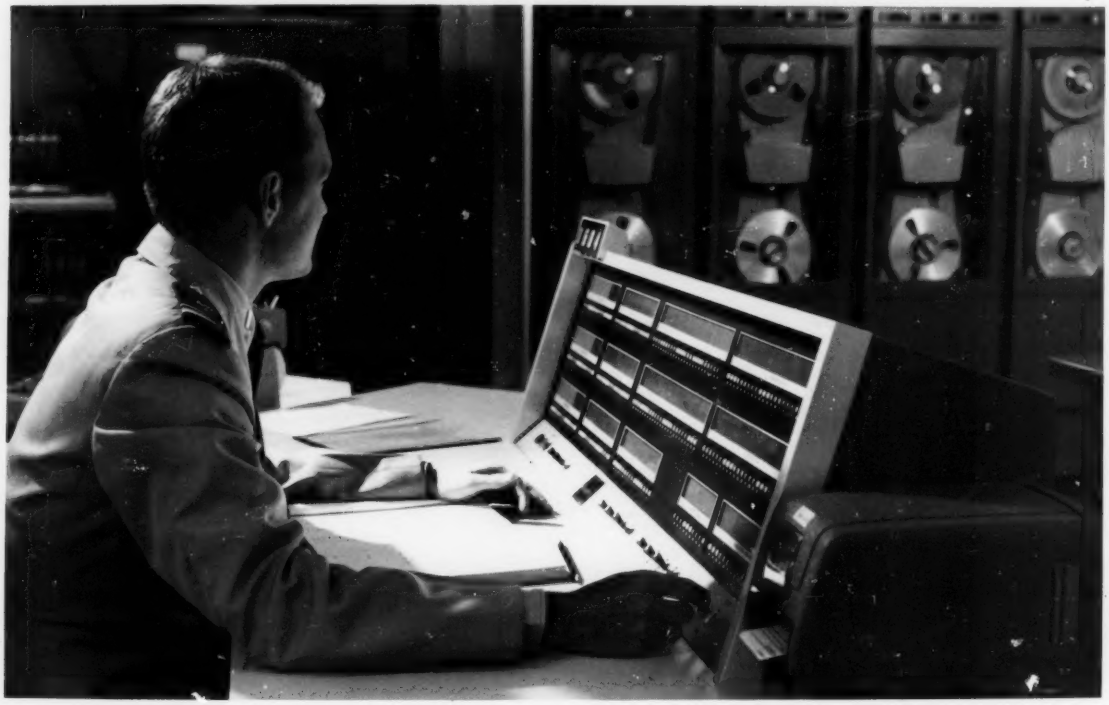

Fleet Numerical Oceanography Center

Fleet Numerical Oceanography Center (FLENUMOCEANCEN) is the master computer center and controller for the worldwide Naval Environment Data Network (NEDN). The mission of FLENUMOCEANCEN is to provide numerical environmental products—analyses and predictions, both meteorological and oceanographic—on an operational basis, to Navy forces.

FLENUMOCEANCEN's earliest predecessor was the Project, NANWEP, a Navy Numerical Weather Problems Group established in 1958 at Fleet Weather Center, Suitland, Maryland, to conduct research in numerical weather prediction techniques. The group was transferred to Monterey, California, in 1959 to work cooperatively with meteorologists at the Naval Postgraduate School (NPS). It was designated the Fleet Numerical Weather Facility in 1961. During 1963-64 the facility established the world's first successful satellite link for intercomputer, environmental data communication.

During the 1966-1969 period, Fleet Numerical Weather Facility pioneered the prediction of ocean acoustic conditions based on synoptic analysis of oceanographic data. The facility was redesignated Fleet Numerical Weather Central in 1968. By 1970, the Four-Processor Primitive Equation forecast Model, which demonstrated atmospheric forecasting skill out to 72 hours, had been developed in conjunction with NPS faculty members. A Satellite Processing Computer was installed at FLENUMOCEANCEN in 1976 to process and merge satellite data into the environmental products developed for transmission Navywide.

In 1979, Fleet Numerical Weather Central was renamed Fleet Numerical Oceanography Center. 1981 marked the installation of the world's first operational ocean mixed layer prediction system at FLENUMOCEANCEN for fleet applications in antisubmarine warfare. The Navy Operational Global Atmospheric Prediction System (NOGAPS) was implemented in 1982 on a very large, newly installed "super" computer.

Since 1982 FLENUMOCEANCEN has brought on-line Navy Operational Regional Atmospheric Prediction System (NORAPS) which has provided high resolution forecasts in many areas of the world. An advanced spectral ocean wave model, designed to improve forecasts of wave and swell conditions on the open ocean, has been expanded into a global model.

Naval Research Reviews

NAVAL RESEARCH REVIEWS.
1987
V.39 I.1 C.3
6- 50 T+

Articles

3 **Contributions to Hydrodynamics: Vortex Motion in Homogeneous and Stratified Media**
by T. Sarpkaya, S.K. Johnson, W.E. Gray, and J.J. Daly

9 **Autonomous Measurement of Space Shuttle Payload Bay Acoustics During Launch**
by Lt. Austin W. Boyd, Lt. Brian, Lt. P. Kosinski, and Lt. Richard L. Weston

19 **Studies of the Marginal Ice Zone along the East Greenland Coast**
by Robert H. Bourke and Robert G. Paquette

28 **NPS Meteorology Studies on the Marginal Ice Zone**
by Kenneth L. Davidson and Peter Guest

36 **Towards the Efficient Solution of an ASW Search Problem**
by James N. Eagle

41 **Naval Tactical Decisions Under Uncertainty: Some Case Studies**
by Donald P. Gaver, Jr.

44 **Steam Condensation: Putting Surface Tension to Work**
by Paul J. Marto

51 **Materials Research at NPS**
by Terry R. McNally and Steven J. Hales

Departments

2 **Introduction**

2 **Note from the Superintendent**

18 **Profiles in Science**

CHIEF OF NAVAL RESEARCH
RADM J. B. Mooney, Jr., USN

TECHNICAL DIRECTOR
Dr. Marvin K. Moss

CHIEF WRITER/EDITOR
W. J. Lescure

SCIENTIFIC EDITOR
Dr. J. T. Lester

MANAGING EDITOR
M. J. Whetstone

ART DIRECTION
Typography and Design
Government Printing Office

About the Cover

Growth and motion of vortices generated by a plate at an angle of attack of 60 degrees. The picture is taken in a recirculating water table and the vortices are visualized by means of aluminum dust. The alternate shedding of vortices takes place practically about all bluff bodies (cylinders, cables, missiles, etc.) and gives rise to large drag, oscillating lift force, and hydro- or aero-elastic oscillations. The flow field may be simulated numerically through the use of the fundamental equations of motion. The visualization of flow helps to our physical understanding of the phenomenon and provides data for comparison with those obtained in numerical experiments. (See article beginning on page 3.)

Photograph is the courtesy of Professor Turgut Sarpkaya (NPS).

Naval Research Reviews publishes articles about research conducted by the laboratories and contractors of the Office of Naval Research and describes important naval experimental activities. Manuscripts submitted for publication, correspondence concerning prospective articles, and changes of address, should be directed to Code OPARI, Office of Naval Research, Arlington, Va. 22217-5000. Requests for subscriptions should be directed to the Superintendent of Documents, U.S. Government Printing Office, Washington, D.C. 20402. *Naval Research Reviews* is published from appropriated funds by authority of the Office of Naval Research in accordance with Navy Publications and Printing Regulations. NAVSO P-35.

Introduction

The Naval Postgraduate School (NPS) was founded as a branch of the Naval Academy in 1909 to educate officers at the state-of-the-art in naval engineering and ordnance. In the last seventy-seven years NPS has undergone significant expansion in both physical size and scope of its educational programs, moving to its current location at Monterey, California in the early 1950's.

NPS supports the Navy through graduate education and research at the Masters, Engineers, and Ph.D. levels. Its numerous programs cover the science, technology and design of weapons systems and platforms, the planning and operations of these weapons and platforms, the management of the complex Navy structure including systems acquisition and logistics planning, and the strategic objectives of military power given the current political realities. Since these programs call for a wide range of academic disciplines, NPS is organized into eleven academic departments totaling approximately 200 regular faculty. The departments include Physics, Mathematics, Computer Science, Aeronautical Engineering, Mechanical Engineering, Electrical and Computer Engineering, Meteorology, Oceanography, Operations Research, Administrative Sciences, and National Security Affairs.

The Navy has long recognized that research is an integral part of graduate education and strongly supports the role of research at NPS. Research efforts of the regular faculty are augmented by approximately 60 adjunct research faculty and postdoctoral fellows. Students undertake research as an integral part of their programs. One student project of particular interest involving the Space Shuttle is described in this issue. All academic departments have extensive research programs, all aspects of which cannot be covered here. The papers included in this issue have been selected from areas thought to be of particular interest to readers of *Naval Research Reviews*. These describe research in the mathematical, physical, and environmental sciences, but cover only a small fraction of the more than 200 research projects underway at any time.

Note from the Superintendent

Research at the Postgraduate School helps to expand our knowledge base. For the officers assigned to study here, it provides the mechanism that allows these officers to apply their sea-going experience with the insights they have gained through their studies at the school. The results presented in their theses should be aimed at the challenges the Navy will face in the future.

The blend of research, graduate education and operational experience has strengthened officers' ability to solve problems and make decisions in a thoughtful, objective and discerning manner.

I take great pride in the Naval Postgraduate School and, because of its continued pursuit of excellence in research, I expect to see the school continue being a vital cog in officer development and in shaping the kind of Navy that will afford national security into the 21st century.

RADM Robert C. Austin, USN,
Superintendent, Naval Postgraduate School

CONTRIBUTIONS TO HYDRODYNAMICS :

Vortex Motion in Homogeneous and Stratified Media

By T. Sarpkaya, S.K. Johnson, W.E. Gray, and J.J. Daly, Department of Mechanical Engineering

Introduction

The research activities at the Naval Postgraduate School (NPS) in the general area of hydrodynamics concern vortex breakdown, harmonically-oscillating flow about smooth and rough bluff bodies, wave forces on offshore structures, hydroelastic oscillation of cables in steady and oscillating flow, impulsively-started flow about various types of bodies, discrete vortex analysis of separated time-dependent flows, and the rise and demise of trailing vortices in homogeneous and density-stratified media. This article focuses on the effect of ambient turbulence and density stratification on the migration of trailing vortices.

Vortices and vortex wakes have become a major theme of aerodynamics research since the advent of the large aircraft, and their evolution required an examination of many fundamental problems in fluid mechanics. Much of the progress made during the past two decades has been extremely useful in understanding the behavior and interpreting the consequences of vortices generated by the control surfaces of bodies submerged in homogeneous and stratified ocean environment.

The flow over a wing of finite span is three-dimensional having both chordwise and spanwise velocity components. The difference in spanwise velocity components causes the fluid to roll up into a number of streamwise vortices distributed along the span. These small vortices roll up into two, counter-rotating, large vortices (trailing vortices) just inboard of the wing tips (see Figure 1). They descend (downwash) gradually because of mutual induction. In the oceans, the motion of a submerged body produces numerous vortices from various control surfaces (e.g., sail planes and stern) which rise (upwash) due to mutual induction. These vortices decay partly due to large-scale instabilities (sinusoidal instability[1]) and linking (Figure 2), leading to vortex rings, and vortex breakdown[2,3] (Figure 3), leading to the bulging and bursting of the vortex core and partly due to small-scale effects (viscous and turbulent diffusion). These, in turn, depend on the intensity and scale of the ambient turbulence.

With a goal of minimizing the adverse consequences of trailing vortices (internal waves, surface signatures, vortex-aircraft interactions, etc.), the relationship between the lifespan of the vortices and the various demise mechanisms are being explored through analysis and experiments with the support of the Office of Naval Research.

Figure 1

Roll-up of vortex sheets over a delta-wing model.

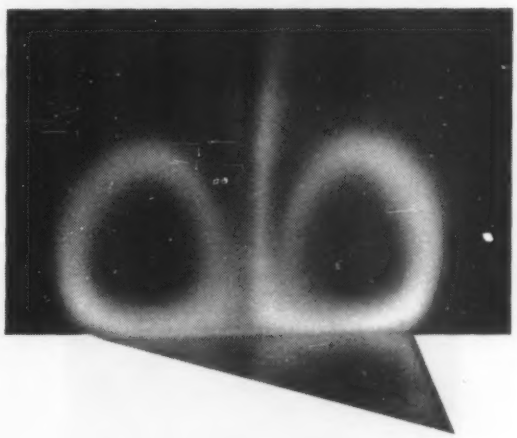

Figure 2

Rise of trailing vortices and the inception of sinusoidal instability (time increases upwards).

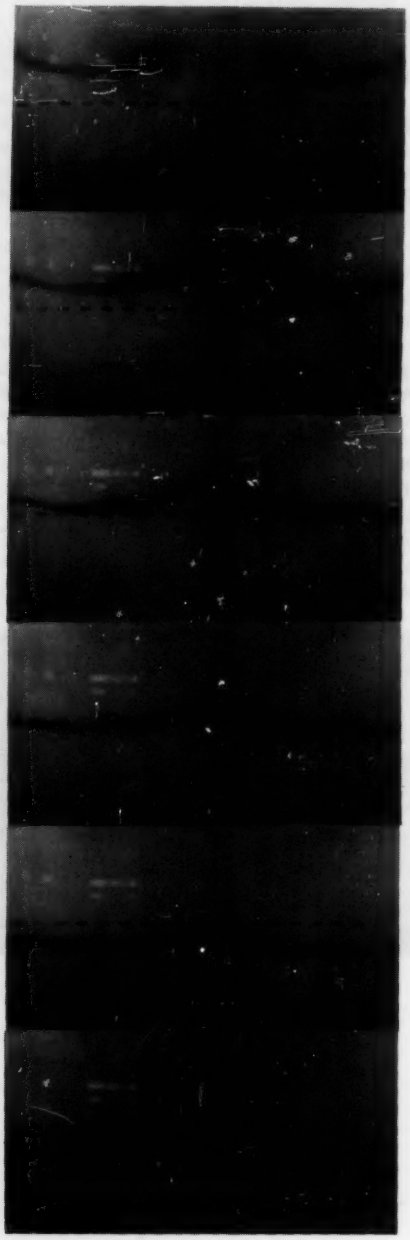

Figure 3

Evolution of vortex breakdown (core bulging and bursting) in trailing vortices (time increases upwards).

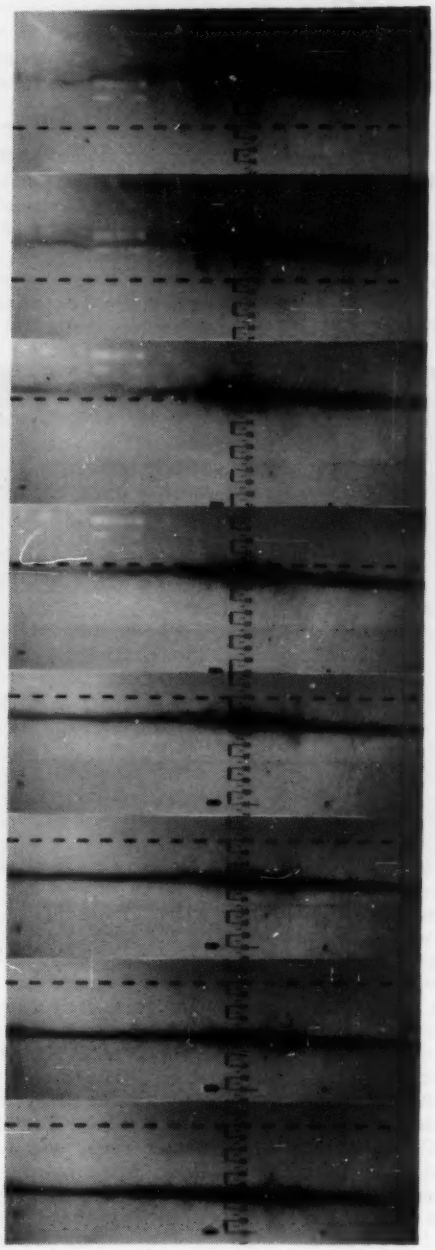

Vortex Motion in Homogeneous Media

In the absence of stratification, the rise of a vortex pair is governed primarily by the relation,[4]

$$H^* = f(t^*, D^*, \epsilon, r^*) \qquad (1)$$

where $H^* = H/b_o$, $t^* = V_o t/b_o$, $D^* = D/b_o$, $\epsilon^* = (\epsilon b_o)^{1/3}/V_o$, $r^* = r_c/b_o$, and H, the vertical displacement of the vortex pair; b_o, the initial separation of the vortices; V_o, the initial mutual induction velocity; t, the time; D, the initial depth of the vortex pair; ϵ, the dissipation rate of the grid-generated turbulence per unit mass, and r_c, the initial vortex core radius. The effect of the aspect ratio and the angle of attack of the lifting surface enter into the Equation (1) indirectly through V_o and b_o [note that $b_o = (\pi/4)B$ where B is the base width of the foil]. Whereas the parameters t^*, D^*, and ϵ^* may be changed independently, r^* is taken as nature provides it ($r^* \approx 0.1$). The primary reason for this is that a century of theoretical and experimental aerodynamics research has been incapable of describing the details of the structure of the tip vortex to be used as initial conditions in a viscous solution. It is surprising, but true, that up until recently, the importance of the wing-tip shape and its influence upon both the initial tangential velocity profile and initial turbulence in the vortex has not been fully appreciated. Here the said influences are characterized in terms of an effective core radius, with full awareness of its shortcomings.

The experiments were performed in a long towing tank (with a cross section of 3 ft by 6 ft).[5,6] Two parallel rails are mounted at the bottom of the tank. A carriage rides smoothly on these rails and provides the test body with a constant velocity through the use of an endless cable and a variable speed motor. The two rails, the carriage and the filling pipes are located under a turbulence management system (polyurethane foam, sandwiched between two perforated aluminum plates).

The ambient turbulence (nearly isotropic) is generated by means of a bi-planar grid. The grid is attached to another carriage, mounted on two parallel rails along the top of the towing tank. The test model is placed in the basin and the tank is filled with water (or stratified as desired through a computer-controlled stratification system). The hollow interior of the model is filled with neutrally buoyant fluorescent dye to seed the vortex core. After sufficient time for equilibrium, the grid is set in motion at the desired speed. When the grid has moved a prescribed distance of x/M (M = mesh size of the grid), the model is set in motion at the same speed. Thus, the horizontal distance between the model and the grid is kept constant.

A large number of grid-turbulence measurements have shown that the turbulence parameter ϵ^* may be written as[4]

$$\epsilon^* = C(V_o/U)^{-1}(M/b_o)^{1/3}\,(x/M)^{-0.767} \qquad (2)$$

where C is a constant (≈ 0.44). Thus, for a given model and angle of attack, i.e., for a given V_o/U and M/b_o, the turbulence parameter varies with x/M as given by Equation (2).

The motion of the trailing vortices was recorded on high-speed film at the test section, together with two digital timers, at regular intervals. It is from these photographs that the data similar to that shown in Figure 4 are deduced. Clearly, the path of the vortices in the turbulent field does not significantly deviate from that of the vortices in the non-turbulent medium until the vortex pair rises at least one initial separation distance. Subsequently, the vortices slow down considerably before the onset of large scale instabilities (mostly vortex breakdown) and eventual dissipation. Figure 4 shows that the smaller the x/M (i.e., the stronger the intensity of turbulence), the smaller is the ultimate rise and the lifespan of the vortex pair. This is primarily due to the fact that turbulence enhances the instabilities leading to the vortex breakdown and, at the same time, diffuses vorticity rapidly, eventually leading to the total destruction of the vortices. This mechanism is far more powerful than the sinusoidal instability leading to the linking of the vortices and to the formation of irregular vortex rings. It remains to be determined what the individual effects of the turbulence intensity and scale are in bringing about the destruction of the vortices due to the vortex breakdown.

Figure 4

Effect of ambient turbulence on the rise of trailing vortices.

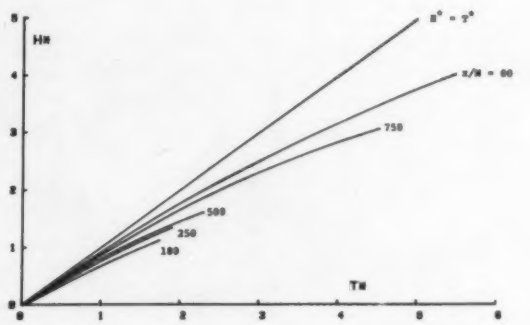

The maximum height H*(max) attained by the vortices is of special importance. Figure 5 shows the maximum height data as a function of ϵ^*. Also shown in this figure is the flight data obtained by Tombach.[6] There is reasonable agreement between the laboratory and flight data in spite of the considerable scatter due to the difficulty of determining the maximum height attained by the vortices. The uncertainties stem primarily from the randomness in the inception of the instabilities leading to the destruction of the vortices. Figure 6 shows the lifespan of the vortex pair as a function of ϵ^*. The data points on the T*(max) axis correspond to the non-turbulence case. Clearly, the effect of turbulence is to reduce both the lifespan and the maximum height attained by the vortices. The data have also shown that the vortices in the non-turbulent medium break up primarily due to linking and in the turbulent medium, mostly due to vortex breakdown.

Figure 5

Maximum height attained by the vortices as a function of the turbulence parameter.

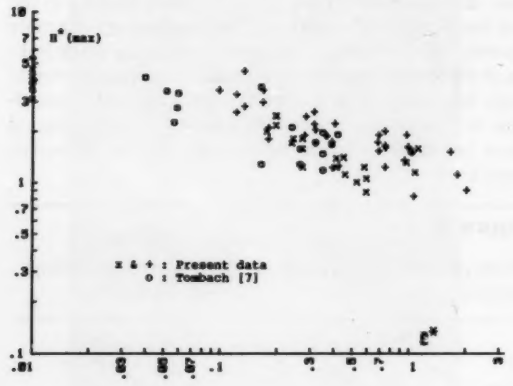

Figure 6

Lifespan of the vortices as a function of the turbulence parameter.

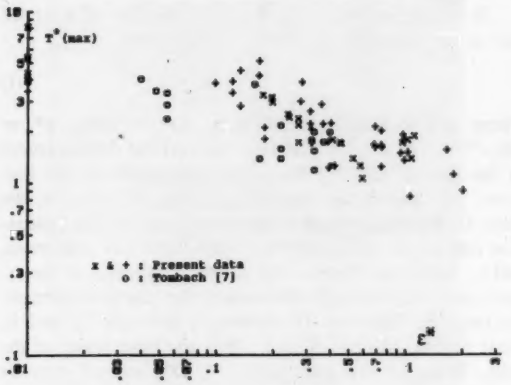

Vortex Motion in Stratified Media

The generation of the internal waves and the rise and demise of the vortices in a stratified medium may be analyzed through the use of the equations of motion for an incompressible fluid for both laminar and turbulent motions provided that a suitable turbulence closure model is adopted and the usual Boussinesq approximation (gravitational acceleration is much larger than the fluid acceleration) is made. For the type of motions considered herein, the Boussinesq approximation is quite valid and has been used in the investigation of all types of internal waves in stratified fluids.

The governing equations of motion in normalized form are

$$\frac{\partial \zeta_m}{\partial t_m} + F_v \left(\frac{\partial u_m \xi_m}{\partial x_m} + \frac{\partial v_m \xi_m}{\partial y_m} \right) = \frac{F_v}{Re} \nabla^2 \xi_m + \frac{\partial \varrho'_m}{\partial x_m} \tag{3}$$

and

$$\frac{\partial \varrho'_m}{\partial t_m} + F_v \left(\frac{\partial u_m \varrho_m}{\partial x_m} + \frac{\partial v_m \varrho_m}{\partial y_m} \right) = F_v n^2 v_m \tag{4}$$

in which the appropriately normalized variables are: ζ the vorticity, t the time, u and v the velocity components, x and y the coordinates of a point, ϱ the density of fluid, ϱ' the fluctuating component of the density, F_v a Froude number, Re a Reynolds number, and n the Vaisala-Brunt frequency (for additional details see Reference 4).

Equations (3) and (4) are valid when $F_v \ll 1$ and buoyancy dominates the flow. When F_v approaches zero, the equations that result from Equations (3) and (4) describe the propagation of linear internal waves. The $F_v \ll 1$ regime is of interest in the present investigation because for submerged bodies of naval interest the Froude number is about 0.01. The results presented below are obtained by considering the full nonlinear equations (3) and (4).

A sufficiently large grid is chosen, the appropriate boundary conditions are imposed, the initial vorticity distribution in the vortex pair is taken to be Gaussian, and the velocities are calculated at all points through the use of the well-known Biot-Savart law. Equations (3) and (4) are integrated through the use of an efficient upwind differencing scheme[4] at each time step. Among the several calculations carried out only one utilizing the initial parameters corresponding to those of an experiment will be reported here, (i.e., $D^* = 8$, $r_c = 0.09$, $n = 0.0135$, and $F_v = 0.018$).

Figures 7 and 8 show the velocity and constant density contours at time $T^* = 3.64$. Clearly, the motion of the vortices gives rise to two regions of circulation with countersigned vorticity (in the upper right and lower left regions of the vortex in Figure 7). Similar regions of circulation develop around the left-half of the vortex pair. These counter vortices not only reduce the rise velocity of the original vortex pair, but also push the pair against each other. Consequently, the vorticity is lost in the overlapping regions of the vortex pair, and the rise velocity is further reduced. As time increases, the countersigned vorticity begins to dominate the flow and the vortex migration stops. With further increases in time, the vortex begins to migrate downward, provided that it is not yet subjected to large scale instabilities (sinusoidal instability and/or vortex breakdown).

The density contours reveal the same phenomena in a different context. As the vortices rise, fluid of greater density is pushed upwards (Figure 8) into regions of lesser density. Since such a migration cannot go on indefinitely, the vortices rise to a maximum height and then begin to sink downwards. The calculations do not take into account sinusoidal instability, vortex breakdown, and ambient turbulence. In reality, of course, the vortex pair begins to break up as it nears the end of its maximum migration and eventually disappears.

The experimental and calculated values are compared in Figure 9. The correspondence between the measured and calculated values is surprisingly good up to the time of maximum rise. This is partly because of the experimental fact that the migration of vortices in a highly stratified medium is inhibited primarily due to the reduction of vorticity of the initial vortices and the creation of the countersigned vorticity.

Figure 7

Velocity field and the evolution of counter-sign vorticity at $T^* = 3.64$.

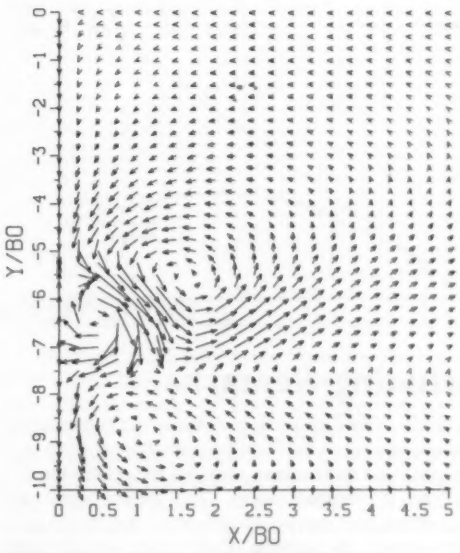

Figure 8

Constant density countours at $T^* = 3.64$.

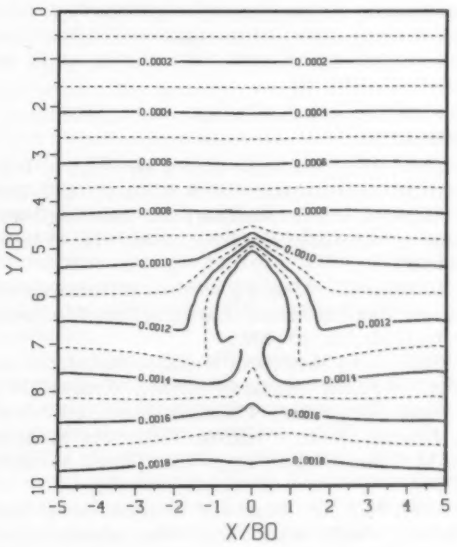

Figure 9

Comparison of numerical and experimental results for the example cited in the text (SP = 0.75, F_v = 0.018).

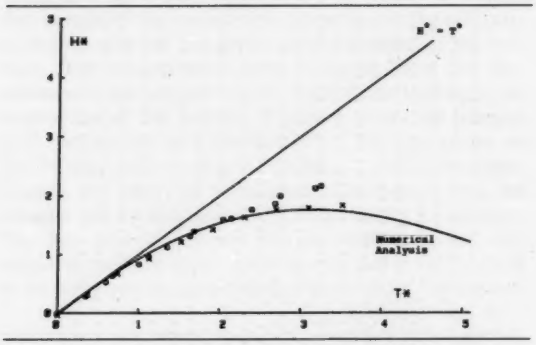

Concluding Remarks

The migration of trailing vortices in the ocean environment is of vital importance to the Navy because these vortices give rise to surface and temperature scars (if they reach the free surface) and to internal waves. The experimental and analytical efforts face numerous difficulties due to the complex interactions of ambient turbulence, stratification, sinusoidal instability, vortex breakdown, and laminar and turbulent diffusion. This article attempted to summarize briefly the efforts undertaken in the hydrodynamics laboratory of the Naval Postgraduate School. The problems investigated concern the effect of ambient turbulence in stratified medium, surface signatures in homogeneous[8] and arbitrarily-stratified ocean, scale effects, numerical investigation of the dependence of the calculated internal wave characteristics on the turbulence model used, etc.

References

1. Crow, S. C., "Stability Theory for a Pair of Trailing Vortices," *AIAA Journal*, Vol. 8 (1970), pp. 2172-2179.

2. Sarpkaya, T., "On Stationary and Travelling Vortex Breakdowns," *Journal of Fluid Mechanics*, Vol. 45 (1971), pp. 545-559.

3. Sarpkaya, T., "Trailing Vortices in Homogeneous and Density Stratified Media," *Journal of Fluid Mechanics*, Vol. 136 (1983), pp. 85-109.

4. Daly, J. J., "Effects of Ambient Turbulence and Stratification on the Demise of Trailing Vortices," M.S. thesis, Naval Postgraduate School, Monterey, CA., 1986.

5. Johnson, S. K., "Trailing Vortices in Stratified Fluids," M.S. thesis, Naval Postgraduate School, Monterey, CA., 1982.

6. Gray, W. E. Jr., "Scars and Striations due to Trailing Vortices," M.S. thesis, Naval Postgraduate School, Monterey, CA., 1985.

7. Tombach, I., "Observations of Atmospheric Effects on Vortex Wake Behaviors," *Journal of Aircraft*, Vol. 10 (1973), pp. 641-647.

8. Sarpkaya, T., "Trailing-Vortex Wakes on the Free Surface," *Proceedings of the 16th Symposium on Naval Hydrodynamics*, pp. 14-18, July 1986, Univ. of Calif., Berkeley, CA.

Biographies

Dr. T. Sarpkaya, a Distinguished Professor in the Department of Mechanical Engineering, joined the Naval Postgraduate School in 1967. He has been teaching and doing research in the general area of hydrodynamics for the past 30 years. He is primarily interested with time-dependent flows, vortex breakdown, discrete vortex models, and marine hydrodynamics. In 1981, his book, *Mechanics of Wave Forces on Offshore Structures* was published.

LCDR Steven K. Johnson graduated from the U.S. Naval Academy with a M.S. degree in Mechanical Engineering in June 1974. In 1982 he graduated with distinction from the Naval Postgraduate School. His thesis "Trailing Vortices in Stratified Fluids" was the basis of his receiving the Newborn Student Research Award, an annual award sponsored by the Sigma Xi Society. LCDR Johnson also was the recipient of the Naval Sea Systems Command Award for excellence in Naval Engineering, and the Navy League Award for highest school-wide academic achievement. He is now serving aboard the USS BUCHANAN (DDG-14) as the Executive Officer.

LT William E. Gray, USN, received his Bachelor of Science degree in Micro-Biology in 1976 from the University of Ohio. He then attended Surface Warfare Officers School, San Diego, California. In 1982 he reported to the Naval Postgraduate School and graduated in 1985 with the degrees Master of Science in Mechanical Engineering and Mechanical Engineer. His thesis entitled "Surface Disturbances Due to Trailing Vortices." He was awarded the Naval Sea Systems Command Award in Naval Engineering recognizing his achievements at the Naval Postgraduate School. Following his graduation he reported to the Naval Reactors Representative Office at Portsmouth Naval Shipyard, Portsmouth, NH where he is currently stationed.

LT John J. Daly, USN, received his Bachelors Degree in Mechanical Engineering from the University of Illinois in 1978. He then attended the Naval Nuclear Power School and after other tours of duty was assigned to the Naval Postgraduate School graduating in 1985 with the degrees Master of Science in Mechanical Engineering and Mechanical Engineer. His Master's Thesis was entitled "Effects of Ambient Turbulence and Stratification on the Demise of Trailing Vortices." Following graduation LT Daly attended Surface Warfare Officers School – Department Head Course in Newport, RI. He reported to USS PETERSON (DD-969) in December 1986 as the Chief Engineer.

AUTONOMOUS MEASUREMENT OF SPACE SHUTTLE PAYLOAD BAY ACOUSTICS DURING LAUNCH

By Lt. Austin W. Boyd, USN
Lt. Brian P. Kosinski, USN
Lt. Richard L. Weston, USN
Space Research Team

Introduction

A method of recording and analyzing the acoustic characteristics of the Space Transportation System (STS) cargo bay has been developed. The experiment is integrated within a NASA Get-Away-Special (GAS) canister. The experimental procedure involves an autonomous prelaunch measurement of acoustic modes using an oscillator, loudspeaker, and three microphones. Acoustic-resonance data are recorded on a solid-state digital recorder using magnetic bubble-memory. The system is then used to record ambient noise prior to and during the launch. Postflight data analysis will provide information relevant to the design of sensitive spacecraft components.

Airborne acoustic vibrations, like structure-borne mechanical vibrations, possess the potential to cause significant damage to payloads aboard the Space Shuttle. Early flights of the orbiters confirmed that such vibrations contributed to the loss of thermal protection tiles and subsequent minor vehicle damage. Similar distress in sensitive spacecraft components has been of continuing interest to contractors and NASA, as components are engineered to withstand the rugged mechanical vibrations and intense sound pressure levels (135 dB SPL) experienced during launch. The Dynamic Acoustic and Thermal Environments (DATE) group of NASA Goddard Space Flight Center and the Aerospace Corporation of El Segundo, CA, have been analyzing data from STS missions. Two conclusions reached by these groups are that a better understanding of the STS cargo bay acoustics is needed and that the acoustics data base should be expanded. Additionally, a more precise analysis is required with regard to the acoustic transients produced at the moment of solid rocket booster (SRB) ignition. The acoustic impulse generated by the ignition of the boosters could be a significant damaging force, but previous experiments have experienced difficulty in characterizing it quantitatively. An analysis of booster ignition acoustics may also provide insight into failure mechanisms of that critical Shuttle component.

Description

Students and faculty at the Naval Postgraduate School (NPS) have designed an experiment to measure the resonant acoustic modes of the Shuttle payload bay and the ambient acoustic environment produced as a result of main engine and booster operation. This project is designed to use the NASA Get-Away-Special (GAS) experiment program and the associated GAS payload canister. This program is designed to facilitate the transportation of compact, self-contained payloads aboard the Space Shuttle at low cost ($10,000). Experiments must exhibit scientific value, be relatively autonomous, and fit within a 5-cubic-foot canister with a maximum system weight of 200 pounds.

The NPS acoustic mapping experiment will operate in three phases. The first phase will measure the acoustic resonance spectrum of the Shuttle payload bay. A loudspeaker will provide a sinusoidal excitation of the cargo bay while the experiment records the resultant acoustic resonances. This spectrum will be dependent upon the payload configuration, and will act as a template for evaluation of the subsequent launch data. The second phase will record the Shuttle prelaunch and launch acoustics. The experiment will be prepared to record the launch approximately 5 minutes prior to liftoff, and will continue recording until the vehicle is exoatmospheric. The final phase will maintain a temperature record and actively heat the electronics, thus determining the thermal characteristics of the new, uninsulated GAS canister lid used in this experiment.

The GAS canister will be configured using an external unpressurized speaker-and-microphone assembly, and a pressurized electronics/power supply section. (See Figure 1). In the unpressurized assembly, a JBL model LE10H-1 electrodynamic loud-speaker is mounted in a Helmholtz-type resonator cavity. This cavity enhances the speaker output at low frequencies and equalizes the ambient pressure on both sides of the speaker cone. Three Endevco 2510 microphones are also mounted in the lid of

Figure 1

A cross section of the Naval Postgraduate School Acoustic mapping experiment as integrated within the Get Away Special canister.

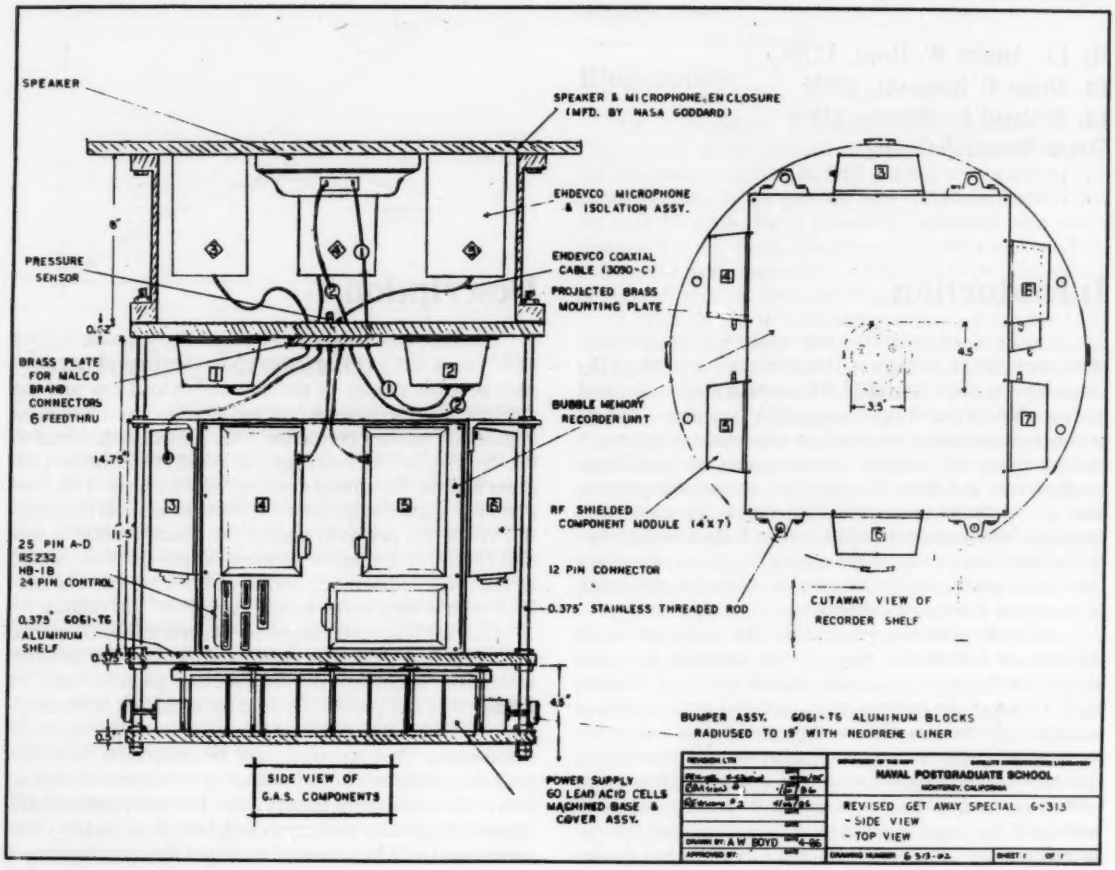
SPEAKER
SPEAKER & MICROPHONE ENCLOSURE (MFD. BY NASA GODDARD)
ENDEVCO MICROPHONE & ISOLATION ASSY.
ENDEVCO COAXIAL CABLE (3090-C)
PROJECTED BRASS MOUNTING PLATE
PRESSURE SENSOR
BRASS PLATE FOR MALCO BRAND CONNECTORS & FEEDTHRU
BUBBLE MEMORY RECORDER UNIT
RF SHIELDED COMPONENT MODULE (4"X7")
12 PIN CONNECTOR
0.375" STAINLESS THREADED ROD
25 PIN A-D RS232 MB-1B 24 PIN CONTROL
0.375" 6061-T6 ALUMINUM SHELF
CUTAWAY VIEW OF RECORDER SHELF
BUMPER ASSY. 6061-T6 ALUMINUM BLOCKS RADIUSED TO 1" WITH NEOPRENE LINER
POWER SUPPLY 60 LEAD ACID CELLS MACHINED BASE & COVER ASSY.
SIDE VIEW OF G.A.S. COMPONENTS
NAVAL POSTGRADUATE SCHOOL
MONTEREY, CALIFORNIA
REVISED GET AWAY SPECIAL G-313
- SIDE VIEW
- TOP VIEW
DRAWN BY: A.W. BOYD 4-86

the cavity, and are mechanically isolated from structural vibrations. Signal transmission between these components and the electronics package occurs through a pressure bulkhead and associated feedthrough connectors. The electronics package is sealed in a 15 psi dry nitrogen atmosphere. The electronics consist of a voltage-controlled oscillator (VCO), matched filter signal-detection circuitry, an accelerometer-based launch-detect circuit, three analog-to-digital (A/D) converters, a solid-state magnetic bubble-memory (MBM) recorder, an NSC 800 microprocessor-based system controller, an autonomous heater system, and a 680 watt-hour DC power supply.

Five key components were developed in support of this experiment. They are (1) a nonvolatile, high density data-storage medium, (2) a microprocessor-based system controller, (3) a matched filter pre-launch detection circuit and associated autonomous experiment turn-on algorithm, (4) a microphone vibration isolation mechanism, and (5) a general purpose high-density power supply. These components were all designed by NPS students and faculty, and have been modularized for use in other experiments and space payloads by the NAVY and NASA. Following a description of the experimental method, each of these critical elements will be described in detail.

Method

The acoustic mapping experiment is initiated on the launch pad after the various payloads are integrated and the payload bay doors are closed. Approximately five hours prior to liftoff NASA ground personnel will activate a GAS control switch on the aft flight deck of the Shuttle. This will close the payload's power control relay allowing the experiment to receive power from its internal supply. No further NASA controlling actions are needed throughout the duration of the experiment. Having received power, the system controller will conduct an initialization routine and route power to appropriate sub-systems. This low power CMOS (Complimentary Metal Oxide Semiconductor) system controller is the only component that is continuously powered. It has the capability to selectively energize all other elements of the system for the purpose of power conservation in the event of possible ground delays.

To determine the resonant acoustic modes of the cargo bay, the system controller will follow its initialization routine with an acoustic sweep. It will command the voltage-controlled oscillator (VCO) to resonate the cargo bay using an amplifier and external speaker assembly which are capable of generating sound-pressure levels of 120 dB SPL (ref. 20 μPa). The VCO will step in 1 Hertz (Hz) increments from 30 Hz to 1054 Hz, at a rate of one Hz per second. The total sweep time will be 17:04 minutes with an average electrical power consumption of 48 watts. The sound will excite the resonances of the Shuttle bay and its payloads, and the resultant acoustic energy will be detected by three independent Endevco 2510 high intensity microphones. This will allow determination of the direction and amplitude of sound-pressure gradients. The microphone signals are conditioned by preamplifiers and filters, and are then sampled by 15 bit A/D converters at a rate of 2.5 kHz. The digitized data are stored in the solid-state magnetic bubble-memory recorder for later retrieval. Acoustic mapping of the cargo bay will be based on this information and will be used as a template for interpretation of the actual launch data.

At the completion of the sweep the system controller will remove power from all components with the exception of the matched filter and launch-detect circuitry. This matched filter component and its associated turn-on algorithm will utilize a fourth external microphone to detect a 600-Hz discrete frequency line which is characteristic of the operation of the Shuttle auxiliary power units (APU's). These APU's are turned on immediately prior to launch. The launch must be aborted for APU refueling if the APU's are left operating in excess of seven minutes. Consequently, the characteristic acoustic signature of the APU is an excellent signal with which to initiate the experiment shortly prior to SRB ignition. In the event of a failure of the matched filter, an accelerometer will detect launch vibrations to provide a backup signal for experiment initiation. Use of this matched filter and autonomous turn-on algorithm eliminates the need for external inputs from NASA at a checklist-intensive period in the launch schedule.

When the 600-Hz frequency has been detected continuously for one minute, the matched filter provides a logic signal to the system controller indicating an imminent launch. The controller then places the previously mentioned recording system of microphones, preamps, A/D converters, and recorder in a "scroll" stage of operation. In this mode, the background noise prior to launch is recorded on two bubble-memory modules using an endless loop format, overwriting data that is 60 seconds old until a launch is confirmed. Ignition of the SRB's is detected by an accelerometer, and at that time, the system controller shifts the recorder into a normal record mode. In this way, the most recent two minutes of prior-to-launch acoustics are retained, in addition to the full spectrum of SRB ignition acoustic transients and powered flight acoustics through the Shuttle's exit from the atmosphere. Total system data storage at the completion of the acoustics recording phase is approximately 12 megabytes.

During the orbital phase of the Shuttle flight, the system controller provides power only to the autonomous heater controller, which alternately cycles a set of 12 heating strips placed near the 25 magnetic bubble-memory modules. These modules are subject to loss of data if exposed to temperatures below −20 degrees Celsius. Initial thermal-control data for GAS canisters suggests that temperature extremes of this magnitude are possible if the Shuttle is oriented with the open payload bay facing deep space for an extended period of time. In addition to the heater controller activity, the system controller will continue to sample the canister temperature, heater status, and a real-time clock once every 10 minutes. It will log these data on a separate bubble-memory module that is dedicated to controller use.

Upon completion of the mission, a correlation of canister temperatures, heater operation, and vehicle attitude will enable determination of the thermal characteristics of GAS canisters which use exposed, uninsulated lids. It will also permit evaluation of the effectiveness of the heating system. Postflight analysis of the acoustics will be performed by the Naval Postgraduate School and the Aerospace Corporation of El Segundo, CA.

The canister development has been funded by the Office of Naval Research (ONR) in conjunction with the Naval Postgraduate School Foundation Research Program ($30,000), the USAF Space Division ($150,000) and the US NAVY TENCAP office ($25,000). System components will be retained alternately at the USAF and NPS sites, with the delivery of one flight ready system due in the winter of 1987. Shuttle launch acoustics have been given increased attention in the aftermath of the STS 51-L accident. Because the acoustics of any flight are highly dependent upon the payload configuration of the cargo bay, the provision of this experiment package will enable acoustic

mapping on a number of different missions. The Get Away Special program enables regular use of an orbiter due to the compact nature of the experiment, low launch costs, and minimal impact upon crew operations.

Technical Description

Due to initial design constraints, a number of enabling elements were required to ensure successful acquisition of launch data. Foremost was the requirement to develop a recording mechanism capable of withstanding vibration during launch without failure or degradation of acoustic data. Commercial tape recorders were studied for possible use, but it was discovered that even the best of space-qualified data recorders could not be guaranteed to be free of mechanically induced noise during the initial vibration transient of the SRB ignition. The mechanical tape recorder is subject to failure, tape slippage, and internal generation of noise when exposed to harsh vibration environments. Additionally, the ability to alternate quickly between scroll and normal recording modes is difficult to achieve in all but the most expensive recording units. Solid-state memory devices (PROM, EPROM, RAM) were investigated as possible solutions. They were rejected as well, due to the lack of flexibility in rewriting data or unacceptable memory volatility upon loss of power.

Figure 2

Lt Austin Boyd and Lt Mike Ziegler demonstrate the operation of the prototype magnetic bubble memory recorder, controller and power supply components.

Magnetic bubble-memory (MBM) was subsequently chosen as the core of this new generation data recorder due to its nonvolatility, immunity to vibration, and low power consumption. A 12-megabyte, 8 bit resolution recorder using the INTEL model BPK 5V75 four megabit bubble-memory module (Figure 2) was subsequently designed and tested at the Naval Postgraduate School (Figure 3). It provides 22 minutes of recording time on three channels using a sampling rate of 2.5 kHz. A scroll and a normal record capability were included to permit overwriting or retention of data as appropriate. Power consumption is kept at a minimal level (15 watts) through the use of a power switching scheme that energizes only the requisite memory modules. Data retrieval is accomplished via a direct link to an IBM PC-AT microcomputer on which floppy disk backups provide data redundancy. This recorder is the first of its kind and is being upgraded using Hitachi bubble memory devices in a third generation unit for use on the Naval Postgraduate School General Purpose Satellite (ORION).

Figure 3

A set of 24 INTEL BPK 5V75 Four megabit magnetic bubble memory modules are used to construct the 12 megabyte data recorder.

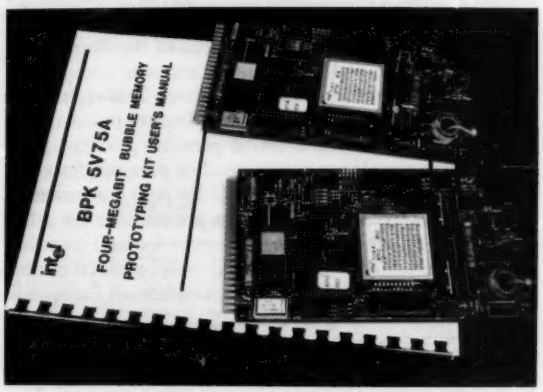

Autonomous operation of an experiment is a requirement of the GAS program. The low launch costs and rapidity of flight assignment are due largely to the lack of crew interaction required by these "space-available" payloads. To accomplish autonomous control of the acoustic mapping experiment, a controller was required which could function reliably for extended periods, accounting for possible launch delays and operating with minimal power consumption. For the purpose of energy efficiency, power switching was identified as one role of the controller, enabling it to selectively energize experiment components. Additionally, the controller was assigned the function of experiment-mode sequencing. In the event that NASA secures the experiment and later reinitiates the launch checklist, the controller must be able to ascertain whether heavy power use operations (such as the acoustic sweep) have been performed and thus not duplicate them. As a result of these design considerations, the control efforts were integrated in an NSC 800 microprocessor-based controller which is supported by 56 kbytes of Eraseable Programmable Memory (EPROM) and 8 kbytes of Random Access Memory (RAM). The ROM stores a series of subroutines designed to direct the three phases of operation, and the RAM is used for housekeeping functions and storage of system status information. CMOS components are used throughout the controller to minimize the power consumption of this continuously powered component A 4-megabit magnetic bubble-memory module is also integrated to allow the controller to maintain a status log of all significant events as a function of time. The storage of the on-orbit temperature samples is an example of such a use for this bubble module. Perhaps the most important mission of this particular module is the retention of information on the status of the experiment during power-down operations. The use of a non-volatile memory log enables the controller to query a status word in the bubble memory following ground aborts, thus ascertaining the status of the experiment chronology.

A dependable algorithm was needed to initiate recorder operation in order to detect the initial launch transients produced by the ignition of the solid-rocket boosters. In consideration of possible launch delays and power supply limitations, the launch recording portion of the experiment was constrained to begin as close to launch time as possible. Although NASA will initially power the GAS canister five hours prior to launch, it would be inefficient to power the recorder in its relatively power-intensive scroll mode for the duration of this prelaunch window. This is particularly true in the event that delays are encountered. It is possible that as many as seven ground aborts could be encountered on a given launch. Consequently, a turn-on signal was sought that occurred close in time prior to the SRB ignition and thus allowed for efficient utilization of the available battery power. Use of the SRB ignition for experiment initiation, as has been done by NASA, would not allow recording of the initial launch acoustic-transients. With the benefit of anti-submarine warfare expertise, a pair of students successfully isolated the characteristic signature of the auxiliary power units, noting the presence of a strong 600-Hz tonal during analysis of the preflight tapes for STS 2, 3, and 4. (Figure 4). In each case the APU's were powered up approximately five

Figure 4

Navy Lt. Austin Boyd analyzes a graphic display of the sound frequency which will automatically "turn on" an innovative experiment in the space shuttle Discovery's cargo bay just prior to lift-off. Identifying the "acoustic signature" of this particular frequency was one of several breakthroughs made by Naval Postgraduate School students in the course of designing their space-bound project.

minutes prior to launch. Information from NASA-Goddard indicated that once the APU was on line, the launch was committed to a "go", or an abort for APU reservicing. Using this 600-Hz signal as an input, a matched filter component was designed using the INTEL model 2920 programmable digital signal-processing integrated circuit. This chip incorporates an EPROM for the storage of digital filter routines that customize the chip to the user's needs. The raw signal from an external microphone is conditioned by a preamp and bandpass filter, and is subsequently processed using an Infinite Impulse Response (IIR) filter program in the INTEL 2920. Upon detection of the 600-Hz signal for 0.5 seconds, the 2920 provides a digital pulse output. A finite state controller then counts the number of uninterrupted occurrences of the 600-Hz signal, thus eliminating a chance occurrence of this critical frequency. After one minute of continuous APU operation, this matched filter provides a logic signal to the system controller for initiation of the scrolling recorder sequence. It should be noted that following the design and testing of this component, production of the 2920 signal-processing chip was discontinued by INTEL. Many programmable digital signal processing chips are commercially available from other manufacturers, however, and the philosophy of the turn-on algorithm remains unchanged. A variant of this component will be flown on an upcoming NASA mission in conjunction with a launch vibration analysis being conducted aboard a SPARTAN freeflyer platform.

Figure 5

The flight ready general purpose DC level power supply consists of 68 Gates brand lead acid cells. This 76 pound unit is capable of providing 680 watt-hours of energy using various voltage configurations.

An analysis of power consumption was conducted using a prototype MBM recorder, matched filter, VCO, heaters, and system controller. Allowing for possible launch delays in addition to a maximum 10 day flight, it was determined that approximately 680 watt-hours of energy would be required for a successful experiment. Sixty eight (68) Gates brand lead acid cells (5 ampere-hour, two volts) were chosen to meet the power supply requirements. These gelled electrolyte batteries are ideal due to their high power density, low cost, and the absence of outgassing during discharge cycles. Power supplies that have been previously flown in GAS canisters have typically been encased in aluminum housings. However, this method of containment proved to be excessively cumbersome for the restraint of 68 cells. An alternative power-supply structure was designed at NPS which utilizes a milled-baseplate receptacle and matching lid for the restraint, but not enclosure, of the batteries. As an offshoot of the design a general purpose architecture was devised which allows simple reconfiguration of the cells to provide voltages within the range of 2 to 136 VDC using only minor wiring modifications. A prototype unit has been successfully tested at NASA-Goddard under a 13.4 G random-vibration load (Figure 5) with no interruption of power on any of 8 volt-

Figure 6

Lt Brian Kosinski prepares the general purpose power supply for a NASA Goddard vibration test. Flight certification of the unit was obtained following 13.4 G load tests in three axes with no power fluctuations.

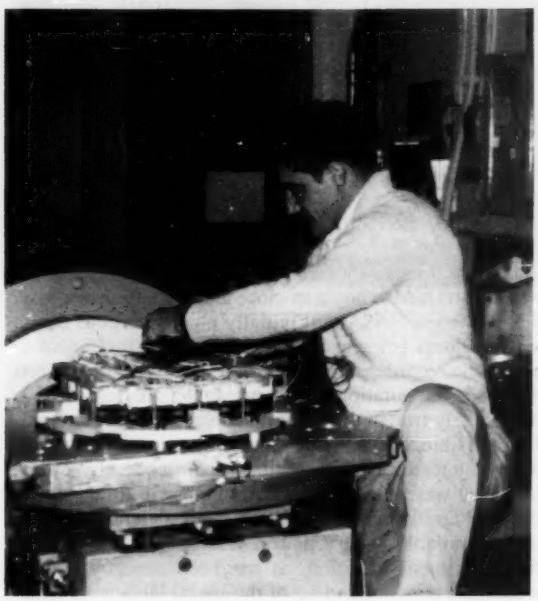

age stacks. The 80-pound flight unit (Figure 6) is presently configured with five parallel stacks of five cells each to provide twenty-five ampere-hours at 10 volts (digital logic supply), and two sets of two parallel stacks of 10 cells each for positive and negative 20-volts (opamps and A/D converters.) The positive and negative 20 volt stacks are also combined to provide a 40-volt potential for the voltage-controlled oscillator audio amplifier and its high power requirement. The remaining three cells are not used in this particular experiment. Information on this simple but effective design of a general-purpose DC power supply has been widely distributed, describing an affordable standard for GAS power applications.

Figure 7

Vibration isolation assembly for one of the three Endevco 2510 microphones used in the acoustic mapping experiment. An elastic suspension system effectively isolates all mechanical vibration between 30 and 1250 hz.

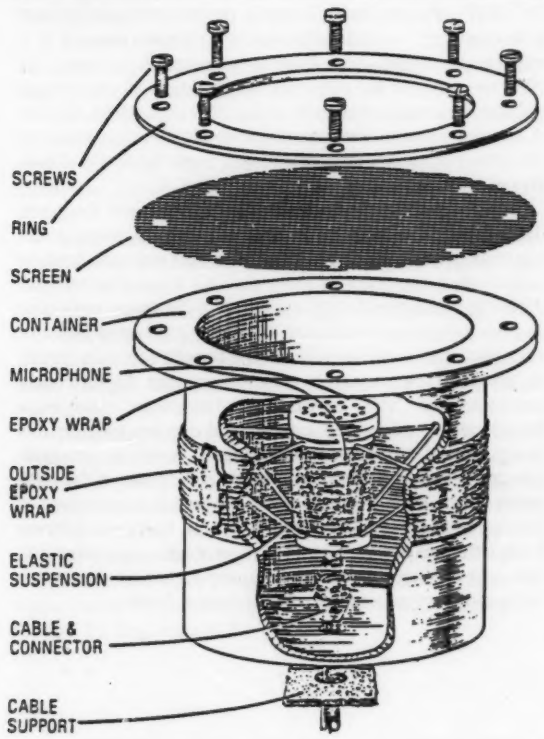

Figure 8

LT. Brian Kosinski (USN), right, and CAPT. Frank Mazur (USMC) test power supply connections on the NPS Get-Away-Special payload. The magnetic bubble-memory recorder occupies the center section of the experiment structure.

Investigation of previous Shuttle microphone-vibration isolators has revealed that they were actually mechanical amplifiers at 110 and 300 Hz. These low frequencies are among those of concern in studies of acoustic damage mechanisms. Due to these previously undetected artifacts, some early NASA acoustic data may be judged as degraded by virtue of the presence of mechanical vibration noise. This noise was impressed upon acoustic data via coupling through the microphone "vibration isolators" and support structures. A vibrating microphone acts, in effect, as an accelerometer. Thus, data from the early acoustic studies of Shuttle launches may be degraded by "acceleration noise" at least at two frequencies (110 and 300 Hz). An effective vibration-isolation design was produced at NPS which possesses a natural frequency of 15 Hz and effectively isolates the microphone from all mechanical vibrations between 30 and 1250 Hz. Using an elastic-thread suspension system, an Endevco model 2510 microphone is mounted in an aluminum shell which then attaches to the lid of the unpressurized GAS canister section. Three such shells are mounted in an equilateral triangle, providing phase and amplitude information by virtue of their geometry. Figure 7 depicts the elastic-thread suspension system and mounting shell.

Conclusions

The maximum height H*(max) attained by the vortices is of special importance. Figure 5 shows the maximum height data as a function of ϵ^*. Also shown in this figure is the flight data obtained by Tombach.[7] There is reasonable agreement between the laboratory and flight data in spite of the considerable scatter due to the difficulty of determining the maximum height attained by the vortices. The uncertainties stem primarily from the randomness in the inception of the instabilities leading to the destruction of the vortices. Figure 6 shows the lifespan of the vortex pair as a function of ϵ^*. The data points on the T*(max) axis correspond to the non-turbulence case. Clearly, the effect of turbulence is to reduce both the lifespan and the maximum height attained by the vortices. The data have also shown that the vortices in the non-turbulent medium break up primarily due to linking and in the turbulent medium, mostly due to vortex breakdown.

A better understanding of the normal-mode acoustics and sound-pressure levels in the Shuttle cargo bay during liftoff is required. With a more complete picture of the acoustic environment during launch, NASA and contractors will be able to design payloads efficiently, ensuring that a correct margin of safety is present to prevent damage to critical components. Spacecraft should not be built to account for acoustic and vibration damage mechanisms that do not exist. However, designers should be afforded information on possible transients which have been undisclosed due to late recorder initiation or masking due to degraded data. Previous Shuttle acoustic analyses have in some cases been unable to focus upon airborne acoustic data due to improper vibration isolation of microphones and unreliable tape-recorder operation following SRB ignition. The Naval Postgraduate School acoustic-mapping experiment will record these acoustic data through the use of properly isolated microphones and a vibration-proof magnetic bubble-memory data recorder. This experiment will also provide an interpretation and analysis of the launch data based upon the resonance characteristics of the orbiter bay observed prior to liftoff. Generic GAS components have been developed as a result of the acoustic-experiment research. An autonomous controller has been designed which is capable of sequencing components and recording significant events. This controller can be modified to satisfy various GAS requirements through simple software alterations. A self contained experiment turn-on circuit and algorithm has been developed which is capable of autonomously initiating operations immediately prior to Shuttle liftoff. A 680 watt-hour power supply has been constructed which is now a generic design for GAS applications at voltages selectable between 2 and 136 VDC. Analysis of Shuttle launch acoustics has been given increased emphasis as a result of the STS 51-L accident. Follow-on flights of this experiment will provide an expanded acoustic baseline for various payload configurations and booster modifications.

Other Space Research at NPS

An improved capability solid state magnetic bubble memory recorder is being developed to prove its feasibility for data storage onboard satellites in lieu of the current technology analog tape recorders. This third generation recorder will use Hitachi 4 megabit bubble memory devices. It will have a data rate of 3.2 megabits/second and will have expandable data storage capacity from 8 megabytes to 128 megabytes. The goal of this MBM recorder is to achieve higher reliability, longer life, and improved performance over conventional tape recorders at a lower cost, while maintaining low power consumption.

A General Purpose Satellite is being developed under USAF/SDIO sponsorship for defense sensor and military laboratory experimenter missions. This 250-pound satellite will provide full support services for small payloads of up to 50 pounds in a 2 cubic foot volume. It will launch from Shuttle into circular orbits up to 1500 km. Using a second generation GAS satellite ejection concept, or an optional deployment from expendable launch vehicles (SCOUT), the satellite will enable government and industry to access the low earth orbit realm for approximately $1.5 million per flight unit. Additional research is funded at NPS to compare the radiation degradation of silicon and gallium arsenide solar cells in the Van Allen belt region. A thermo-acoustic refrigerator with ultralow temperature IR sensor cooling applications has been funded and will fly as a GAS payload in FY's 89/90.

All research conducted by the NPS Space Research Team is performed by groups of master's-level engineering students with faculty support. Current research funding represents a spectrum of Navy and Air force interests, indicating widespread application of NPS space expertise in operational environments. A highly motivated cadre of officers, often working without the benefit of thesis credit, is involved in research experience that significantly enhances the NPS curriculum. Hands-on experience broadens the officers' educations and exposes participants to real-world engineering challenges. A strong graduate education with an operational focus is the tenet of the NPS experience. That philosophy is reflected in a summary of the Space Research Team efforts, where Navy and Marine Corps fleet experience is used to generate innovative and low-cost engineering solutions in support of current space technology requirements of the armed forces.

Bibliography

Boyd, A.W.; "Design Considerations for the ORION Satellite: Structure, Propulsion and Attitude Control Subsystems for a Small General Purpose Spacecraft"; Naval Postgraduate School M.S.E.E. Thesis; July, 1987.

Boyd, A.W., Fuhs, A.E.; "A Design for Small, General Purpose, Low Earth Orbit Satellites"; Proceedings, 37th Annual Congress, International Astronautic Federation (IAF), Innsbruck, Austria; October, 1986.

Boyd, A.W., Fuhs, A.E.; "General Purpose Satellites: A Concept for Affordable Low Earth Orbit Vehicles"; AIAA Aerospace Sciences Meeting, Reno, NV; January, 1987.

Butler, D.; "Get-Away-Special (GAS) Thermal Design Summary"; NASA X-732-83-8; July, 1983.

D'Ercole, T.M.; "A Solid State Data Recorder for Space Based Applications Using Magnetic Bubble Memory"; Naval Postgraduate School M.S.E.E. Thesis; March 1986.

Frey, T.J.; "A 32-Bit Microprocessor Based Solid State Data Recorder for Space Based Applications"; Naval Postgraduate School M.S.E.E. Thesis; March 1986.

Jordan, W.D.; "A Matched Filter Algorithm for Acoustic Signal Detection"; Naval Postgraduate School M.S.E.E. Thesis; June 1985.

Kosinski, B.P.; "Design, Development, and Testing of a General Purpose Power Supply for Space Transportation System Get-Away-Special Experiments"; Proceedings, AIAA Region Six Student Conference; May, 1986.

Kosinski, B.P. and Mazur, F.; "Comparison of Bubble Memory Architectures and the Design of a Solid State Digital Recorder for Satellite Applications"; Naval Postgraduate School M.S.E.E. Thesis; September, 1987.

On F.J.; "Evaluation of Space Transportation System (STS) OV-102 Orbiter Payload Bay Acoustic Environment"; NASA Technical Memorandum 84958; December, 1982.

Palmer, S.E., Garett, S.L., Wilson, O.B., Yoon, S.W.; "Autonomous Measurement of Normal Acoustic Modes in STS Cargo Bay"; Proceedings, AIAA Shuttle Environment Operations Conference, Houston TX, 1985.

Payload Bay Acoustic and Vibration Data from STS (DATE Report 002-005); NASA, 1981-1983.

Profumo, V.J.; "Experimenter's Planning Guide for Department of Defense Space Test Program"; Aerospace Corp., El Segundo, CA; 1983.

Stehle, C.D.; "Vibration Isolation of a Microphone"; Naval Postgraduate School Masters Thesis; September, 1985; (DTIC Report No. ADA 161 018).

Wallin, J.W.; "Microprocessor Controller with Nonvolatile Memory Implementation"; Naval Postgraduate School M.S.E.E. Thesis; December, 1985.

Wheatley, J., Hoffler, T., Swift, G.W., Migliori, A.; "Understanding Some Simple Phenomena in Thermoacoustics with Applications to Acoustical Heat Engines"; American Journal of Physics, 53, 147, (1985).

Biographies

Lt. Austin W. Boyd, Jr., USN, an antisubmarine warfare pilot, is a graduate of the Space Systems Engineering curriculum at NPS. He served as Project Director of the Space Research Team during 1985-1986. He is the 1987 recipient of the AIAA "CAPT. Michael J. Smith Award for Excellence in Astronautics" at NPS. Lt. Boyd is now assigned to the Naval Military Personnel Command.

Lt. Brian P. Kosinski, USN, an engineering duty officer, is a graduate of the Space Systems Engineering curriculum at NPS. He served as the Space Research Team Project Director during 1986-1987. He is now assigned to the Space Technology Office of SPAWAR.

Lt. Richard L. Weston, USN, a surface warfare officer, is a graduate of the Weapons Systems Engineering curriculum at NPS. He is now serving as Weapons Officer aboard the USS Waddell (DDG 24).

Profiles in Science

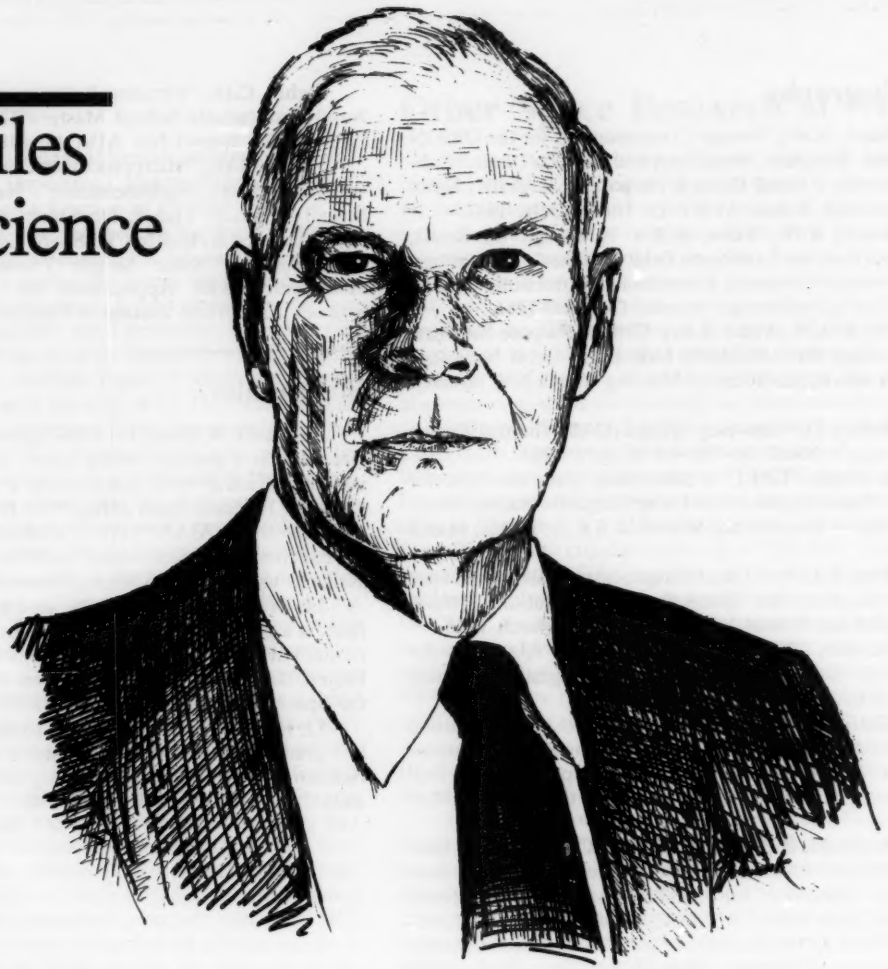

Richard W. Hamming

In the late 1940's, when Dr. Richard W. Hamming was managing the Bell Laboratory computer centers in Murray Hill, New Jersey, he encountered a series of unexpected failures in the lab's error correcting machines. His subsequent assessment of fundamental issues of machine reliability and maintainability led to the birth of coding theory and the development of "Hamming codes."

The error detecting and error correcting codes, along with the underlying theory created by Hamming, provided an important framework for improvements in the reliability and maintainability of naval electronic equipment and computers.

He joined the Naval Postgraduate School in 1976 as Professor of Computer Science. He teaches courses in information and coding theory, simulation and modeling, mathematics, and an advanced seminar on computer science topics. The author of nine books and more than 75 journal articles, Hamming continues active research in numerical methods, software, simulation and system performance and measurement.

Hamming, a member of the National Academy of Engineering, has received honors such as the Emmanuel R. Piore Award from the Institute for Electrical and Electronic Engineers (IEEE) for "contributing to the advancement of science and the betterment of society in the field of information processing," the Harold Pender Award from the University of Pennsylvania for "pioneering work in algebraic coding theory," and the Turing Prize from the Association for Computing Machinery (ACM).

Hamming's contributions were recently recognized by the IEEE through the establishment of the Richard W. Hamming Medal. This major award, including a $10,000 prize, will be awarded annually for exceptional contributions to information sciences and systems. It is sponsored by AT&T Bell Laboratories.

STUDIES OF THE MARGINAL ICE ZONE ALONG THE EAST GREENLAND COAST

By Robert H. Bourke and Robert G. Paquette
Department of Oceanography

Introduction

From the viewpoint of U. S. naval strategists, the Arctic Ocean has always been considered a potential warfare theater due to its contiguous boundary with the Soviet Union. Over the past several decades, however, naval operations in the Arctic have been quite limited and primarily of an investigatory nature to test and develop submarine operations under ice-covered waters. Recent advances in Soviet submarine-launched missile capabilities and their routine deployment on submarines operating in Arctic waters has brought an increased awareness to naval planners of the real potential for warfare in these waters. It is therefore prudent that studies be conducted of the hostile Arctic environment and its potential impact on naval operations, including platforms, weapons and sensors.

The study of polar oceanography has a long history at the Naval Postgraduate School (NPS) dating back to the mid 1960's when NPS faculty conducted sound speed and thermal microstructure studies from drifting ice camps in the Arctic Ocean.[1,2] Since the early 1970's, a course in polar oceanography has been offered at NPS, one of the few places in the U. S. to do so. This course was originally presented at the Naval Arctic Research Laboratory at Point Barrow, Alaska and was continued at Monterey only after closure of the Laboratory in 1979.

Beginning in 1971, NPS faculty have been involved in physical oceanographic studies of the marginal ice zones (MIZ) of the Pacific and Atlantic Arctic basins. To date, eleven ice-breaker cruises have been conducted in the ice-covered waters of the Chukchi, Beaufort, Bering and Greenland Seas during both summer and winter conditions. This research has been under the direction and sponsorship of the Arctic Submarine Laboratory, Naval Ocean Systems Center, San Diego, California. These studies have primarily been directed towards characterizing the water masses, currents, fronts, finestructure, and mesoscale eddies found in these dynamically active regions. NPS faculty were also actively involved in the international, multidisciplinary Marginal Ice Zone Experiment (MIZEX) sponsored by ONR and conducted in 1984 in Fram Strait off the east coast of Greenland. In recognition of this long-term commitment to Arctic research, the Chief of Naval Research established at NPS in 1977 a research Chair in Arctic Marine Science which today brings to NPS Arctic scientists of wide reknown and with widely varying areas of expertise.

In the sections that follow we have chosen to describe the results of our more recent efforts, namely the oceanographic characteristics of the East Greenland Current, rather than provide a broad overview of marginal ice zone oceanography. Many features of the MIZ are similar in both the Atlantic and Pacific, e. g., the association of a strong front with the ice edge. However, a hallmark of the MIZ is its extreme variability in both space and time. Hence, it is perhaps more instructive to restrict our description to a specific locale.

The remainder of the paper concerns discussions of the water masses, circulation and transport of the waters flowing over the East Greenland continental shelf and slope. Applications to naval operations are not explicitly addressed but are self evident, namely with regard to underwater acoustics and submarine operations under ice.

Oceanography of the EGC

The East Greenland Current (EGC) is the major outlet for Arctic Ocean surface water into the Atlantic Ocean and forms the western limb of the cyclonic gyre which occupies most of the Greenland Sea (Figure 1). It flows south over the East Greenland continental shelf. It's eastern boundary lies close to the shelf break where the current is concentrated into a high speed jet as a result of the strong topographically-generated oceanographic front, the East Greenland Polar Front (EGPF), formed there. This front separates the cold, ice-covered waters of Arctic origin to the west from the warmer, saltier North Atlantic-derived waters to the east.

A comprehensive review of the characteristics of the EGC and its associated water masses was conducted by Aagaard and Coachman based on older data up to and including the 1964 and 1965 EDISTO expeditions. They identified three major water masses in the EGC whose names and properties have been slightly modified since then. Polar Water (PW), which extends from the surface to 150 to 200 m, is characterized by temperatures less than 0°C and salinities less than 34.5 ‰. A sharp thermohaline gradient separates PW from the underlying warm ($T > 0°C$) and salty (salinity maximum of 34.88 to 35.0 ‰) Atlantic Intermediate Water (AIW). AIW is itself a modified product of Atlantic Water (AW) ($T > 3°C$, $S > 34.9$ ‰; Swift and Aagaard brought into the region by the West Spitzbergen Current (WSC). Beneath the AIW, commencing at about 800 m. lies the nearly homogeneous Greenland Sea Deep Water (GSDW) having temperatures colder than 0°C and a limited salinity range of 34.87 to 34.95 ‰.

Warm salty water from the temperate regions of the North Atlantic flows into the Greenland Sea as the Norwegian Atlantic Current where a portion of it branches to form the West Spitzbergen Current. Some of this water, upon encountering the ice edge between 79°N and 80°N, sinks to intermediate depths of 200–500 m and enters the Arctic basin where it is traceable throughout as a warm ($T > 0°C$), salty layer. However, an uncertain but major portion of the WSC turns west, then south, to join with the EGC between latitudes 75°N to at least 82°N. This warm, southward flowing current, termed the Return Atlantic Current (RAC), is observed as both a surface and subsurface flow and forms the eastern boundary of the EGPF.

The near-surface water of the WSC is comprised of AW. As the WSC turns west and then south, the AW becomes cooler and slightly more dilute due to interaction with the ice edge. Hence, the waters which comprise most of the RAC are predominantly of the type AIW. In summer some AW may be present in the core of the RAC, especially at latitudes above 77°N.

Figure 1

Bathymetry (meters x 100) and currents in the Greenland Sea derived from a variety of sources (from Paquette et al., 1985). Fram Strait separates Greenland and Spitsbergen.

Recent Observations in the East Greenland Current

Commencing in 1981 the Polar Oceanography Group at NPS conducted several extensive surveys of the East Greenland Current (EGC) from the ice breaker NORTHWIND. The NORTHWIND surveys were conducted in October–November 1981 and August–September 1984 and 1985 and included the region between 75°N and 82°N. The NORTHWIND 81 cruise provided the first detailed observations of the temperature and salinity properties and baroclinic flow characteristics of the EGC.[6,7] Transects across the front, constructed from closely spaced oceanographic stations, illustrate frontal conditions at the onset of freezing. A much more extensive set of cross-sections were obtained during the summer of 1984 which demonstrated both seasonal and interannual changes.[8,9]

Frontal Features

Two vertical cross-sections of temperature and salinity from September 1984 are introduced to describe some of the features of the EGPF and to also highlight some of the features described above. The crossing along 79°55′N (Figure 2) indicates that the front (observed by the near-vertical slope of the isotherms and isohalines) is positioned in deep water more than 100 km east of the continental slope. The front is closely aligned with the ice edge which at this latitude trends northeastward toward the north coast of Svalbard. Farther to the south the front and, as will be seen, the high speed jet of the EGC converge onto the shelf break near 79°N remaining aligned with it at least as far south as 73°N.[4] A transect along 78°10′N (Figure 3) illustrates this alignment with the continental slope and also shows that warm AIW overlies the shelf, e.g., compare the positions of the 1°C isotherms in Figures 2 and 3. The latitude at which the EGPF converges onto the shelf break varies both seasonally and annually in response to the position of the ice edge but generally is constrained between 78°N and 79°N. This variability is closely coupled with the volume flow rate and heat flux variations experienced by the WSC. For example, the ice edge across Fram Strait melts back to higher latitudes during periods of greater warmth and flow rate.

Figure 2

Temperature (solid line) and salinity (dashed line) transect along 79°55′N. The East Greenland Polar Front, observed by the near-vertical slope of the isotherms and isohalines, is displaced about 120 km east of the continenta1 shelf break. The Return Atlantic Current is identified by the core of water warmer than 3°C.

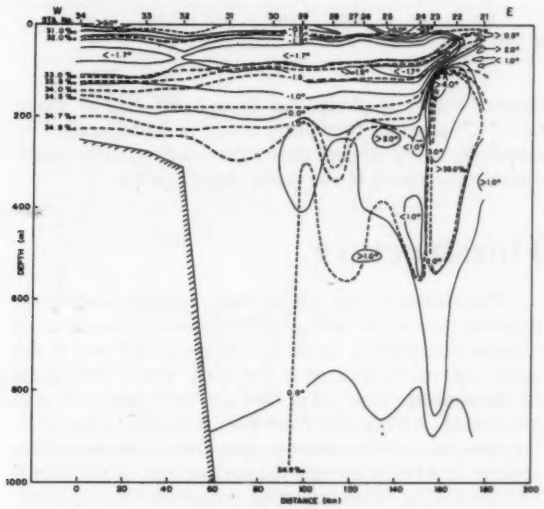

In both these transects, a warm (> 3°C) core of RAC is observed nestled close to the front causing the temperature gradient to be strongest there. The core has frequently been observed to be separated into horizontal and vertical filaments; their north-south length scales have not been well defined. The temperature-salinity characteristics of the core waters apparently vary with latitude both decreasing slowly with decreasing latitude due to continuous mixing with PW along the frontal boundary.

Based on the trend of the 0°C isotherm the mean slope to the EGPF is approximately 4 m/km in summer,[8] becoming two or three times steeper in winter.[6] North of about 77°30′N, the front is often separated into an upper and a lower portion. The extension of the upper frontal boundary to the east is probably often due to the formation of an extensive cold surface layer by the melting of nearby ice. Southward, where the RAC flows parallel and beneath the ice edge, less melting occurs and the front is generally continuous to the surface.

Shelf Processes

The bathymetry of the East Greenland shelf is marked by a series of banks and interconnected troughs (Figure 4) which influence the circulation and water mass structure of the overlying waters. The predominant water overlying the shelf is PW which in Figure 3 is seen to extend to depths of 150–200 m. In the winter this water is near the freezing point and, due to convective mixing and advection, may be isothermal to 50 m or more. Summer insolation causes a warming and dilution of the surface layer from a winter temperature of −1.7°C and a winter salinity having a maximum of about 33.8 ‰. These effects are visible ln Figures 2 and 3. The lens of cold (< − 1.5°C) water centered near 50 m in Figure 3 is of particular interest in that it is a residuum of water brought to the freezing temperature during the preceding winter. This water has been little modified since winter and thus indicates that vertical mixing of heat and salt is near zero in that depth zone. The layer is of lower salinity than waters of similar temperature but located near the EGPF. In 1984 much of this water was constrained between a narrow salinity band of 32.1 to 32.5 ‰ while in 1979 it was found ln the salinity range 33.2 to 33.4 ‰. This difference appears to be a result of the qreater freezing stress experienced in 1979, i.e., the number of freezing degree days was substantially greater in 1979 than in 1984 resulting in more ice formation and increased brine production. A comparison of shelf PW with PW from the Arctic basin or farther east in deep water indicates that the PW over the shelf is modified by coastal and local processes leading to substantial dilution.

Figure 3

Temperature and salinity transect along 78°10′N. At this latitude and farther southward the EGPF is aligned with the upper continental slope. Warm AIW overlies much of the shelf.

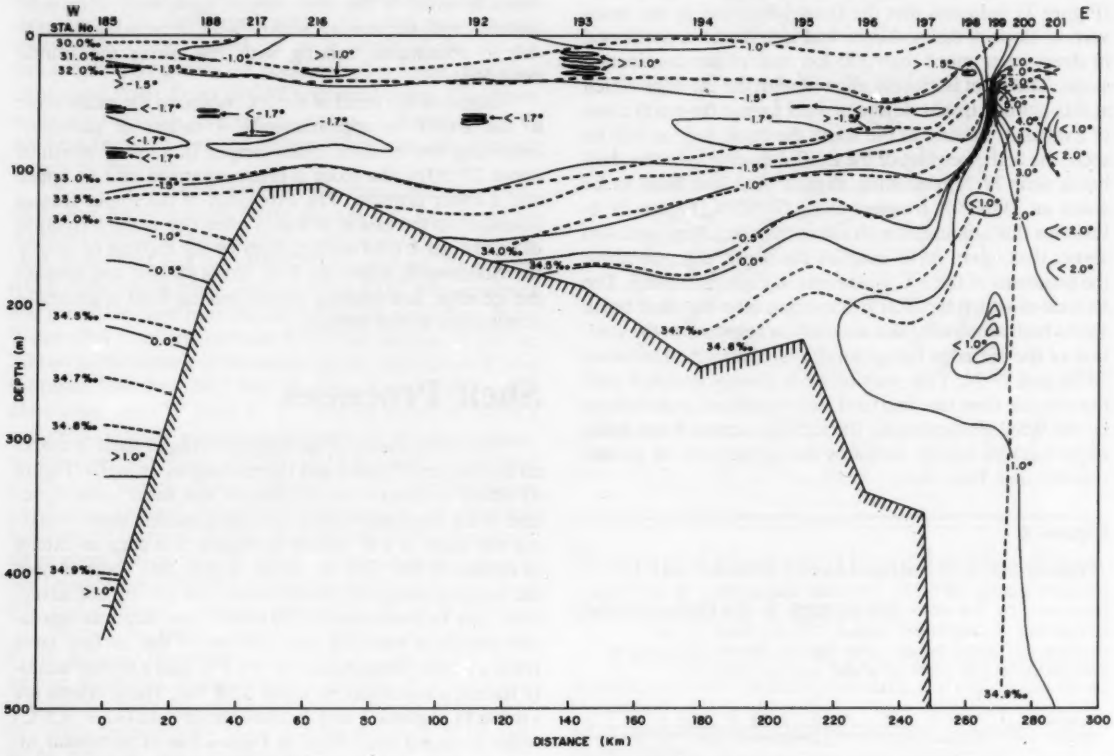

Beneath the PW is AIW which covers the deeper parts of the shelf region westward to the Greenland coast. In shallow areas, such as Belgica Bank seen near Stations 216 and 217 in Figure 3, the bottom shoals into the PW essentially eliminating all the AIW in these shallow areas. Overlying the shelf break and upper continental slope, many of our transects have shown that warm patches of AIW (temperatures > 1°C) are present. In Figure 3 such a patch appears to be forming. These occur sporadically in time and space and their generation mechanism has not yet been identified.

The troughs which cut across the Greenland shelf act as channels permitting the warm, salty AIW to penetrate far back onto the shelf extending its influence on shelf processes much more than otherwise possible. Water warmer than 1°C and saltier than 34.9 ‰ can be seen along the entire length of Belgica Trough (Figure 5) extending to the southern reaches of Norske Trough (Figure 3). The bottom waters of Westwind Trough are not as warm (< 0.5°C) since, as previously noted, at the latitude of its mouth the EGPF is more than 100 km seaward, effectively diminishing much of the warm source waters.

Finestructure

Finestructure, the temperature inversions resulting from interleaving of AIW and PW, generally is restricted to areas immediately to the east of the EGPF and in the upper 300 m. Compared to the early winter 1981 data, the finestructure observed in 1984 was weak and not widely distributed. An example from 1981 is shown in Figure 6. Finestructure of this nature is presumed to be formed by cooling of AIW at or near the surface east of the EGPF and descending westward along isopycnals into the frontal region. The finestructure lenses are markedly filamented

in both the cross- and along-frontal directions with maximum estimated along-front length scales of approximately 30 km.[7] The effect of the ship's drifting in and out of these lenses is observed in Figure 6 where a large intrusion centered near 275 m is present in the upward traverse of the CTD but is totally absent in the downward traverse taken some 20 min. earlier.

The effect of these finestructure lenses on low-frequency acoustic propagation was examined by Sleichter.[10] Using a range-dependent transmission-loss model, he found that the presence of finestructure served to increase the overall complexity of the transmission loss curve causing target signals to fade in and out in response to the multipath, interference patterns.

Figure 4

Bathymetry (in meters) of the northeast continental shelf of Greenland (from Tunnicliffe, 1985). A series of shallow banks and interconnected troughs influences the circulation and water mass structure of the overlying waters.

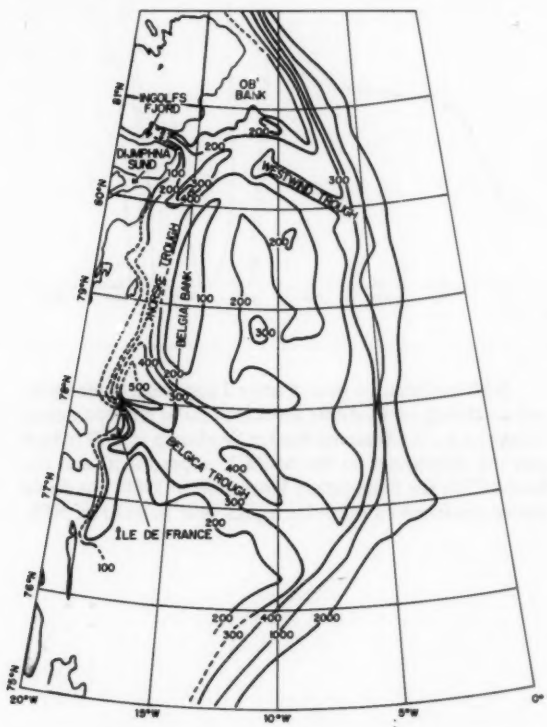

Circulation and Transport

The circulation over the East Greenland shelf is dominated by a narrow, swift-moving flow associated with the EGPF and an anticyclonic rotation centered on Belgica Bank (Figure 7). The latter is a near-surface baroclinic (density driven) flow extending to about 150 m, the approximate boundary between PW and AIW. The northward flow along the coast has been substantiated by ice drift measurements using NOAA-7 imagery.[8]

Vertical velocity sections across the EGPF and shelf illustrate the nature of the flow of the EGC. A section along 77.5°N (Figure 8) shows the limited horizontal and vertical extent of the frontal jet, 50 km and 100 m, respectively. In 1984, maximum southward baroclinic speeds of 0.12 m/s to 0.67 m/s were computed. In early winter 1981, when the frontal gradient was even sharper, maximum southward speeds of 0.80 m/s to 0.96 m/s were obtained. Farther west over the shelf current speeds are much reduced, of the order of 0.05 m/s to 0.1 m/s. Near the Greenland coast a northward flow of up to 0.12 m/s was encountered.

Recent current-meter measurements taken during the MIZEX 1984 experiment by Muench[11] at 100 m and 400 m depth indicate the vertical shear is about the same as indicated in Figure 8 but that the current speed at these depths is approximately twice as fast, suggesting that the additional flow due to the slope of the sea surface is not negligible. A mean southerly baroclinic transport, across both the shelf and the front, of 1.47 Sv (10^6 m^3/s) was determined. Considering the northward coastal flow of 0.58 Sv, the net flow of the EGC in 1984 was 0.89 Sv southward.

Future Plans

Future research cruises to the MIZ are planned on a nearly annual basis. During the summer of 1986, we conducted a bathymetric and oceanographic survey of northern Baffin Bay and Nares Strait. We also plan on expanding our instrumentation suit to include the ability to make current-meter observations using both moored arrays and expendable probes. The moored arrays are expected to provide long-term observations, remaining in place for about a year.

In order to more fully assess the impact of the complex MIZ environment on acoustic propagation, we are obtaining a series of drifting buoys which will not only measure standard atmospheric parameters but oceanographic and acoustic ones as well. The buoys will be equipped with a thermistor chain and two or more hydrophones. Our plan is to make ambient noise and transmission loss measurements in the MIZ and develop predictive models which will simulate the measurements.

Figure 5

Temperature and salinity transect along the axis of Belgica Trough. AIW warmer than 1°C extends far back on the shelf eventually flowing into Norske Trough near Station 231.

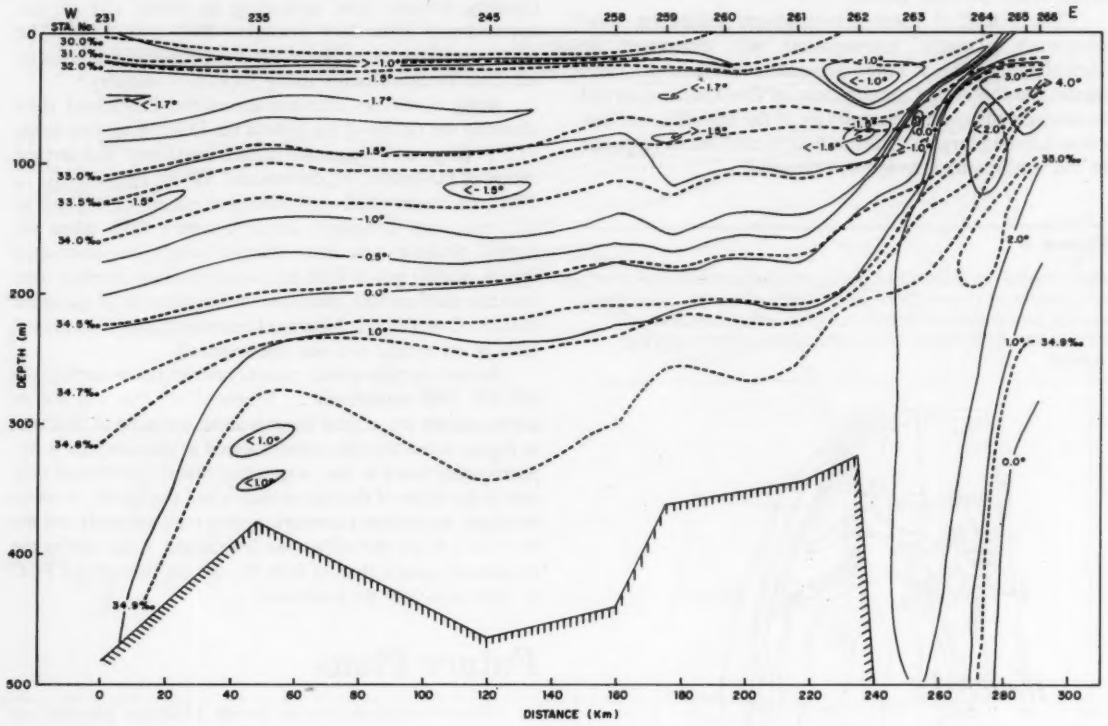

The oceanography faculty at NPS has recently been augmented with the addition of two numerical modelers, Professors Burt Semtner and David Smith, who have extensive experience in modeling arctic processes. Their expertise will provide a natural coupling between field experiments and predictive modeling of the dynamic processes indigenous to the MIZ.

Because of the expertise in sea-ice mechanics and sea-ice distribution characteristics brought to NPS by several former Arctic Chair incumbents, an ongoing research program has been developed in this area. The primary emphasis is to establish the spatial and temporal distribution of sea-ice thickness, an important factor in ice-penetration studies.

NPS has been the host of several important conferences and workshops on various aspects of polar environmental science, e.g., the Seasonal Sea Ice Workshop in 1979 (which was the forerunner to the MIZEX experiment) and the Second Sea Ice Penetration Workshop in 1986. No doubt future conferences on polar topics will be held at NPS.

Figure 6

Temperature and salinity profiles (both up and down traverses are shown) from a 1984 frontal station which demonstrate the large temperature inversions or finestructure indicative of interleaving of cold, fresh Polar Water with warmer, saltier AIW (from Paquette et al., 1985).

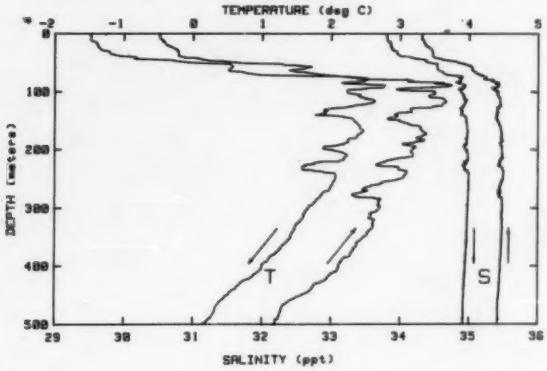

Figure 7

Pictoral representation of the near-surface density-driven (baroclinic) circulation over the East Greenland continental shelf. The length of the arrows is suggestive of the relative speed with maximum speeds near the EGPF (from Tunnicliffe, 1985).

Figure 8

Vertical baroclinic current velocity section along 77.5°N (contours in m/s). The jet of the EGPF indicates speeds of up to 0.34 m/s. Northward flow (dotted lines) of 0.1 m/s over Norske Trough is seen near Stations 226 and 227.

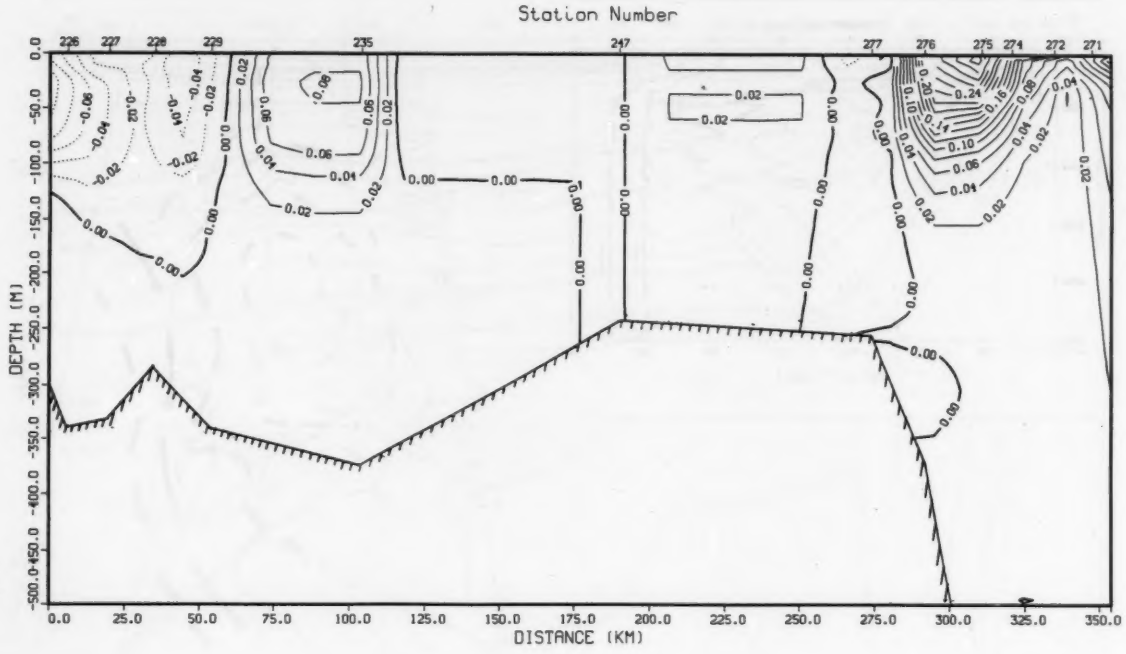

References

1. Denner, W.W., V.T. Neal, and S.T. Neshyba, "Modification of the Expendable BT for Thermal Microstructure Studies," *Deep-Sea Research.*, 18, pp. 375-378, 1971.

2. Neshyba, S., V.T. Neal, and W. W. Denner, "Temperature and Conductivity Measurements under Ice Island T-3," *Journal of Geophysical Research.*, 76, pp. 8107-8119, 1971.

3. Aagaard. K., and L.K. Coachman, "The East Greenland Current North of the Denmark Strait, I," *Arctic*, 21(3), pp. 181-200, 1968a.

4. Aagaard, K., and L.K. Coachman, "The East Greenland Current North of the Denmark Strait, II," *Arctic*, 21(4), pp. 267-290, 1968b.

5. Swift, J.H., and K. Aagaard, "Seasonal Transitions and Water Mass Formation in the Iceland and Greenland Seas, *Deep Sea Research.*, 28A(10), pp. 1107-1129, 1981.

6. Perdue, W.F., Oceanographic Investigation of the East Greenland Polar Front, Master's Thesis. Naval Postgraduate School, Monterey, CA., 1982.

7. Paquette. R.G., R.H. Bourke, J.L. Newton, and W. F. Perdue, "The East Greenland Polar Front in Autumn," *Journal of Geophysical Research*,90(C3), pp. 4866-4882, 1985.

8. Tunnicliffe, M.D., An Investigation of the Waters of the East Greenland Current, Master's Thesis, Naval Postgraduate School. Monterey, CA., p. 136, 1985.

9. Bourke. R.H., J.L. Newton, R.G. Paquette, and M.D. Tunnicliffe, "Circulation and Water Masses of the East Greenland Shelf," accepted for publication in *Journal of Geophysical Research.*

10. Sleichter, W.T., Modeling Acoustic Propagation Across the East Greenland Polar Front, Master's Thesis, Naval Postgraduate School, Monterey CA., p. 106, 1984.

11. Muench, R.D., G.S.E. Lagerloef, and J.T. Gunn, "1984-85 Current Observations in the East Greenland Current: a Preliminary Description," MIZEX Bulletin, No. VII, pp. 41-53, 1986.

Biographies

Professor Robert H. Bourke heads up the Polar Oceanography Group at the Naval Postgraduate School. He has made eleven ice breaker cruises to the Pacific and Atlantic marginal ice zones during the past 15 years. In addition to conducting polar research, he is also active in the field of environmental acoustics.

Emeritus Professor Robert G. Paquette has a long history of polar research having participated in cruises to the Arctic Ocean in 1951 and 1952 as well as during the decade of the 1970's. Although now retired, he continues to be active in data reduction and analysis efforts.

NPS METEOROLOGY STUDIES ON THE MARGINAL ICE ZONE

By Kenneth L. Davidson
Peter S. Guest
Department of Meteorology

Introduction

Understanding the annual and inter-annual variability of the Fram Strait/Greenland Sea Marginal Ice Zone (described by Bourke and Paquette[1] in this issue) is of scientific interest because of its impact on increasing military and civilian activities in this area. Until the ONR-sponsored Marginal Ice Zone Experiments (MIZEX), no comprehensive meteorology research had been done in marginal ice zones (MIZ). Limited meteorological studies were conducted in the Bering Sea MIZ (MIZEX-WEST 1983).[2-5] However, our meteorological understanding of this area has been minimal.

NPS investigators conducted meteorological studies in summer MIZEXs (June-July) in 1983 and 1984 and will participate in winter MIZEXs (March-April) in 1987 and 1989. In addition to MIZEXs, we have conducted several studies of mid-latitude open-ocean atmospheric boundary layer (ABL) properties.[6-10] From these studies, it became apparent that atmosphere-ocean coupling is controlled by properties throughout the ABL, not just at the immediate air/sea interface. MIZEX has provided the opportunity to study the role of the ABL in coupling weather patterns with both underlying ice and ocean features. The large horizontal temperature and roughness gradients which occur in the MIZ cause complex interactions between the atmosphere, ocean and ice resulting in highly variable (in space and time) conditions.

The following sections will discuss meteorological studies in the ONR-supported East Greenland Sea MIZ (MIZEX-EAST) program in which NPS investigations have a central role, recent results pertaining to MIZEX meteorological scientific objectives and plans for winter experiments in 1987 and 1989.

Figure 1

A summary of processes, geophysical scales and information sources relevant to MIZ studies.

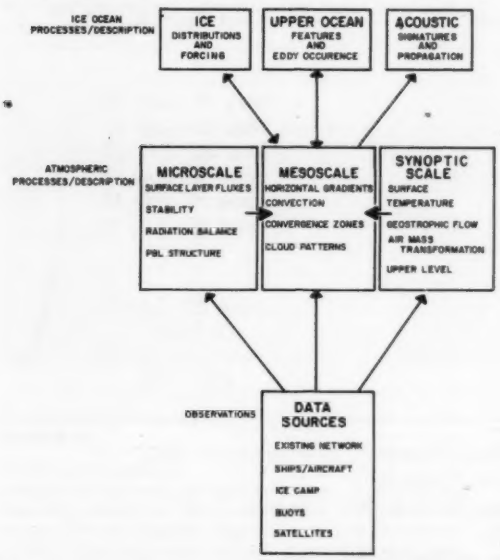

Mizex-East Meteorological Studies

Meteorology studies were a major part of MIZEX-EAST because oceanography, ice and acoustic studies require detailed time and space specifications of momentum and energy transfer from the atmosphere. A number of factors are important to this atmospheric forcing in the vicinity of the MIZ. The most important factor is the geostrophic wind (pressure gradient) forcing, but the relation between the geostrophic wind and the wind stress at the surface is complicated by curving wind trajectories and the horizontal variability of surface roughness and temperature, inversion strength and height, and ABL structure which occurs in the MIZ.

The nature and scope of the MIZEX meteorological effort, designed to examine MIZ atmospheric forcing, is illustrated by Figure 1, which represents the coordinated objectives in both the past summer and future winter experiments. The scale of features, the data sources, and the orientation of the MIZEX meteorological program are emphasized in Figure 1. The central position is given to the mesoscale processes in the interaction between atmosphere and ice/ocean features. These mesoscale processes were difficult to observe on surface platforms (ships and buoys) in the MIZ because the large number of platforms required to sufficiently resolve these processes has not been economically feasible.

A study encompassing the scales and processes shown in Figure 1 can be undertaken only by coordinated ABL measurements from several platforms. Surface, rawinsonde and aircraft meteorological observations, along with satellite imagery and airborne remote sensor data were used. Ships and aircraft involved in the MIZEX-84 meteorological program are listed in Table 1. Institutions and agencies investigating the ABL are also listed in Table 1.

Shipboard, aircraft and ice-floe-mounted turbulence and mean profile sensors were used to obtain information on MIZ microscale properties. The spacing of the platforms enabled surface flux properties to be measured simultaneously over water and ice regions. MIZ mesoscale properties were obtained from quantities measured on the platforms, as well as extensive rawinsonde launches from the ships. Rawinsondes were launched simultaneously from as many as five ships at least four times per day. Eight launches per day (every three hours) were made on the *Polarstern* throughout the experiment, as well as from the *Haakon Mosby, Valdivia* and *Polar Queen* during a six-day period at the end. Synoptic features were obtained from the existing observing network, Figure 2, augmented by the in situ measurements and an extensive interpretation of satellite imagery (Lindsay et al., 1986).[11]

Figure 2

Existing meteorological observing network in the vicinity of Fram Strait/East Greenland Sea MIZ with surface and upper air (rawinsonde) stations indicated.

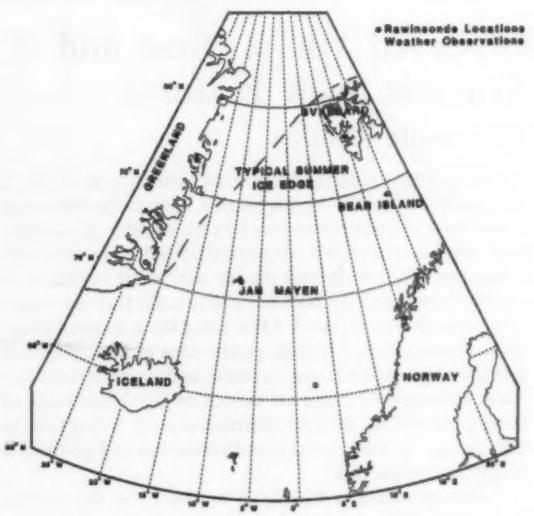

Table 1
Meteorology Platforms and Groups in MIZEX 84

	Meteorological Group*	Field Periods
SHIPS:		
USNS LYNCH	PMTC	May 18–June 28
MV POLARQUEEN	NPS/PSC	May 29–July 29
MV KVITBJORN	BIO/AES	May 30–July 30
MS HAAKON MOSBY	NPS/UW	June 12–July 15
FS POLARSTERN	AWI	June 11–July 18
FS VALDIVIA	AWI	June 20–July 18
AIRCRAFT:		
NOAA P-3	WLP/PMEL	June 20–July 7 (6 FLTS)
FALCON-20	AWI	June 22–July 14 (20 FLTS)

*AWI—Alfred Wegener Institute for Marine and Polar Research, Bremerhaven, FRG
AES—Air Environmental Services, Toronto, Ontario, Canada
BIO—Bedford Institute for Oceanography, Halifax, Nova Scotia, Canada
NPS—Naval Postgraduate School, Monterey, CA
PMEL—Pacific Marine Environmental Laboratory, NOAA, Seattle, WA
PSC—Polar Science Center, University of Washington, Seattle, WA
PMTC—Pacific Missile Test Center, Point Mugu, CA
UW—Department of Atmospheric Sciences, University of Washington, Seattle, WA
WPL—Wave Propagation Laboratory, NOAA, Boulder, CO

Observed Micro, Meso and Synoptic Scale Features

Microscale Results:

Microscale features have sizes generally less than 1 km. During MIZEX, the microscale features studied were related to surface processes such as the transfer of momentum, heat, moisture and suspended particles (aerosol) between the atmosphere and the ice and water surfaces. A profile tower used by NPS for microscale flux measurement is shown in Figure 3. Measuring these transfer processes enables more accurate predictions of ice movement and melting, upper-ocean currents and temperature, and lower atmospheric phenomena such as fog. Knowledge of locally produced aerosol distributions is important in climatological studies and in interpretation and prediction of optical properties.

The momentum transfer from the air to the surface is influenced by the aerodynamic roughness of the surface. This roughness is parameterized by the neutral drag coefficient which relates the momentum transfer to the wind speed. Drag coefficient results from MIZEX-83 were described by Guest and Davidson (1987)[12] in terms of ice concentration, ice floe roughness and size. They estimated wind stress by determining the turbulent kinetic energy dissipation rate near the surface. Similar results from MIZEX-84 have been described by Anderson (1987).[13] In general, both studies found that drag coefficients in the East Greenland Sea MIZ region were higher than those reported for other MIZ regions.

An example of results obtained by Guest and Davidson[12] in MIZEX-83 is shown in Figure 4. It is a summary of neutral drag coefficient, C_{DN}, as a function of upwind ice concentration. The mean value of 4.0×10^{-3} for ice concentration of 70 to 90% is higher than previously reported (Overland, 1985).[14] The bars indicate the large variability within given concentrations. The large variation in C_{DN} for given ice concentration is explained by differences in ice floe size and roughness. Small rough floes formed by wave action exert twice the drag as relatively large flat floes with the same concentration, and three to four times as much as the adjacent open ocean.

Figure 3

Turbulence tower left center, and wind profile tower, right. These 2.2 m and 6 m towers were used to measure heat and momentum fluxes over an ice flow in the East Greenland Sea MIZ. The polar bear was an uninvited visitor.

Figure 4

Drag coefficients, C_{DN}, or roughness length, z_o, as a function of upwind ice concentration. Bars indicate standard deviation. Solid circles are the mean and open circles are the median (from Guest and Davidson (1987)). The roughness length is another way of expressing the relationship between wind stress and wind speed.

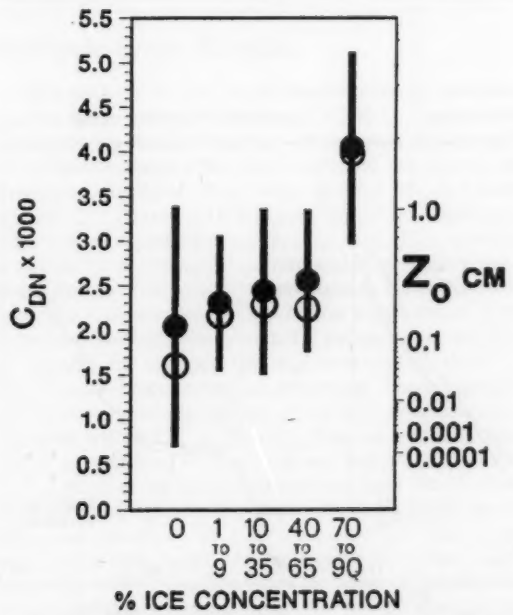

Aerosol measurements were also made by NPS participants in MIZEX-83. Borrmann *et al.*, (1987)[15] interpreted total aerosol concentrations and size distribution with respect to synoptic scale features. Size distributions before, during and after an atmospheric frontal passage show that the concentration of particles in the 1-to-10-mm size range decreased by a factor of 30 (Figure 5). This is a significant naturally occurring decrease in this region far from anthropogenic sources.

This discontinuity was caused by the changing trajectories of sampled air which were first from ocean to ice and then, after frontal passage, from ice to ocean. It is notable that the concentrations of smaller sizes, 0.1 to 0.5 mm, change only slightly with the frontal passage. Particles of this size have distant sources while larger particles have local (MIZ) sources. These results show that the adjacent MIZ ocean and ice regions have much different aerosol production properties for aerosol with sizes larger than 1 mm.

Figure 5

Aerosol size distribution before (upper curve), during and after (middle and lower curves) passage of a cold front. The solid line depicts the global background aerosol size distribution of Jaenicke (1979), (from Borrmann et al., *1987).*

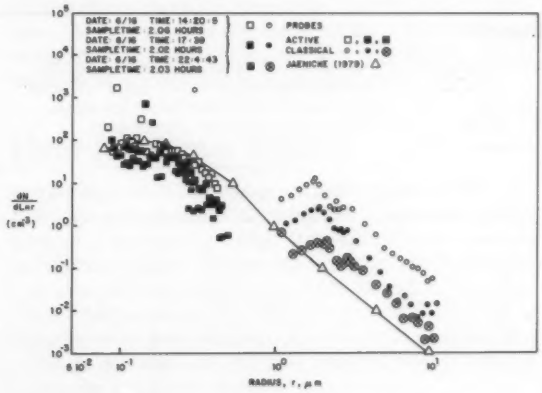

Mesoscale Results:

The mesoscale includes features which exist within 200 km horizontal distances but larger than 1 km. They need to be described using all four dimensions. MIZ mesoscale features are now being examined on the basis of coordinated analyses of combined data bases by MIZEX meteorology investigators. Because these features exist at spatial scales less than the standard synoptic observing network and for periods of hours versus days, our best description will result only from analyses of combined ship, satellite and aircraft data. These analyses will yield mesoscale information on both thermodynamic and dynamic properties of the atmosphere.

Variations in surface temperature between the relatively warm Atlantic water and the cool ice and mixed ice-polar water regions cause spatial variations in the ABL which have been reported by Fairall and Markson (1986)[16] on the basis of aircraft measurements in MIZEX-83. Their measurements were made in conjunction with NPS studies (Fairall was a member of the NPS ABL group during MIZEX-83). The MIZ effects on temperature and humidity are illustrated in Figure 6, which shows profiles of virtual potential temperature and specific humidity for three wind directions relative to the ice edge. When winds were parallel to the ice edge (Figure 6a), distinct mixed layers extending up to 500 meters were observed over both ocean and ice surfaces. The 6 C temperature difference between the two profiles could yield a 5 ms^{-1} wind difference at the top of the layer due to baroclinic (thermal wind) effects. When winds were slightly on ice (Figure 6b), there was a large difference (350 meters) in the inversion height with the lower ABL over the ice. This yields a baroclinic (thermal) wind component of 7 ms^{-1} due to the sloping inversion. When the winds are directly on-ice (Figure 5c), the profiles look almost identical in the upper part of the ABL but are quite different in the lower layer. Cooling when the air moved over the ice caused the lower layer to be stable which greatly reduced the coupling between the upper part of the ABL and underlying ice surface.

Thermodynamic variations across the MIZ are now being examined with the more extensive MIZEX-84 data set. Results from MIZEX-84 are illustrated by Figure 7 which has percentages of occurrences of inversion heights obtained from a ship in the ice (*Polarstern*) and from a ship in the adjacent water (*Valdivia*). These results were obtained by investigators from the Alfred Wegener Institute for Polar and Marine Research, Bremerhaven, FRG and they will be part of the combined data set examined by NPS investigators. The most important feature of these results, which agrees with the examples of Fairall and Markson (1987),[16] is the distinct lower inversion levels

Figure 6

Virtual potential temperature, θ_v (solid line) and specific humidity (dashed line) versus altitude over water (1) and over ice (2) for cases of winds (a) parallel to ice edge, (b) slightly on ice and (c) on ice (from Fairall and Markson 1987).

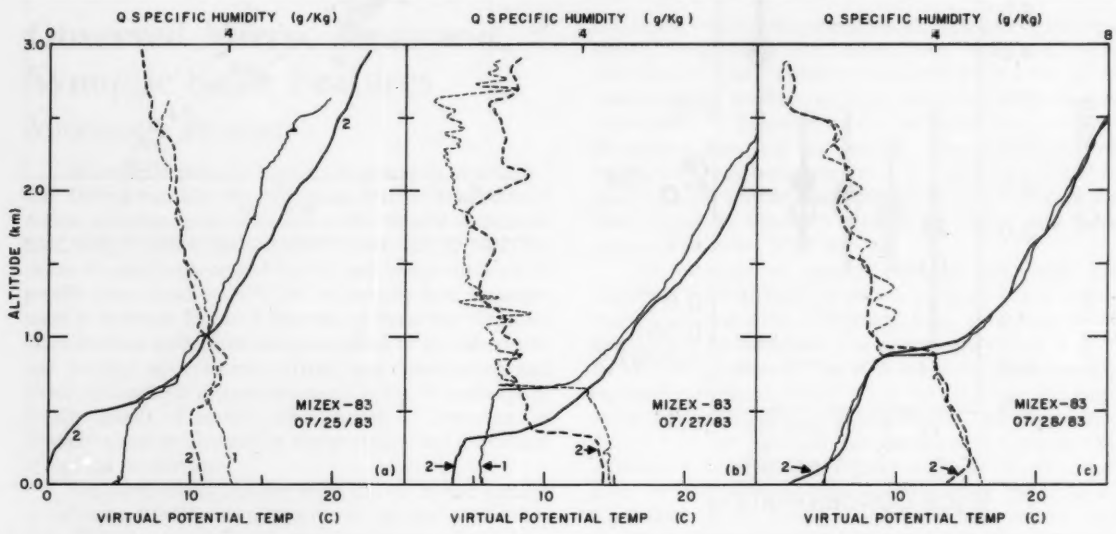

occurring over the ice (*Polarstern*) than those occurring over the water (*Valdivia*).

Another common MIZ mesoscale feature which NPS investigators have studied is fog. The onset of foggy conditions is of two types, frontal and stratus-lowering. Stratus-lowering fog occurs during sea to ice winds when an already present stratus-deck lowers to the surface. This type of fog can be predicted on the basis of general synoptic conditions, i.e., when winds become on-ice. Frontal fog occurs when the wind is generally parallel to the ice edge. This type occurs when a mass of fog with a distinct edge reaches the observer. These fronts are confined to the ABL and must be associated with mesoscale processes, although the exact nature of these processes is not known.

Figure 7

*Histogram of the inversion base over the ice (*Polarstern, *96 observations) and over the open water (*Valdivia, *86 observations).*

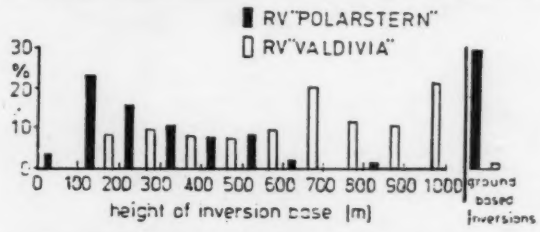

Synoptic Scale Results:

Phenomena which can be identified using standard weather maps with resolutions of > 200 km are termed "synoptic". No standard weather observations are reported in the East Greenland Sea MIZ, but there are stations on Greenland, Svalbard, Bear Island and Jan Mayen Island (Figure 2). During MIZEX-84, five ships measured meteorological parameters within the MIZ. This network of standard meteorological stations and ship observations, along with satellite imagery, were used to make the most complete synoptic description of the summertime East Greenland Sea MIZ ever obtained (Lindsay, *et al.*, 1986).[11]

During the summer, this region is characterized by relatively mild meteorological conditions. The surface air temperature in the ice regions of the MIZ almost always remained within 5°C of freezing. Relative humidity was usually greater than 80% and fog was present 40% of the time. The wind speeds and directions, from the *Haakon Mosby* (Figure 8) and other ships, show several events of high wind speeds (> 10 ms^{-1}), all of which have been associated with synoptic or large mesoscale events (Lindsay *et al.*, 1986).[11] Surface maps for some of the days in the time series are shown in Figure 8. The high wind events are due to occluded mid-latitude cyclonic storms moving into the area from the south and east, the tightening of pressure gradients due to highs and lows adjacent to the MIZ, and the formation of weak storms in the MIZ. These events never produced wind speeds in excess of 20 ms^{-1}. There was no prevalent wind direction because the cyclonic storms passed on both sides of the *Haakon Mosby* (Figure 8) and the other ships. The circumpolar vortex, which is associated with most mid-latitude storms and moves to the north in the summer, was still located well to the south and did not influence the MIZ. The baroclinicity (horizontal temperature gradient) of the MIZ or the location of the MIZ to the lee of the large Greenland land mass may have created five small (large mesoscale, 100–200 km) systems, which formed within the MIZ and dissipated within a day or two, during MIZEX-84.

When the wind speed was greater than 7 ms^{-1}, it dominated the movement of ice. However, the location of the ice edge was generally not related to wind forcing. Apparently, the melting of ice when it was pushed over warm Atlantic water was so rapid that the ocean temperatures, rather than the wind forcing, controlled the location of the ice edge. The wind forcing was the mechanism which controlled ice concentration in the MIZ ice region. When wind forced the ice toward the open ocean, concentrations decreased, while the ice became compacted during sea to ice forcing. The ice movement was to the right of the surface wind forcing by approximately 45 degrees, in agreement with traditional Ekman-layer concepts and observations. A more detailed discussion of the relation between synoptic scale wind forcing and ice morphology during MIZEX-84 is provided by Campbell *et al.*, (1987).[17]

Plans for Winter MIZEX

Objectives of the planned winter MIZEXs (1987 and 1989) are to understand the processes responsible for the advance of the winter ice edge, and their effect on acoustics and electromagnetic remote sensing under much different conditions than in summer (MIZEX 87/89 Science Plan, 1986).[18] Meteorological activity at the winter ice edge is expected to be more intense due to larger temperature and moisture contrasts and the more intense synoptic storms which are present in winter.

Of particular interest in the winter MIZ region is the occurrence of mesoscale cyclogenesis (Arctic lows) which has been the focus of recent studies (Rassmusen, 1985[19] and Wilhelmsen, 1985[20]). Arctic lows are intense systems which form rapidly and may have winds exceeding 30 ms^{-1} within a few hours of initial development. A climatology of Arctic low tracks formulated by Wilhelmsen (1985)[20] clearly shows their frequent occurrence and some evidence of generation in the MIZ. In general, generation and maintenance processes for Arctic lows are not well understood (Kellogg and Twitchell, 1986).[21] However, it is believed that they gain a significant portion of their energy from surface fluxes. The surface flux contribution to these mesoscale systems is believed to be more crucial

Figure 8

(Below) Time series of wind speed (line) and direction (barbs) observed over water on Haakon Mosby *and (above) surface pressure patterns for selected days.*

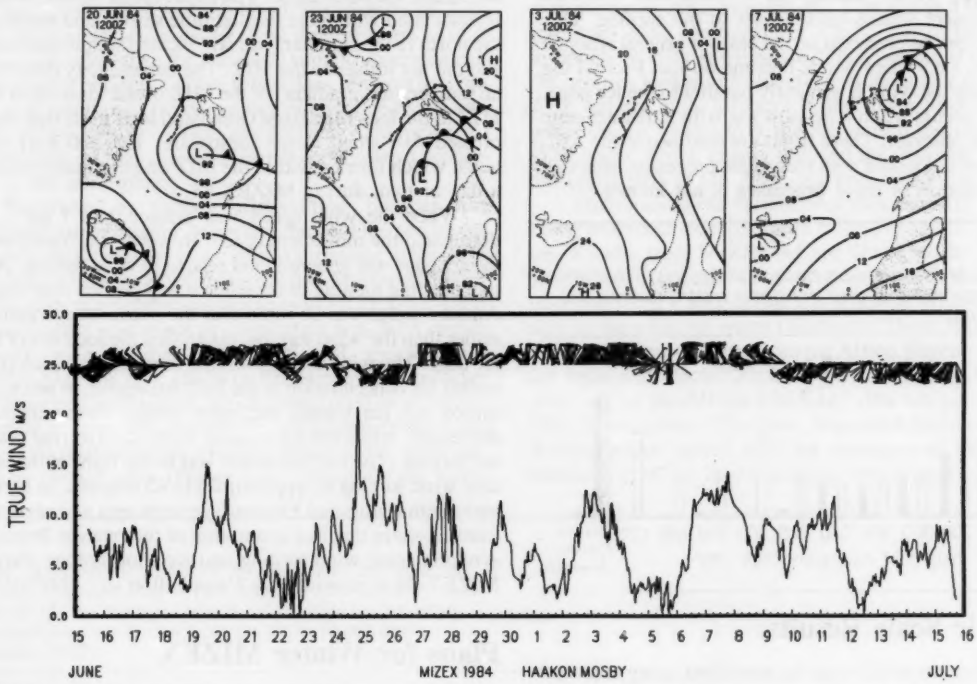

To their formation and structure than lower latitude systems.

The approach used to study the MIZ during MIZEX-87 and 89 will be similar to the summer experiments, diagramed in Figure 1. Features observed are given considerable emphasis in the plans. The features include the surface fluxes and vertical profiles over adjacent ice and ocean regions. The type of results illustrated in section 3 will be sought. Limitations will exist because the number of ships will be reduced from the six in MIZEX-84. Only three ships, one inside and two outside the ice, will be involved in 1987. The in-ice ship will have capability of both ice floe and shipboard measurements. No meteorological aircraft are planned for 1987 but two are likely (Falcon-20 and NOAA-P3) for 1989. In 1989, as an addition to previous efforts, will be possible the deployment of up to 15 buoy-mounted meteorological systems and an ice camp with meteorological equipment. Measurements planned for ships, aircraft, buoy and ice camp have been described in the MIZEX 87/89 Science Plan.[18]

Acknowledgments

The Naval Postgraduate School participation in MIZEX was funded by the Naval Air Systems Command Arctic Program now within the ONR Applied Research and Technology Program, the ONR Arctic programs and the Naval Ocean Systems Center, EOMET program.

References

1. Bourke, R.H. and R.G. Paquette, "Studies of the Marginal Ice Zone along the East Greenland Coast," Naval Research Reviews, (1987), pp. Y1-Y2.

2. Overland, J.E., R.M. Reynolds, and C.H. Pease, "A model of the atmospheric boundary layer over the Marginal Ice Zone," *Journal of Geophysical Research, 88* (1983), pp. 2836-2840.

3. Macklin, S.A., "Wind drag coefficient over first-year ice on the Bering Sea," *Journal of Geophysical Research, 88* (1983), pp. 2845-2852.

4. Pease, C.H., S.A. Salo and J.E. Overland, "Drag measurements for first-year sea ice over a shallow sea," *Journal of Geophysical Research, 88* (1983), pp. 2853-2826.

5. Walter, B.A., J.E. Overland and R.O. Gilmer, "Air-ice drag coefficients for first-year sea ice derived from aircraft measurements," *Journal of Geophysical Research, 89* (1984), pp. 3550-3560.

6. Davidson, K.L., T.M. Houlihan, C.W. Fairall, and G.E. Schacher, "Observation of the temperature structure function parameter, C_T^2, over the ocean," *Boundary-Layer. Meteorology, 15* (1978), pp. 507-523.

7. Davidson, K.L., C.W. Fairall, P.J. Boyle and G.E. Schacher, "Verification of an atmospheric mixed-layer model for a coastal region," *Journal of Climate and Applied Meteorology, 23* (1984), pp. 617-636.

8. Fairall, C.W., K.L. Davidson and G.E. Schacher, "Applications of a mixed-layer model to aerosols in the marine boundary layer," *Tellus, 36 B* (1984), pp. 203-211.

9. Schacher, G.E., K.L. Davidson, T. Houlihan, and C.W. Fairall, "Measurements of the rate of dissipation of turbulent kinetic energy, ϵ, over the ocean," *Boundary Layer Meteorology, 20* (1981), pp. 321-330.

10. Boyle, P.J., K.L. Davidson and D.E. Spiel, "Characteristics of over-water surface stress during STREX," *Dynamics of Atmospheres and Oceans,*[10] 1987, pp. 343-358.

11. Lindsay, R.W., K.L. Davidson, M. Gube-Lenhardt, P.S. Guest, R. Picard and C. Wamser, "Synoptic weather events of MIZEX-84," *Journal of Geophysical Research,* 1986 (submitted).

12. Guest, P.S., and K.L. Davidson, "The effect of observed ice conditions on the drag coefficient in the Summer East Greenland Sea," *Journal of Geophysical Research,* 1987, (in press).

13. Anderson, R.J., "Wind stress measurements over rough ice during MIZEX-84," *Journal of Geophysical Research,* 1987, (in press).

14. Overland, J.E., "Atmospheric boundary layer structure and drag coefficients over sea ice," *Journal of Geophysical Research, 90* (1985), pp. 9029-9049.

15. Borrmann, S.H., K.L. Davidson and M.E. Miller, "Surface measurements of aerosol size distributions in the Marginal Ice Zone during MIZEX-83," *Journal of Geophysical Research,* 1987, (in press).

16. Fairall, C.W. and R. Markson, "Mesoscale variations in surface stress, heat fluxes and drag coefficients in the Marginal Ice Zone during MIZEX-83," *Journal of Geophysical Research,* 1987, (in press).

17. Campbell, W.J., P. Gloersen, E.G. Josberger, O.M. Johannessen, P.S. Guest, N. Mognard, R. Schuchman, B.A. Burns, N. Lannelongue and K.L. Davidson, "Mesoscale and large-scale sea ice morphology in MIZEX-84," *Journal of Geophysical Research,* 1987, (in press).

18. MIZEX Bulletin, Winter MIZEX-87/89 Science Plan, MIZEX Bulletin VIII, CRREL Special Report 86-9, April 1986.

19. Rasmussen, E., "A case study of a polar low development over the Barents Sea," *Tellus, 37A* (1985), pp. 407-418.

20. Wilhelmsen, K., "Climatological study of gale-producing polar lows near Norway," *Tellus, 37A,* (1985), pp. 451-459.

21. Kellogg, W.W. and P.F. Twitchell, "Summary of the workshop on Arctic Lows 9-10 May 1985, Boulder, Colorado," *Bulletin of the American Meteorological Society, 67,* (1986), pp. 186-193.

Biographies

Dr. Kenneth L. Davidson is professor of meteorology at the Naval Postgraduate School. His research since 1966 has been on the structure of the Atmospheric Boundary Layer over water and ice. His primary interests have been on air-sea and air-ice interaction and boundary properties which affect electromagnetic and optical wave propagation. He is a member of the science group for the Marginal Ice Zone Experiment (MIZEX) in the East Greenland Sea and coordinates the meteorology investigation.

Peter S. Guest is a research meteorologist and is pursuing a Ph.D. in meteorology at the Naval Postgraduate School. He has collected and analyzed meteorological data for the MIZEX 83, 84. His research has concentrated on surface exchange processes and boundary layer structure in marginal ice zones.

Towards the Efficient Solution of an ASW Search Problem

By James N. Eagle
Department of Operations Research

Introduction

The problem addressed here was motivated by search problems encountered by antisubmarine warfare (ASW) forces. In particular, we postulate that a target submarine has been detected by a long-range sensor. After the detection, the target's location is not known precisely but is given as a probability distribution over some, possibly large, area of ocean. A mobile ASW platform with a specified maximum speed is then required to close the submarine for attack or surveillance. The searcher is provided with the initial target distribution and statistical information on historical target tracks. The searcher's problem is to select a track which will maximize the probability of detect ing the target by some specified future time.

This problem is made difficult by the target and searcher motions allowed. Evasive target motion causes old detection information to "age" and become less useful for search. It also allows the target the opportunity to escape to regions where search is less effective or perhaps impossible. Limiting the searcher's speed places constraints on the search tracks allowed. The searcher cannot transit immediately to the best position to begin the search. Instead, it is necessary to anticipate future target motion (i.e., "lead the target") and block possible avenues of escape.

The initial work on the moving target search problem did not consider constraints on the search path. Typically it was assumed that the searcher could distribute search effort over the entire search region, no matter how large, during a finite time interval. This was essentially an assumption of an infinite search speed. If the searcher is an aircraft and the target is a submarine, then such an assumption of infinitely divisible effort is probably not that unreasonable. If, however, the searcher is an ASW ship or another submarine, the modelling constraints on the search path become more important.

Efficient solution procedures have been found for the infinitely divisible effort problem. Professor Alan Washburn of the Naval Postgraduate school (NPS) has provided such algorithms.[1,2] Necessary and sufficient conditions for search plans maximizing the probability of detection were given by Brown, who also introduced an efficient solution procedure.[3] This moving target search problem is considered well solved.

It was noted by Washburn that when the assumption of an infinite divisibility of search effort is not allowed (that is, search effort must be allocated in discrete units), algorithms which previously gave optimal solutions can converge to suboptimal search paths. If, in addition, path constraints are added (that is, a searcher in one region has immediate access to only some set of adjacent regions), then the problem becomes more complex still.

Trummel and Weisinger have shown that, even for a stationary target, the discrete effort, constrained search-path problem is at least as difficult as finding a path through a network which visits each node once before visiting any node twice[4] (Figure 1.). It is known that finding such a *Hamiltonian path* is a difficult problem to solve efficiently. It is a member of a class of problems, called NP-complete, which have proven difficult computationally.[5] It is not surprising, therefore, that efficient solution procedures for the constrained search path problem have been slow to develop.

Figure 1

A Hamiltonian Path.

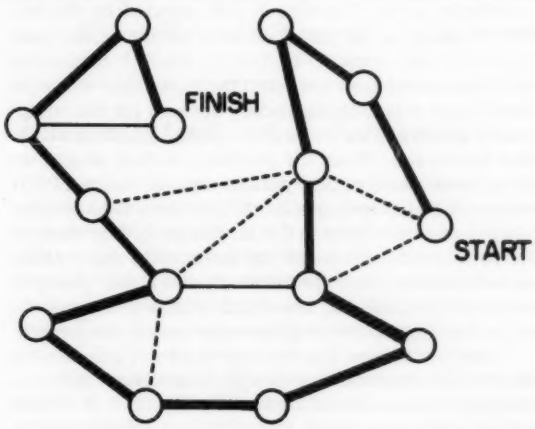

In this paper, three solution methods are described which were developed at the Naval Postgraduate School (NPS). These procedures represent a step towards efficient solution of the constrained search path problem. The initial work on this problem was done by Stewart, who introduced an approximate solution technique in 1979.[6,7] The effectiveness of Stewart's algorithm compared to those presented here has yet to be determined.

To model this problem conveniently, it is made discrete in both space and time. Specifically, the search area is divided into a set of N cells among which the searcher and target must move. And these moves must occur at regularly spaced, discrete points in time. We will use the following notation:

C = the set of all cells = $\{1,2,\ldots, N\}$,
C_j = the set of cells accessible in the next time period when the searcher is currently in cell j,
q_j = the probability of target detection when the target is in cell j and a search is conducted in cell j,
p_{ij} = the probability of the target moving in 1 time period from cell i to cell j,
P = a square matrix with elements p_{ij} (i.e., the target transition matrix),
s_t = the cell searched at time t,
$s = (s_1, s_2, \ldots, s_k)$ = a search path,
π_j = the probability that the target is in cell j,
$\pi = (\pi_1, \ldots, \pi_n)$ = target probability distribution over C.

Given an initial target distribution π and a specified time horizon T, the searcher's problem is to find that T-time period search path maximizing the probability of detecting the target.

Formulation as a Dynamic Program

The search problem can be formulated and solved optimally as a dynamic program. The essence of this procedure is expressing an optimal solution when t searches remain in terms of the solution when $t - 1$ searches remain. Then, in principle at least, the optimal solution for any planning horizon can be determined recursively from the optimal solution when only 1 search remains.

With any t-time period search path, s, there is an associated vector $a = (a_1, \ldots, a_N)$ where a_i is the probability of detecting the target given that the target starts in cell i and search path s is followed. If the target's starting cell is not known precisely but is given as a probability distribution π, the probability of detection when s is used is the dot product πa.

Now assume the searcher is in cell i at time $(T - t)$. (That is, t searches remain in the problem.) Furthermore, let A(t,i) be the set of a-vectors associated with all possible t-time period search paths s beginning at time $(T - t)$. Then give a target distribution at time $(T - t)$ of π, the maximum obtainable t-time period probability of detection is

$$\max_{a \in A(t,i)} \pi a. \qquad (1)$$

And the optimal t-time period search path is that s associated with the maximizing vector a.

Solving this problem for any planning horizon requires that we find the optimal solution when $(t + 1)$ time periods remain in terms of the solution when t-time periods remain. That is, we must construct the vector sets $\{A(t + 1,1), A(t + 1,2), \ldots, A(t + 1,N)\}$ from the vector sets $\{A(t,1), A(t,2), \ldots, A(t,N)\}$. Also, each vector in $A(t + 1,i)$ must have associated with it a $(t + 1)$-time period search path.

To illustrate this construction, let b be any element of A(t,j) and s be the t-time period search path associated with b. Now the a-vector associated with the (t + 1)-time period search path (j,s) is

$$a = e_j q_j + P_j b,$$

where e_j is an N-vector of 0's except for a 1 in the j^{th} place, and P_j is the target transition matrix P with row j multiplied by $(1 - q_j)$. (To demonstrate this formally, the components of a and b are interpreted as probabilities of detection when t + 1 and t searches, respectively, remain in the problem.) The entire set A(t + 1,i) is then all N-vectors, a, such that

$$a = e_j q_j + P_j b, \qquad (2)$$

where j is in C_i, and b is in A(t,j).

The dynamic programming recursion begins by setting A(1,i) to be the set of N-vectors, a, such that

$$a = q_j e_j,$$

where j is in C_i. The 1-time period search path associated with this vector is simply cell j. Continued application of Equation (2) allows the recursive construction of the vector sets A(t,i) with a t-time period search path associated with each vector.

The set A(t,i) constructed in this manner may contain some vectors which will never maximize (1) for any target distribution π. The s associated with each of these "dominated" vectors can not be an optimal t-time period search path. It can be shown that the vectors b which are dominated by the remaining vectors in A(t,i) are exactly those b which can be expressed as a convex combination of the remaining vectors. To keep the size of the vector sets A(t,i) from growing too rapidly as the procedure moves backward in time from time T − 1 to time 1, the dominated vectors are removed from A(t,i) and not used in the construction of A(t + 1,j).

Testing a vector for dominance can be accomplished by solving a mathematical optimization problem called a linear program, but simpler methods can be devised. Removing a from A(t,i) whenever there exists, a vector b in A(t,i) such that $b_i \geq a_i$ for each component i will eliminate some of the dominated vectors. This is much easier to implement that the linear programming procedure, but does not reduce A(t,i) to its minimal size. This results in more computer storage being required to save A(t,i) in each stage of the dynamic program.

Moving Horizon Policies

Computational experience with this problem has shown that available computer storage for the vector sets A(t,i) generally limits the maximum number of time periods for which the problem can be solved. A modification to the dynamic programming procedure which reduces these computer storage requirements is to use *moving horizon policies.* However, the procedure is no longer guaranteed to be optimal, and must be classified as a heuristic.

To determine the m-time period moving horizon (m-TPMH) policy, the vector sets A(m,i), i = 1,..., N, with associated optimal m-time period search paths, s, are first generated. Now assume that t > m time periods remain in the problem, the searcher is in cell i, and the target distribution is π. The search cell selected by the m-TPMH policy is the initial element of that search path associated with vector b in A(m,i), where b maximizes πb. If that search does not detect the target, then the target distribution π is probabilistically updated for the unsuccessful search and the process is repeated to determine the next search cell. When the problem solution progresses to the point where m time periods remain, the m-TPMH policy selects the optimal s for the remaining time periods.

For any time horizon t ≥ m, this procedure chooses the next search cell under the assumption that m time periods remain in the problem. If m = 1, this policy is *myopic.* That is the next search cell is chosen to maximize the probability of detecting the target on the next search.

One would hope that as m approaches T, the moving horizon policies would always perform better. However, examples can be constructed where the (m + 1)-TPMH policy performs worse than the m-TPMH policy. Nonetheless, this heuristic appears to give reasonable results, and because the number of a-vectors that must be stored does not increase with increases in the planning horizon, problems with longer planning horizons can be attempted.

Various small search problems have been solved at NPS with the optimal dynamic programming method and the moving horizon modification.[8,9] A 9-cell, 10-time period problem required 19.3 CPU minutes and 2 Mbytes of storage on an IBM 3033 mainframe computer to solve optimally by dynamic programming. Then using this optimal solution, the 10-TPMH policy extended the time horizon to 40 time periods in an additional 2 CPU seconds.

Figure 2

Searcher's Path through a Network.

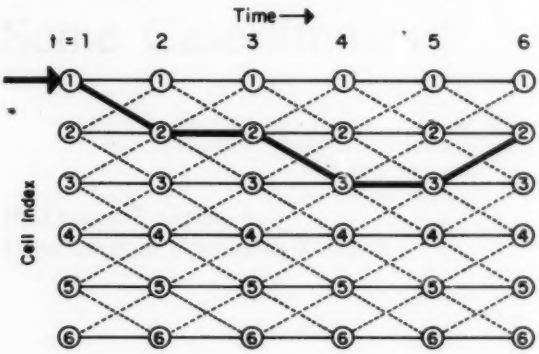

Formulation as a Network

Another way to consider this problem is to view the searcher's track as a path through a rectangular network consisting of T columns, each of which contains N nodes (Figure 2). The idea for this formulation is due to Stewart.[6] Each cell in column t is connected with an arc to the accessible cells in column t + 1. The searcher moves along T − 1 feasible arcs from the starting cell, s_1, in column 1 to some destination cell, s_T, in column T.

The target also moves through the network from column 1 to column T. The target's initial location is given by the probability distribution π over the cells in column 1 and it moves to a cell in column 2 according to the Markov transition matrix P. Since the target and searcher may be operating at different speeds, the cells accessible in a single time period from a specified cell may differ for the two platforms.

Given the transition matrix P, an initial target distribution π, and a search path $s = (s_1, \ldots, s_T)$, the probability of detecting the target during T searches is

$$PD(\pi,s) = 1 - \pi \left(\prod_{i=1}^{T} P_{s_i} \right) 1, \qquad (3)$$

where 1 is a N-vector of ones and, as before, P_j, is P with row j multiplied by $(1 - q_j)$. The searcher attempts to find that feasible search path s maximizing Equation 3.

To present an algorithm for this problem, we must first define a search plan, S, as an Nx(T − 1) matrix of cell numbers where elements S_{it} is the cell searched at time t + 1 when cell i was searched at time t. Given a starting cell s_1 and a search plan S, the entire search path, s, and thus PD(s) can be determined. The algorithm is as follows:

1. Specify an initial target distribution π and transition matrix P.
2. Select an initial search plan S and a starting cell s_1.
3. From S and s_1, determine the initial search path $s = (s_1, \ldots, s_T)$ and, from (3), the resulting PD(s).
4. Set $PD_{MAX} = PD(s)$.
5. For t = 2 to T:
   a. Vary s_t over all values s_t' in $C_{s_{t-1}}$.
   b. For each s_t' determine the new S′ and s′, and PD(s′).
   c. If $PD(s') > PD_{MAX}$, save S′, s′, and set PD_{MAX} to PD(s′).
   d. Continue to next value of t.
6. If no increase in PD_{MAX} is obtained when t = T, then STOP.
7. Otherwise set S to S′, s to s′ and return to 5.

This algorithm attempts to move from a search plan S to an improved plan S′. S′ will differ from S by only 1 element. The new search path s′ will be identical to s up to some time k, but can differ from s from time k + 1 to time T.

This algorithm converges to a local optimum which may or may not be a global optimum. Like the moving horizon procedure, it can be applied to relatively large problems but provides only a lower bound to the optimal PD. This procedure has been applied to several 25-cell, 10-time period problems and, in each case, required less than 2 CPU seconds to find a solution.[10] The test problems were small enough to solve optimally, and in most cases the network solution was optimal. There were exceptions however. Some starting search plans resulted in particularly poor final solutions. More testing is needed before general conclusions can be reached as to this method's effectiveness.

Conclusion

There has yet to be developed a solution procedure for the constrained search problem which appears efficient enough to deter further investigation. The methods presented here are steps in the proper direction, but there is more to accomplish. Relatively small example problems have been solved, but these methods have not been tested on large search problems. This work is continuing.

References

1. WASHBURN, A.R., "Search for a Moving Target: The FAB Algorithm," *Operations Research*, **31,** 1983, pp. 739-751.

2. WASHBURN, A.R., "On Search for a Moving Target," *Naval Research Logistics Quarterly*, **27,** 1980, pp. 315-322.

3. BROWN, S.S., "Search for a Moving Target in Discrete Time and Space," *Operations Research*, **28,** 1980, pp. 1275-1289.

4. TRUMMEL, K.E. and WEISINGER, J.R., "The Complexity of the Optimal Searcher Path Problem," forthcoming in *Operations Research*.

5. GAREY, M., JOHNSON, D., *"Computers and Intractability: A Guide to the Theory of NP-Completeness,"* W.H. Freeman and Co., 1979.

6. STEWART, T.J., "Search for a Moving Target When Searcher Motion is Restricted," *Computers and Operations Research*, 1979, **6,** pp. 129-140.

7. STEWART, T.J., "Experience with a Branch-and-Bound Algorithm for Constrained Searcher Motion," in *Search Theory and Applications*, K.B. Haley and L.D. Stone (eds.). Plenum Press, New York, 1980.

8. EAGLE, J.N., "The Optimal Search for a Moving Target When the Search Path is Constrained," *Operations Research*, **32,** 1984, pp. 1107-1115.

9. EAGLE, J.N., "The Approximate Solution of a Simple Constrained Search Path Moving Target Problem Using Moving Horizon Policies," *Naval Postgraduate School Technical Report NPS55-84-009.*, 1984.

10. EAGLE, J.N., YEE, J., "An Approximate Solution Technique for the Constrained Search Path Moving Target Search Problem," *Naval Postgraduate School Technical Report NPS55-85-015*, 1985.

Biography

Dr. James N. Eagle attended the U.S. Naval Academy, graduating with distinction in 1969. After qualifying in submarines, he attended Stanford University as a Burke Scholar, receiving his M.S. and Ph.D. in the Department of Engineering-Economic Systems. After completing his active naval duty in 1982, he joined the faculty of the Naval Postgraduate School, where he teaches in the Department of Operations Research. His research interests include military applications of operations research, especially search theory and tactics development.

NAVAL TACTICAL DECISIONS UNDER UNCERTAINTY:

Some Case Studies

By Donald P. Gaver, Jr.
Department of Operations Research

Introduction

Many important military (and civilian) decisions are made in an environment of substantial uncertainty. In important cases, the uncertainty derives from lack of knowledge of an adversary's options, skills, and aptitude for creative response to novel challenges. Success in this area is best understood from the scientific perspective of cognitive and behavioral psychology; success is believed to depend upon individual flair, experience and the development of judgment and common sense.

Uncertainty of a somewhat different type arises when the aftermath of a decision is attributable to a variety of natural causes that conspire to produce a kind of statistical stability. Examples are seen in the diverse outcomes of certain gambling games, human life (and disease) durations, the dispersion of shots on a pistol target, the miss distances of missiles around an aim point, the errors made in identifying the location of a target platform by direction-finding systems, the lengths of periods of reliable operation displayed by important pieces of equipment, the nature of noise in electric circuits, the error-freedom of pieces of software and even the behavior of weather; examples are many and often of considerable practical importance and scientific interest.

The *calculus of probability* is a powerful tool for dealing with situations such as the above. If one can treat the phenomena in question as random phenomena, subject to the laws of probability theory, then the consequences of candidate decisions can be evaluated, and the apparent best candidate chosen. Modern *statistical theory* contributes to the above process by providing procedures for examining data so as to assist in the formation of the relevant probability model. The implications of the model are then checked for validity, after which it may be incorporated into a decision-aiding tool. It is currently being forcefully argued that subjective assessments made by experts deserve to be incorporated into the decision process, and that this may be done formally and quantitatively, perhaps with the aid of Bayes' formula. Of course the requirements for careful validation of data models, and expert inputs, are still present.

The ideas briefly sketched above are not at all new, but have been recently evolving in a rapid and heterogeneous way. We wish to describe their use in several specifically Navy-related contexts. It will further be argued that the results that flow from research in the areas of probability and stochastic process theory, and statistical theory and data analysis, including statistical computing, will continue to improve understanding of the environment of Navy planning and decision making, and will thus tend to enhance decision quality.

Military Tactical Applications

The study of certain elements of Naval activities using probabilistic and statistical tools gathered momentum during World War II, when scientists were asked to analyze specific operations (e.g. antisubmarine warfare) and make recommendations for improvements. As a consequence, P.M.S. Blackett in Britain, and P. Morse, G. Kimball, B.O. Koopman and others in the U.S. founded the field of operations research. The output of operations-research studies can ideally furnish needed information to decision makers, and we outline below several recent studies that have been carried out by students and faculty in the Operations Research Department of the Naval Postgraduate School.

Example 1: Cruise Missile Activation

Imagine that a cruise missile is to be fired at a high-value target (hvt), e.g. a carrier in the midst of a task force. The hvt is surrounded by a number of support vessels or low-value targets (lvt); these are ideally arranged in a systematic manner, but in fact are in motion changing stations, etc., and so tend to be scattered somewhat randomly around the hvt. As the missile approaches the hvt its seeker must be activated by a certain range in order to home in on the hvt. One sees that if the seeker is activated too soon, it will likely encounter a lvt before reaching the hvt, attack the lvt, and hence be wasted. On the other hand, if the seeker is activated too late, it remains blind to the lvt but may also pass over the hvt, and again be wasted. It is crucial that the decision as to where to activate the seeker take into account the uncertainty in the actual location of the hvt. If the hvt were actually located perfectly the missile seeker activation could take place just short of the hvt location, with perfect results. Analysis of data on location accuracy reveals the nature of the dispersion between true location and estimated hvt location, and this dispersion can be quantified in terms of probability distributions. These can then be incorporated into a model that also contains the estimated density of the possibly distracting lvt swarm, and the resulting model explored to yield, for example, the optimal activation range approximately maximizing missile hit probability. The model can also be used to explore the sensitivity of the optimal activation range to important operational parameters. These analyses are reported in reference 2.

Example 2: Torpedo-Setpoint Determination

A problem conceptually similar to the first example arises when a torpedo-firing operation by a submarine against an opponent submarine is to be conducted. The attacking submarine commander who has gained contact with his opponent estimates the latter's target range, course, speed, and type, largely using passive methods. Because of this, the target is not alerted and maneuvering. When the attacker prepares to fire a torpedo, he must preset the point in space (ocean) with respect to the target at which a fired torpedo becomes acoustically active (may search), and changes to a search mode. Such a point is called the *enabling run offset* (ERO) and must be a compromise chosen with these conflicting issues in mind: the ERO may be too short (indeed negative) if an inaccurate range estimate places the target much further away than it really is, in which case the torpedo "flies by" its target in an oblivious state; if ERO is too long, then the target is alerted early by the torpedo sound and may take action to successfully evade until torpedo fuel is exhausted. Again a compromise quantity must be sought that accounts for target range, course, and speed determine *and* for the evasive tactics followed by a target that suddenly knows an attack is launched. A study of this problem together with an algorithm that provides the attacker with guidance for setting the ERO, is reported in reference 2.

Combat Logistics

Adequate materiel readiness is essential in order that military, or specifically naval, operations be successfully pursued. Inevitably, some essential system modules such as aircraft engines, avionics, and computers, computer software, and command-and-control linkages will fail unpredictably or "at random" during or before a crucial operation. Adequate properly located replacements, spare parts and repair facilities are needed to insure combat capability. Of course combat itself has dynamic elements with chance components. Thus it is desirable to develop analytical planning tools that assist decision-makers with the task of combining logistics factors and combat requirements so as to achieve (nearly) optimum combat capability under resource constraints. To reach such a goal it is useful to consider a combined *combat logistics model.* We discuss a simplified version of such a model, with emphasis on contributions from stochastic process and statistical theory.

Example 3: Defense of a High-Value Point Against a Surge Attack

Suppose a geographically concentrated point such as a Navy carrier is to be initially defended against air attack by a simultaneously-arriving "surge" of B missiles or bombers by means of a defending force of D aircraft. If the incoming attack is initially detected at a flying time t_a from its target (a weapon release perimeter) then actual combat between the available defenders, D(O) in numbers, where $D(O) \leq D$, may begin at engagement time $t_e < t_a$. The interesting outcome of the combat is

measured by a *leakage* figure: perhaps either the mean number of bombers surviving to the bomb-release line, $E[B(t_r)]$, *or* the probability, $P_b(t_r)$, that b or more bombers (e.g. b = 1) survive. Now suitable combat models can be formulated that permit calculation of the above quantities, *conditional* upon knowledge of D(O), the number of defenders available at attack time. Such models require as additional inputs weapon characteristics, attack and defense platform vulnerabilities, and the command-and-control capacities of each force. Other factors remaining equal, however, possession of an appropriately sized and *available* defense capability, D(O), is a distinct advantage. But D(O) is itself a random quantity that depends upon the numbers of platforms, of spare system modules originally allocated for support of the group (squadron) of defenders, and in particular on the number of such modules available within and backing up each of the defensive platforms. In short, availability at attack time depends upon the activity (for training, etc.), and consequent failures, experienced before the attack occurs, and upon the responsiveness of the repair/replacement facilities. The latter responsiveness depends upon the proper numbers and allocation of repair crews and facilities to shops, and upon the degree of versatility (extent of cross training) of the repair personnel. Again, suitable models can be constructed to represent the delays incurred in the repair process. Given hypothetical figures for the number of platforms, spares and personnel, and for the failure and repair-time characteristics of modules, the model permits access to the probability distribution of D(O), the number of defenders available at the moment of a random attack. Using this distribution, it is then possible to "remove the initial condition on D(O)" in the combat model, and thus to relate combat (in)effectiveness directly to the complement size and characteristics of the defenders, and also to the adequacy of the logistic support facilities. The combined combat-logistics model provides a linkage between combat effectiveness and logistics backup for use by decision-makers.

A combat logistics model of exactly the above type is the subject of a dissertation for the degree of Ph.D. in Operations Research at the Naval Postgraduate School, by Major Abdul L.R. Al-Zayani of Bahrain.[3] Although the existing model is at a pilot level, it already demonstrates the value of state-of-the art methods for approximating and computing properties of the complicated multistate-valued stochastic processes that represent the behavior of both combat and logistics aspects of the situation.

Importance of Methodological Research

Modern research results in probability theory and modeling, and in statistical theory and data analysis have considerable application in the development of useful models and decision-aiding techniques of the types described earlier. Such recent innovations as *robust-resistant statistical methodology* are useful for processing data on target identification, location and motion from distinct sources when the latter data are non-Gaussian (for example they may suffer from extreme outliers or maverick observations). The classical linear Gaussian distribution-based methodologies are often quite vulnerable to such "bad data"; their uncritical use may unnecessarily degrade the overall performance of an information-gathering or weapon system. *Robust empirical-Bayes* procedures recognize the variability among the failure rates of individual platforms, thus allowing for more precise and economical sparing policies. *Diffusion approximation* and *large deviation* techniques furnish relatively simple approximations to complex stochastic models for combat, computer and communication and maintenance and repair facilities. New techniques for *Monte Carlo computer simulation*, including graphical techniques for data exploration, also provide insights into system dynamic behavior useful to decision-makers. Statistical methodology applied to remote-sensing data also allows for the nonintrusive elucidation of operational environments near the air-sea interface. The list is extensive.

Finally, it is important to note that the value of the decision-aiding tools fashioned from research findings is enhanced by the cooperative efforts of experienced and educated naval officers. The insight of these officers serves well to nudge the efforts of operational and natural scientists in fruitful directions.

References

1. Becker, Kevin J., LT, USN, "An Analytical High Value Target Acquisition Model," M.S. Thesis, Naval Postgraduate School, March 1986.

2. Peppe, Patrick K., LT, USNR, "Probabilistic Optimization of Mk-48 Torpedo Enabling Run Offset," M.S. Thesis, Naval Postgraduate School, September 1986.

3. Al-Zayani, Abdul-L.R., Bahrain Defense Force," Formulation and Analysis of Some Combat-Logistics Problems", Ph.D. Thesis, Naval Postgraduate School, September 1987.

Biography

Dr. Donald P. Gaver is a Distinguished Professor of Operations Research at the Naval Postgraduate School, where he has been a faculty member since 1970. Previously, he was a Professor at Carnegie-Mellon University and has had visiting posts at Stanford, U.C. Berkeley, and University of Dortmund. He has served as a member of a National Academy of Science panel, and as an Advisor to the National Research Council. He has been an associate editor of the Journal of the American Statistical Association, is a fellow of that Association. Professor Gaver teaches and carries out research in the areas of probability modeling and statistical methodology development and data analysis.

STEAM CONDENSATION:

Putting Surface Tension to Work

By Paul J. Marto
Department of Mechanical Engineering

Introduction

Since 1765, when James Watt conceived the idea of using a separate surface condenser in a steam engine,[1] the condenser has become an important component in steam power systems. Heat rejection in the condenser is vital to a steam power cycle, and condensers are designed to reject heat at the lowest possible vapor temperature (and therefore pressure) so that a high thermo-dynamic efficiency is achieved. In the last century, the surface condenser has evolved considerably as designers have understood more about the complex heat transfer processes which occur when steam flows into a bundle of water-cooled tubes.[2]

Today, considerable interest exists in the Navy to make propulsion systems smaller, lighter and, where feasible, more efficient.[3,4] These higher-power-density systems will require compact surface condensers where enhanced heat transfer occurs on both the inside (i.e., the cooling water side) and on the outside (i.e., the steam side) of the tubes. The benefits of using heat transfer enhancement in naval condensers have been explored recently and reductions in condenser size of as much as 30 percent were shown to be possible.[5]

Since the early 1970s, a great deal of attention has been focused on heat transfer enhancement techniques for use in a variety of heat exchanger applications.[6,7] Most of the work, however, deals with single-phase heat transfer such as turbulent flow of water in a tube, and not as much information is available when change-of-phase occurs, such as in a steam condenser. In this more complex situation, additional research needs to be performed before fruitful solutions will be possible.

When a vapor condenses on a cold surface, the condensate which is formed creates a thermal barrier which reduces heat transfer. For several decades, numerous techniques have been proposed to reduce the thickness of the condensate layer, but as yet, none of these techniques has been successfully put into practice in steam condensers. Because of the very high surface tension of water, however, this property may be utilized effectively to thin the condensate layer on horizontal tubes which can lead to dramatic increases in heat transfer for steam condensers. Since 1980, a research program at the Naval Postgraduate School has been studying how the high surface tension of water can be put to advantage in thinning the condensate film on horizontal tubes. This research has been focused on two entirely separate techniques. In one case, the use of very thin coatings of polymer materials (such as Teflon, which is used in "no stick" frying pans) to alter the *properties* of the tube surface has been investigated, whereas, in the second case, the use of fins or fine wires to alter the *geometry* of the tube surface has been explored.

In Search of Permanent Dropwise Condensation

Although dropwise condensation of steam has been studied for over 50 years, permanent hydrophobic coatings have not as yet been developed to the satisfaction of condenser designers. Recently, both noble metals and organic polymers have been used as permanent hydrophobic coatings,[8] and progress has been made toward understanding the variables which affect the long-term endurance of these coatings when exposed to steam.[9-11]

At the Naval Postgraduate School, a wide variety of polymer materials has been studied for use as coatings on condenser tubes. Fluorinated polymers are known to have surface free energies less than the surface tension of water. The high surface tension of water causes it to roll up into droplets on a polymer-coated surface rather than to form a continuous liquid film, and it is well known that this dropwise mode of condensation can generate heat transfer coefficients more than 10 times those of filmwise condensation. However, the problem in the past has been to find a durable polymer coating which can be applied in an ultra-thin layer to avoid insulating the condenser tube appreciably. (The organic coatings are poor thermal conductors, so the coatings must be applied to a thickness of approximately 1 micron or less.) Therefore, an important part of the research has been to test the long-term steam endurance of various ultra-thin polymer coatings using a specially built endurance apparatus.

More than one dozen polymer coatings were tested and those which showed sustained endurance after thousands of hours of exposure to steam were selected for heat transfer performance evaluation. Figure 1 is a photograph showing the endurance of a fluoroacrylic coating, developed at the Naval Research Laboratory.[12] The substrate material was titanium which is a lightweight, corrosion-resistant metal being proposed for naval condenser tubes. It was roughened with a glass bead spray prior to being coated, in order to improve adherence. In Figure 1(a), after exposure to steam for 700 hours, the appearance of the dropwise condensation is very good (many small, spherically-shaped droplets is a sign of good dropwise conditions). However, when examined after 17,000 hours of operation (Figure 1(b)), the coating shows signs of deterioration with large, flattened drops being evident. Apparently, the very thin (2-3 microns thick) coating absorbs sufficient water with time to reduce its effectiveness as a hydrophobic material. This is not evident with a gold coating which continued to show excellent dropwise behavior after 17,000 hours (Figure 1(c)). Figure 2 gives comparison data for the measured steam-side condensation heat transfer coefficient on a horizontal tube for several of the polymer coatings; comparisons are with an electroplated silver coating and with filmwise condensation data on an uncoated tube. Some of the coatings

Figure 1

Photographs showing the quality of dropwise condensation on coated specimens.

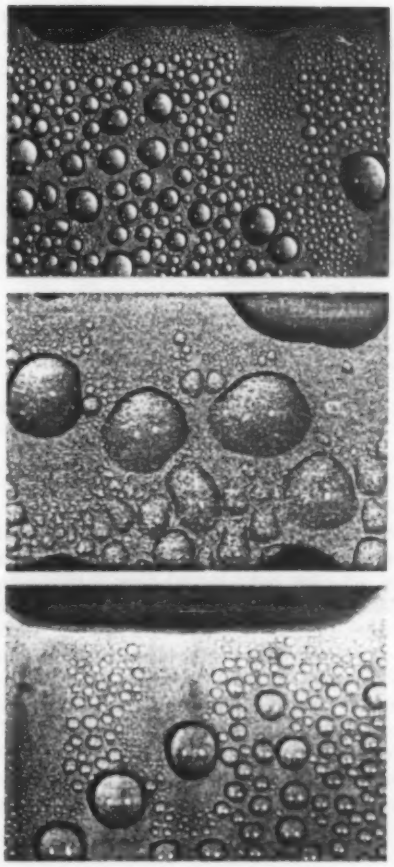

(Emralon-333[a] and No-Stik[b]) showed no improvement over the filmwise case because these coatings were too thick (10-50 microns). However, the Parylene-D[c] and Fluoroacrylic coatings showed enhancements of 3 to 5 times the filmwise data, depending upon coating thickness. The best heat transfer enhancement was with the electroplated silver coating which exhibited an increase of approximately 7 times the uncoated, filmwise tube.

(a) Trade name of a fluorocarbon lubricant developed by Acheson Colloids Company.

(b) Trade name of a thermally conducting plastic coating developed by Plasma Coatings, Inc.

(c) Generic name for members of a thermoplastic polymer series developed by Union Carbide Corporation.

Figure 2

Heat transfer results for dropwise condensation on coated horizontal tubes.

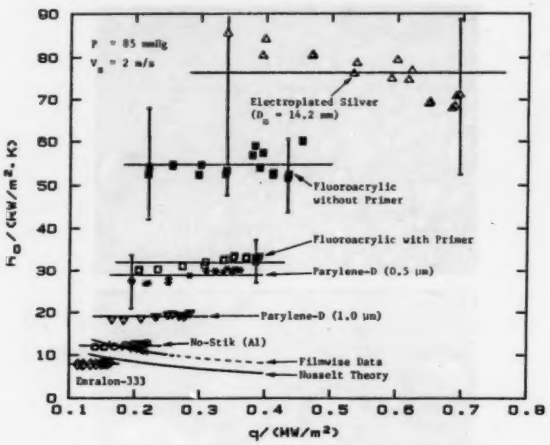

Even with these promising findings, some very important questions remain to be answered. For example, what combination of molecular structure and thickness of an organic coating, and what substrate surface roughness will yield long-term adherence and excellent hydrophobic conditions? Can metal powder dispersions be used within organic coatings to enhance the effective thermal conductivity of the coating? How uniformly can these coatings be applied to long condenser tubes? Can these coatings be applied to installed tubes in an existing condenser? What heat transfer enhancement can be achieved reliably? These questions, as well as questions pertaining to relative cost, must be addressed in order to conclude this seemingly endless search for the "perfect" coating.

Film Condensation on Extended Surfaces

Finned Tubes

The use of extended surfaces to increase the surface area of a heat exchanger is well known,[13] and one of the most common types of extended surfaces in use today is the integral-fin tube. During condensation on this type of tube, the fins not only increase the surface area, but they can also create large surface-tension forces near the fin tips due to the small radius of curvature of the film in this region. These forces thin the condensate film near the tip of the fins,[14] as shown schematically in Figure 3, which leads to higher heat transfer rates. This effect should be more pronounced for sharply profiled fins and for high-surface-tension liquids, such as water. Historically, however, finned tubes have been used only for low-surface-tension liquids like the refrigerants (e.g., Freon 11). They have not been used in steam condensers because it was thought that the high surface tension of water would cause the condensate to bridge over between fins, causing flooding to occur between fins, and adversely affecting heat transfer performance.

Figure 3

Condensate film profile on a finned surface.

The main thrust of the research at the Naval Postgraduate School has, therefore, been to obtain steam condensation data for a wide variety of horizontal finned tubes under carefully controlled conditions, with the objective of examining the effects of fin spacing, thickness, height and shape on heat transfer performance.[15] Test data have been obtained for over 60 different tube samples under both vacuum and atmospheric conditions. Figure 4 shows the variation of the steam condensation heat transfer coefficient with heat flux for a smooth tube and for one family of finned tubes under vacuum conditions. These tubes were made of copper, and had a 19 mm fin root diameter. Rectangular-shaped fins were machined into the walls of these tubes, with both fin height and fin thickness held constant at 1.0 mm. However, each tube had a different fin spacing (i.e., distance between fins) of 0.5, 1.0, 1.5, 2.0, 4 and 9 mm. It is clear from these results that an optimum fin spacing exists near 1.5 mm (i.e., about 10 fins per inch) and at this optimum spacing, an enhancement over the smooth tube of approximately 3.5 is possible. When these data are plotted as the enhancement ratio (the ratio of the finned-tube steam condensation coefficient to the smooth-tube value at a specified heat flux and based upon the smooth-tube surface area) versus the fin spacing, the optimum is more evident, as shown in Figure 5,

Figure 4

Variation of steam condensation heat transfer coefficient with different fin spacings.

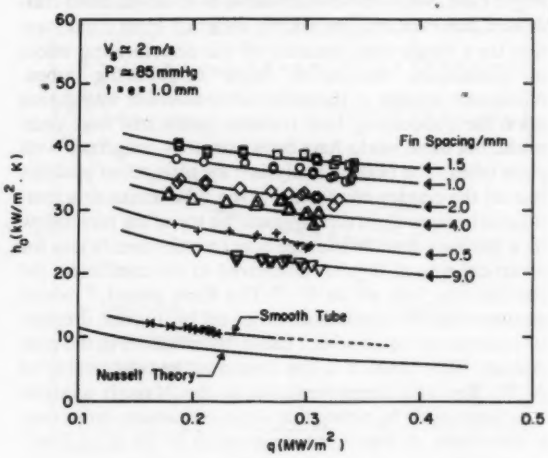

Figure 5

Dependence of steam-side enhancement ratio on fin spacing.

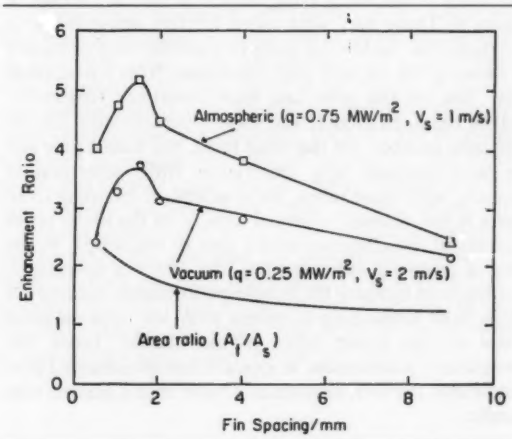

and the enhancement ratio increases with operating pressure. Also, it is clear that the enhancement ratio is always larger than the area ratio, indicating the beneficial effect of surface tension in thinning the condensate film on the fins. This effect of fin spacing is much more important than the size and shape of the fins,[16,17] although fin material can also alter the results considerably.[18] Poor conductivity metals such as stainless steel and titanium yield poor results as extended surfaces.

Wire-Wrapped Tubes

As an alternative to the use of integral fins, a fine wire may be coiled around a smooth tube to thin the condensate film *between the wires.*[19] As shown in Figure 6, when wires are fixed to the tube surface (they don't have to be bonded to the surface), a low pressure region is developed in the film near the base of the wires due to the concave shape of the condensate film. As a result, the condensate along the tube wall is pulled toward the wires and is therefore thinned *between the wires.* This thinner condensate reduces the thermal resistance across the film, leading to enhanced heat transfer between wires. Beneath the wires, the combination of a thick condensate film, and possibly a thermal contact resistance between the wires and the tube wall, reduces the heat transfer rate in this region to a small value. Thus, the addition of wires to a smooth tube enhances the heat transfer process between wires and reduces the heat transfer process beneath the wires. This is unlike the finned tube, where the major heat transfer occurs at the fin tips, which depends upon fin metal conductivity. With wire-wrapped tubes, the wire thermal conductivity plays a very minor role in the heat transfer process. However, it is very important to know what wire diameter and wire pitch will give the best thermal performance. For this purpose, a series of measurements were completed at the Naval Postgraduate School for nine wire-wrapped tubes. Fine titanium wires were coiled around 19 mm diameter smooth copper tubes and were anchored in place at their ends. Three different wire diameters of 0.5, 1.0 and 1.6 mm were used, and for each wire size, three different nominal spacings of 1, 2 and 3 mm were fabricated. The vacuum runs for these tubes yielded the steam condensation heat transfer coefficient data shown in Figure 7. The best configuration appears to be for a wire pitch (i.e., center to center distance between wires) of 2.5 mm (thus about 10 wires per inch). In this case, an enhancement over the plain tube of about 1.8 is possible.

Figure 6

Condensate film profile on a wire-wrapped surface.

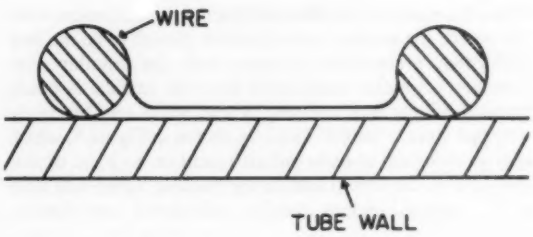

Figure 7

Effect of wire pitch on steam condensation heat transfer coefficient for wire-wrapped tubes (Wire Diameter = 0.5 mm).

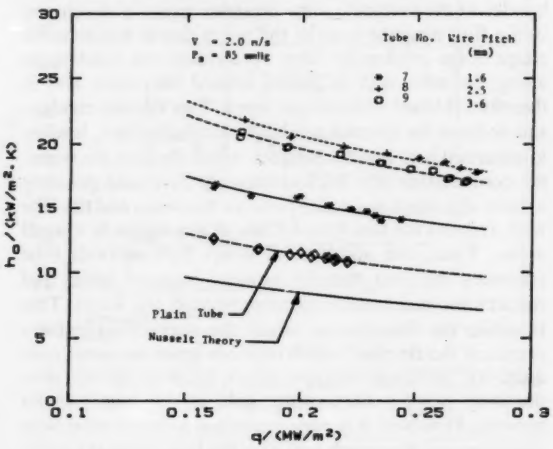

Figure 8

Photograph of wire-wrapped "roped" tube.

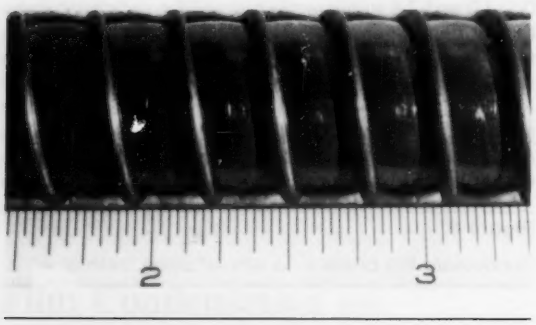

When the results of the three different wire diameters were compared, the smallest wire diameter proved to be the best performer, presumably because with the smaller wire diameter a smaller fraction of the tube surface is being blocked off for heat transfer. These wires can be easily wrapped around "roped" tubes, as shown in Figure 8, which will provide heat transfer enhancement on both the steam-side (due to the wires) and on the cooling-water-side (due to the internal ridges causing additional turbulence).

Tube Bundle Performance

All of the information described above pertains to a single tube. Shell-side condensation in an actual naval condenser, however, may be widely different from condensation on a single tube because of the deteriorating effect of condensate inundation from neighboring tubes. Numerous studies of the effect of condensate inundation upon the condensing heat transfer coefficient have been made, but these works have been primarily concerned with plain tubes. The Nusselt analysis[20] for plain tubes assumes that all the condensate from a given tube drains as a continuous laminar sheet directly onto the top of the tube below it. It predicts that the average heat transfer coefficient for a vertical row of N tubes compared to the coefficient for the top tube falls off as $N^{-1/4}$ The Kern model,[21] which assumes that the condensate drops off by discrete droplets or columns of liquid which cause disturbances in the condensate film, predicts a less conservative relationship of $N^{-1/6}$. Recently, improvements to the Nusselt analysis have been made by noting that when condensate drops onto a lower tube, it does not spread much in the axial direction. Evidence indicates that the degree of spreading may be influenced by the amount of condensate and the tube spacing.

The effect of inundation for enhanced tubes is not clearly established at present. However, some preliminary data taken at the Naval Postgraduate School are shown in Figure 9. These data were taken for five active tubes in a vertical row. Additional tubes in a bundle were simulated by flooding the top tube with condensate from a perforated tube. The smooth tube data were correlated reasonably well by the Kern model, and show a considerable fall-off with tube number. On the other hand, the finned tube and the wire-wrapped tube experience little deterioration because, with these tubes, the condensate dropping from above is not allowed to spread axially on the lower tubes because of the presence of the fins or the wires. In the case of dropwise condensation, the effect of inundation is actually to *increase* the bundle performance because the drops from above help to sweep away the large stagnant drops on the lower tubes in the bundle. From this preliminary information, it appears that an enhanced tube bundle may perform substantially better than a smooth tube bundle.

Figure 9

The effect of condensate inundation on the thermal performance of enhanced tubes.

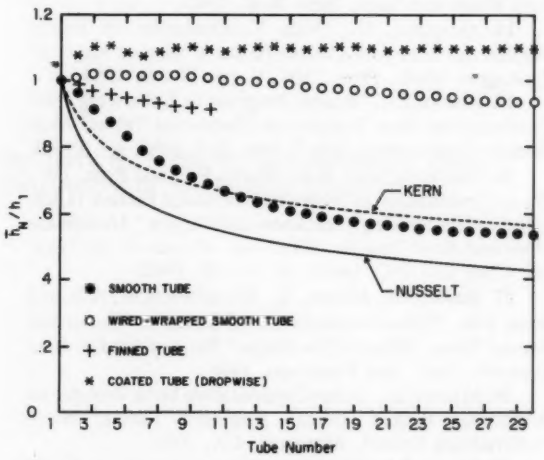

Conclusions

Significant insight has been gained in the use of surface tension to enhance steam condensation heat transfer on horizontal tubes. This enhancement may be obtained either by altering the free energy of the surface (with dropwise condensation) or by altering the geometry of the surface (with filmwise condensation). Each of these techniques has merit depending upon design constraints, and should be studied further under realistic naval condenser conditions in tube bundles where vapor velocity effects, condensate inundation effects and non-condensable gas effects are present. The potential for considerable steam-side enhancements has been demonstrated, and when this is coupled with water-side enhancements, the payoff in naval condenser volume and weight could be of significant benefit to tomorrow's naval steam propulsion systems.

Acknowledgements

This research program has been supported by the David W. Taylor Naval Ship Research and Development Center and by the National Science Foundation. The author wishes to thank Dr. James Griffith of the Naval Research Laboratory for providing several NRL-developed hydrophobic coatings for evaluation.

Biography

Dr. Paul J. Marto is a Distinguished Professor of Mechanical Engineering, Naval Postgraduate School. He teaches in the areas of heat transfer, thermodynamics and nuclear power systems. In addition to his research interests in condensation, he has published a variety of papers involved with nucleate boiling phenomena. He is a Fellow of the American Society of Mechanical Engineers and a Technical Editor for the *Journal of Heat Transfer.*

References

1. Silver, R.S., "Some Aspects of the Development of the Condenser From the Time of James Watt," *Symposium to Commemorate the Bicentenary of Watt's Patent,* University of Glasgow, UK, September, 1969, pp. 27-90.

2. Marto, P.J., "Heat Transfer and Two-Phase Flow during Shell-side Condensation," *Heat Transfer Engineering,* Vol. 5, Nos. 1-2, 1984, pp. 31-61.

3. Knauss, Donald T. and Kornbau, Raymond W., "Benefits of Spirally Enhanced Tubes for Steam Condensers in Minimum-Weight Cooling Systems," DTNSRDC PAS-83/42, David W. Taylor Naval Ship Research and Development Center, Bethesda, MD, October 1984.

4. Knauss, Donald T. and Kornbau, Raymond W., "An Assessment of Heat Transfer Augmentation in Propulsion-Plant Steam Condensers," DTNSRDC-PAS-84/23, David W. Taylor Naval Ship Research and Development Center, Bethesda, MD, April 1985.

5. Marto P.J. and Nunn, R.H., "The Potential of Heat Transfer Enhancement in Surface Condensers," *I. Chem. E. Symp. Series,* No. 75, pp. 23-39, 1983.

6. Bergles, A.E., "Enhancement of Heat Transfer," *Proceedings of the Sixth International Heat Transfer Conference,* Vol. 6, 1978, Toronto, pp. 89-108.

7. Webb, R.L., "The Use of Enhanced Surface Geometries in Condensers: An Overview," *Power Condenser Heat Transfer Technology,* Marto, P. J. and Nunn, R. H. (Eds.), Hemisphere Publishing Corp., New York, 1981, pp. 647-672.

8. Tanasawa, I., "Dropwise Condensation: The Way to Practical Applications," *Proc. Sixth International Heat Transfer Conference,* Vol. 6, pp. 393-405, Toronto, Canada, 1978.

9. Woodruff, D.W. and Westwater, J.W., "Steam Condensation on Electroplated Gold: Effect of Plating Thickness," *Int. J. Heat Mass Transfer,* Vol. 22, pp. 629-632, 1979.

10. O'Neill, G.A. and Westwater, J.W., "Dropwise Condensation of Steam on Electroplated Silver Surfaces," *Int. J. Heat Mass Transfer,* Vol. 27, pp. 1539-1549, 1984.

11. Holden, K.M., Wanniarachchi, A.S., Marto, P.J., Boone, D.H., and Rose, J.W., "The Use of Organic Coatings to Promote Dropwise Condensation of Steam," *J. Heat Transfer,* to be published, Vol. 109, 1987.

12. Field D.E., Griffith, J.R., "Cross-Linked Fluoropolymer Coatings," *I&EC Product Research and Development,* Vol. 14, pp. 52-54, March 1975.

13. Incropera, Frank P. and Dewitt, David P., "Fundamentals of Heat and Mass Transfer," Second Edition, John Wiley and Sons, New York, 1985.

14. Gregorig, R., "Film Condensation on Finely Rippled Surfaces with Consideration of Surface Tension," Z. Angew. Math. Phys., Vol. V, pp. 36-49, 1954.

15. Marto, P.J., "Recent Progress in Enhancing Film Condensation Heat Transfer on Horizontal Tubes," *Heat Transfer Engineering,* Vol. 7, Nos. 3-4, 1986, pp. 53-63.

16. Wanniarachchi, A.S., Marto, P.J., and Rose, J.W., "Film Condensation of Steam on Horizontal Finned Tubes: Effect of Fin Spacing, Thickness and Height," *Multiphase Flow and Heat Transfer,* HTD-Vol. 47, eds. V. K. Dhir, J.C. Chen and O.C. Jones, pp. 93-99, 1985.

17. Marto, P.J., Mitrou, E., Wanniarachchi, A.S. and Rose, J.W., "Film Condensation of Steam on Horizontal Finned Tubes: Effect of Fin Shape," *Proc. of 8th Int. Heat Transfer Conf.,* San Francisco, 1986.

18. Mitrou, E., "Film Condensation Heat Transfer on Horizontal Finned Tubes," Engineer Thesis, Naval Postgraduate School, Monterey, CA, 1986.

19. Marto, P.J., Mitrou, E., Wanniarachchi, A.S. and Katsuta, M., "Film Condensation of Steam on a Horizontal Wire-Wrapped Tube," Proc. 2nd ASME-JSME Thermal Engineering Joint Conference, Vol. 1 Hawaii, March 1987, pp. 509-516.

20. Jakob, M., "Heat Transfer," Vol. 1, John Wiley and Sons, Inc., New York, 1949, pp. 667-673.

21. Kern, D.Q., "Mathematical Development of Loading in Horizontal Condensers," *AICh E Journal,* Vol. 4, 1958, pp. 157-160.

MATERIALS RESEARCH AT NPS

By Terry R. McNelley and Stephen J. Hales
Department of Mechanical Engineering

Introduction

Metals are useful partly because they can bend permanently before they break, i.e. they can deform plastically. Metal plasticity is usually evaluated by measurement of the percentage elongation during tensile testing and the result is referred to as the ductility of the material. Ductility of structural metals is typically 10–50% at ambient temperature and perhaps attains 100% at elevated temperatures.

Some metallic alloys are superplastic under certain processing and deformation conditions. Superplasticity is the ability of such alloys to exhibit verv large, neck-free tensile elongation; an extreme example of such deformability, 5550% elongation, was reported by Higashi and coworkers.[1] More commonly, ductility in tension above 200% elongation to fracture is considered superplastic,[2] and many superplastic alloys exhibit maximum elongations of 500 to 1000%. Such extensive ductility is attained only in a narrow range of temperatures and deformation rates and then only with a suitably processed material. An example is illustrated in Figure 1, which shows a tension test specimen of an Aluminum-Magnesium alloy deformed ~600% to fracture; the test was done at a temperature of 300°C and strain rate equal to 5×10^{-3} sec^{-1}.

This phenomenon is much more than a laboratory curiosity. Several Titanium-based alloys are processed superplastically to form complicated components such as landing gear doors for the Air Force's B-1 aircraft, and superplastic Nickel-base alloys facilitate the manufacture of numerous complex gas turbine engine components. A wide variety of structural forms may be fabricated from superplastic Al alloys. A recent example is the oil cooler inlet duct, indicated by the arrow in the photograph in Figure 2, for the Navy's P-3 anti-submarine aircraft.[3] Other commercial components range from door panels for automobiles to equipment enclosures for scientific and medical instrumentation and even to architectural panels.

The foregoing examples emphasize that superplasticity allows the designer to fabricate complex shapes from a single piece of metal. This in turn will usually lead to weight savings and improvements in system performance and maintainability. The superplastically formed inlet duct for the P-3 replaced an assembly of some 30 individual parts and fasteners, with substantial weight savings. Also, fatigue and corrosion often begin at fastener holes or other sites where components are joined, and thus superplastic forming of components will help extend service lives of Naval platforms and improve their maintainability. Some additional examples of Naval application of this technology include parachute boxes, backrests and equipment packs for aircraft ejection seats; helicopter engine air intakes; and stores carriers for attack aircraft. Not all applications are for aircraft: two superplastic aluminum parts have been used to replace a fifteen-part welded assembly for a Naval compass stabilizer unit for use aboard ship.

Figure 1

Undeformed (top) and superplastically deformed (bottom) test samples of an Al-10 wt.% Mg-0.5 wt.% Mn alloy. The material was thermomechanically processed by warm rolling at 300°C and then tested in tension at 300°C using a strain rate of 5 × 10^{-3} S^{-1}. Elongation attained was ~ 600%.

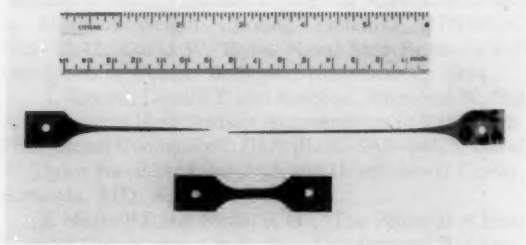

Figure 2

Oil cooler inlet duct, indicated by the arrow, is superplastically formed from an Aluminum alloy. This one-piece component replaced an assembly of numerous parts and fasteners and is fabricated for the Lockheed P-3 Orion aircraft (photo courtesy of Lockheed Corp.).

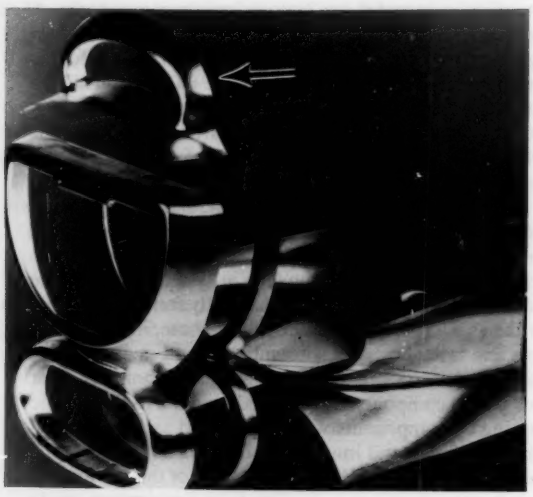

Under what conditions may a metal behave superplastically? From the perspective of applied mechanics, all superplastic metals have one important feature in common, namely a highly strain-rate sensitive flow stress. [2,4-6]. This is often described by the relation

$$\sigma = K\dot{\epsilon}^m$$

where σ is the flow stress of the metal at a strain rate $\dot{\epsilon}$, K is a material constant and m is the strain rate sensitivity coefficient. It is observed experimentally[7] and readily demonstrated analytically[8] that elongation to failure increases as m increases. When m = 1, behavior would be Newtonian viscous and materials such as hot glass, which exhibit a linear stress vs. strain-rate relationship, are ideally superplastic. Superplastic metals generally have m values nearer to 0.5.

The strong stress dependence of the strain rate, as described by the coefficient m, arises from deformation mechanisms that depend in turn upon microstructural considerations.[2,4-6] These microstructural prerequisites are:

- ☐ A fine grain size. Typical superplastic metals exhibit grain sizes below 10 μm; models for behavior generally presume that the superplastic strain rate $\dot{\epsilon} \alpha d^{-p}$ where d is the grain size and p = 2 or 3. Thus, finer grain size will enhance the superplastic response.
- ☐ A second phase. As superplastic forming is generally done at warm temperatures, where pure metals and single phase alloys would experience grain growth, a second phase is generally necessary to retard grain growth. This phase must deform with the matrix and generally must be uniformly distributed.
- ☐ Mobile high-angle grain boundaries and equiaxed grains. The predominant mode of deformation during superplastic flow is grain boundary sliding; this requires high-angle (disordered) boundaries and also that the boundaries be mobile to relieve stress concentrations that would otherwise result from grain boundary sliding. Equiaxed grains will accommodate better the grain rotation that accompanies grain boundary sliding.

Superplastic Al Alloys

The discovery of superplasticity is usually attributed to Pearson in 1934.[9] Sherby and Wadsworth[2] have pointed out, however, that Bengough[10] first reported "enormous enlongations" attained in specially processed brass as early as 1912. Even so, the phenomenon remained in the laboratory until Underwood's 1962 review of Soviet work in the field; then, superplasticity was thought to be attainable only in a few alloys of eutectic or eutectoid composition.[6] Indeed, the first Al-base alloy for which superplastic ductilities were reported was Al-33 wt.% Cu.[11]

This is the eutectic composition at the Aluminum end of the Al-Cu phase diagram, and as late as 1970, the opinion continued to be expressed that no useful superplastic Al-base alloys were likely, as the various possible eutectic systems, like Al-Cu, involved phases that would render the alloys too brittle at ambient temperature.[5] Some time thereafter however, research in Britain resulted in the commercialization of Supral alloys; these are based on the Al-Cu system, but have Cu content of only 5-6 wt. %, well below the eutectic.[12] In order to maintain the fine structure necessary for superplasticity, Zr is added to form fine Al_3Zr particles; these pin boundaries of recrystallized grains and prevent them from growing during superplastic forming.

Subsequent work using similar approaches has led to superplastic versions of existing alloys such as the high-strength Al alloy designated 7475 and alsó to superplastic Al-Li alloys.[3,13,14] There are, however, some significant problems with all of the Al-base superplastic alloys. The limited volume fractions of second phase attainable with additions of elements such as Zr results in rather coarser grain sizes, 10-20 μm, than attainable in other superplastic alloy systems. This, in turn, results in relatively higher temperatures, ~500°C, i.e. 80% of aluminum's melting temperature, being required for superplastic forming, as well as lower strain rates being required to sustain high ductility. Low strain rates present a particular problem in that production rates in superplastic forming generally are low and this tends to offset reduced tooling costs associated with the process. Finally, cavitation resulting from tensile separation of grain boundaries is an acknowledged[16,17] problem in superplastic aluminum alloys, and this results in degraded ambient temperature properties of components formed by the process. Current research in many laboratories is addressing these problems and solutions are being developed. For example, cavitation may be limited by use of back pressure during forming.[16]

It has been noted that the processing used to induce elevated temperature superplasticity results in highly refined grain structures, and it is generally perceived that such structural refinement may have application beyond superplastic forming. For instance, grain-refined Al alloys have stress-corrosion resistance superior to conventional alloys. Stress-corrosion cracking is a severe limiting factor in use of high-strength Al alloys in marine environments; indeed, the conventional 7475 Al alloy is heat-treated in such a way as to give up considerable strength to gain resistance to stress corrosion, and application of processing studies such as that at NPS may facilitate use of many alloys at higher strength levels than is now possible.

Research at NPS Thermomechanical Processing

The program at NPS has focused upon the Al-Mg system and has addressed various issues in addition to superplasticity. The Al-Mg system is the basis for several moderate-strength alloys, many of which are used in marine applications. The first research at NPS considered various methods of processing to refine microstructures and strengthen these alloys;[18] the thermomechanical process (TMP) most generally utilized in the research is illustrated in Figure 3 and has as its central feature mechanical working at warm temperature by rolling. By warm is meant a temperature below the Mg-solvus, but above 200°C. As such, the processing is most applicable to relatively high Mg-content alloys, i.e. 6-10 wt.% Mg.

Because the rolling takes place below the Mg-solvus temperature, the intermetallic β phase (Al_8Mg_5) will precipitate during the rolling in conjunction with introduction of dislocations. The microstructure of such a warm rolled Al-10 wt.% Mg -0.1 wt.% Zr alloy is shown in Figure 4, a micrograph obtained by transmission electron microscopy. Owing to the extreme distortion experienced by the material during the rolling process, it is hard to differentiate the features. The high dislocation density obscures the grain structure and the β phase is only occasionally discernable as highly faulted precipitates ~ 0.5 μm in size.

Figure 3

A schematic of the thermomechanical processing method showing initial solution treating and hot working as well as the warm working. Strains attained during the warm rolling are > 2.0, i.e. more than 80% reduction.

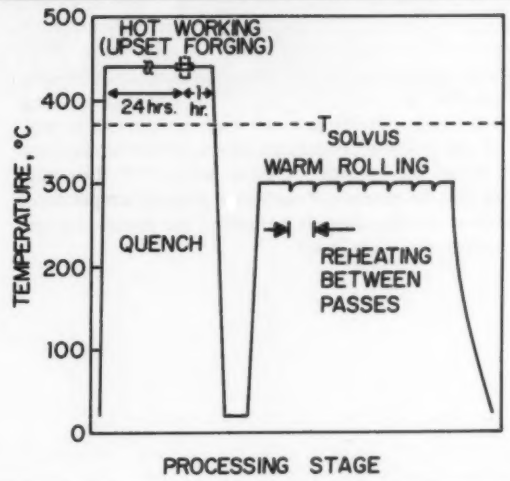

Superplasticity

The structure shown in Figure 4 does not satisfy the microstructural prerequisites outlined previously, and yet as shown in Figure 5, the ductility exceeds 500% during the tension testing at 300°C at a strain rate of about 5×10^{-3} S^{-1}. More recent research[19-21] has examined the behavior of such alloys and concluded that these warm-rolled alloys undergo a type of recrystallization often termed continuous.[22] In these Al-Mg alloys, this is seen as a more or less gradual conversion of the heavily dislocated structure of Figure 4 into one consisting of fine, recrystallized grains 1-5 μm in size. Indeed, during deformation, it was observed[21] that such recrystallized grains coarsened gradually during superplastic deformation. The effect of this is also seen in the lower plot of Figure 5. There, the stress for a given strain rate is seen to increase with strain during a mechanical test. As the superplastic strain rate is directly related to the stress and inversely related to the grain size, grain growth during deformation at constant strain rate will be accompanied by such apparent hardening.

The alloy characterized in Figures 4 and 5 possesses an ambient temperature (25°C) tensile strength of ~ 70 Ksi (~500 MPa), with 15 percent elongation to fracture during ambient temperature testing. Thus, this processing results in a relatively high-strength alloy of good ductility which is also superplastic at lower temperature, 300°C, when compared to other superplastic Al alloys. Further, the strain rate at peak ductility, 5×10^{-3} S^{-1}, is higher by a factor of 25 when compared to that reported for the 7475 Al alloy,[13,14] and this would be of considerable importance in enhancing production rates when using superplastic forming. Especially noteworthy is the observation[20,21] that these warm-rolled alloys do not cavitate during superplastic flow at warm temperature. It is believed that this is the result of the highly refined grain structure retained during the superplastic deformation, and the relatively low temperature (300°C) at which the deformation is occurring. It was noted[19,20] that these alloys will undergo normal rapid recrystallization upon heating to a temperature above the Mg solvus and that resultant grain sizes are 10-20 μm. At such temperatures, e.g. 450°C, these now-recrystallized alloys cavitate as observed with other superplastic Al-base alloys,[16,17] thus suggesting that the absence of cavitation at lower temperatures with these Al-Mg alloys is a result of the processing and not simply the alloy itself.

Figure 4

A transmission electron micrograph illustrating the high dislocation density in the warm-rolled condition of an Al-10 wt.% Mg-0.1 wt.% Zr alloy. A faulted β (Al_8Mg_5) precipitate is indicated by the arrow at the right-center of the micrograph.

Figure 5

Tension test data for the material of Figure 4 showing superplastic ductility of ~500% at strain rates near 10^{-2} S^{-1} (top plot). Stress versus strain-rate data is at the bottom where it is seen that the material hardens during deformation with a decrease in the coefficient m.

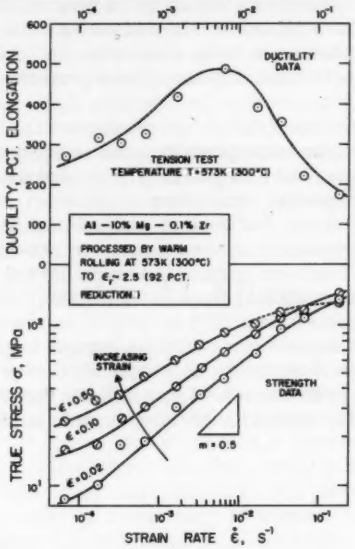
DUCTILITY, PCT. ELONGATION
DUCTILITY DATA
TENSION TEST TEMPERATURE T=573K (300°C)
Al – 10% Mg – 0.1% Zr
PROCESSED BY WARM ROLLING AT 573K (300°C) TO ϵ_T = 2.5 (92 PCT. REDUCTION)
TRUE STRESS σ, MPa
INCREASING STRAIN
STRENGTH DATA
m = 0.5
STRAIN RATE $\dot{\epsilon}$, S^{-1}

Microstructural Evolution

Superplasticity, and associated difficulties such as cavitation, are very sensitive to microstructure and to changes in microstructure during processing and deformation. More extensive application of superplastic forming to Al alloys will require better understanding of microstructural evolution and the potential problems associated with it. The research program at NPS is currently focusing on study of microstructural evolution during processing and superplastic deformation of these higher Mg, Al-Mg alloys. In addition, the program is examining the effects of lithium additions to these alloys and also the possibility of adapting the processing methodology to other Al-base alloys.

For example, Figure 6a illustrates the effect of static annealing at 300°C of the rolled structure of Figure 4. The structure following superplastic deformation at this same temperature (300°C) and at a strain rate near that of peak ductility, $2 \times 10^{-3}\ S^{-1}$, is shown in Figure 6b. After annealing only, the as-rolled structure has been replaced by a recrystallized microstructure of grain size 1–5 μm. The grains are essentially dislocation free, although some grains contain subgrain boundaries in which individual dislocations are discernible. Such a subboundary is seen in Figure 6a, running roughly vertically and just to the right of center of the micrograph. The grain boundaries are free of precipitates except for the β which is found to form preferentially at triple points. Here, the β is seen as the mottled-appearing regions at the upper left and also on the right side of the micrograph. In comparing the β to that present in the as-rolled condition, coarsening to a size of 1–2 μm is evident, although no faulting is seen within the particles.

After superplastic deformation (Figure 6b) under conditions where the sample experienced the same time at temperatures as that in Figure 6a, the grain size is still 1–5 μm, suggesting time at temperature is the primary factor controlling coarsening. The grains in the deformed material are somewhat less equiaxed than those in material experiencing only annealing and show some local distortion near the β precipitates. The β is slightly finer, $\sim$ 1 μm in size, and is again substantially faulted. Some dislocations within grains are also apparent, and these may have been generated in conjunction with accommodation processes during grain boundary sliding. The highly refined structures documented here should have application in other areas as well as superplasticity; these structures should have much improved resistance to stress-corrosion cracking in comparison to structures normally found in high-Mg alloys. Existing alloys such as Al 5083 alloy, widely used in ship superstructures and related marine application, may benefit from such grain refining processing methods.

Figure 6

Transmission electron micrographs of an Al-10 wt.% Mg-0.1 wt.% Zr alloy (a) warm rolled and then recrystallized by static annealing at 300°C. Note the subgrain boundary dividing the center grain. In (b) is shown this same material superplastically deformed to a strain of $\sim$ 200% at a strain rate of $2 \times 10^{-3}\ S^{-1}$ and temperature 300°C.

Future Directions

The fineness of microstructure demonstrated in Figure 6 is noteworthy. Other wrought superplastic Al-base alloys will exhibit grain structures at least four or five times coarser than those of this research. The fine structures result in relatively low deformation temperatures (300°C here versus 450-500°C for other Al-base alloys) and high strain rates for optimum ductility. The low deformation temperatures are thought especially important in the avoidance of the cavitation problem so often noted in such alloys. This all suggests potentially excellent ambient temperature properties as noted above, and current research is evaluating this area.

Finally, the mechanisms involved in the recrystallization process noted here are not well understood. Improved understanding of the modes of recrystallization in Al is a current topic of research at NPS. This understanding would have relevance to the development of refined grain structures in Al alloys and potential widespread application in areas demanding high performance materials for use in Naval aircraft and ships.

Acknowledgements

This research activity has been supported by the Naval Air Systems Command; also, the Office of Naval Research has provided support through the NPS Foundation program, especially for Postdoctoral Associates.

Biographies

Dr. Terry R. McNelley is Professor of Materials, Department of Mechanical Engineering, Naval Postgraduate School. He teaches in the areas of materials science, welding, and physical and mechanical metallurgy. His research interests are in processing and microstructural control in high-carbon steels and in Aluminum alloys as well as in superplasticity.

Dr. Stephen J. Hales is Adjunct Research Professor of Materials, Department of Mechanical Engineering, Naval Postgraduate School. He has conducted research in powder metallurgy Ni-base alloys including dynamic compaction of superalloy materials and his current interests are in thermomechanical processing, recrystallization and superplasticity in Al alloys.

References

1. Higashi, K., Oknishi, T. and Nakatani, Y., "Superplastic Behavior of Commercial Aluminum Bronze," *Scripta Metallurgica*, Vol. 19 (1985), pp. 821-823.

2. Sherby, O.D. and Wadsworth, J., "Development and Characterization of Fine-Grained Superplastic Materials," *Deformation Processing and Structure*, G. Krauss, ed., American Society for Metals, Metals Park, OH (1984), pp. 355-390.

3. Wadsworth, J., Nieh, T.G. and Mukherjee, A.K., "Superplastic Aluminum Alloys—A Review," *Aluminum Alloys—Their Physical and Mechanical Properties, Vol. II*, E.A. Starke and T.H. Sanders, eds., Chameleon Press, Ltd., London (1986), pp. 1239-1253.

4. Gifkins, R.C., "Mechanisms for Superplasticity," *Superplastic Forming of Structural Alloys*, N.E. Paton and C.H. Hamilton, eds., The Metallurgical Society of AIME, Warrendale, PA (1982), pp. 3-26.

5. Johnson, R.H., "Superplasticity," Metallurgical Reviews, Review No. 146, Vol. 15 (1970), pp. 115-134.

6. Underwood, E.E., "A Review of Superplasticity and Related Phenomena," *Journal of Metals*, Vol. 14, No. 12 (1962), pp. 914-919.

7. Woodford, D.A., "Strain Rate Sensitivity as a Measure of Ductility," *Transactions ASM*, Vol. 62 (1969), pp. 291-293.

8. Burke, M.A. and Nix, W.D., "Plastic Instabilities in Tension Creep," *Acta Metallurgica*, Vol. 33 (1975), pp. 793-798.

9. Pearson, C.E., "The Viscous Properties of Extruded Eutectic Alloys of Lead-Tin and Bismuth-Tin," *Journal of the Institute of Metals*, Vol. 54 (1934), pp. 111-134.

10. Bengough, G.D., "A Study of the Properties of Alloys at High Temperatures," *Journal of the Institute of Metals*, Vol. 7 (1912), pp. 123-146.

11. Holt, D.L. and Backofen, W.A., "Superplasticity in the Al-Cu Eutectic Alloy," *Transactions of the ASM*, Vol. 59 (1966), pp. 755-768.

12. Watts, B.M., Stowell, M.J., Baikie, B.L. and Owen, D.G.E., "Superplasticity in Al-Cu-Zr Alloys, Part I: Material Preparation and Properties," *Metal Science Journal*, Vol. 10, No. 6 (1976), pp. 189-197.

13. Wert, J.A., Paton, N.E., Hamilton, C.H. and Mahoney, M.W., "Grain Refinement in 7075 Aluminum by Thermomechanical Processing," *Metallurgical Transactions A*, Vol. 12A (1981), pp. 1267-1276.

14. Wert, J.A., "Grain Refinement and Grain Size Control," *Superplastic Forming of Structural Alloys*, N.E. Paton and C.H. Hamilton, eds., The Metallurgical Society of AIME, Warrendale, PA (1982), pp. 69-83.

15. Grimes, R., "Superplasticity in Aluminum-Lithium Based Alloys," *Superplasticity,* B. Baudelet and M. Suery, eds., Centre National de la Recherche Scientifique, Paris (1985), pp. 13.1-13.12.

16. Ridley, N. and Pilling, J., "Cavitation in Superplastic Alloys – Experimental," ibid, pp. 8.1-8.17.

17. Suery, M., "Cavitation in Superplastic Alloys – Theoretical," ibid, pp. 9.1-9.19.

18. McNelley, T.R. and Garg, A., "Development of Structure and Mechanical Properties in Al-10.2 Wt. Pct. Mg by Thermomechanical Processing," *Scripta Metallurgica,* Vol. 18 (1984), pp. 917-920.

19. McNelley, T.R., Lee, E.W., and Mills, M.E., "Superplasticity in a Thermomechanically Processed High-Mg Al-Mg Alloy," *Metallurgical Transactions A,* Vol. 17A (1986), pp. 1035-1041.

20. Lee, E.W., McNelley, T.R. and Stengel, A.F., "The Influence of Thermomechanical Processing Variables on Superplasticity in a High-Mg Al-Mg Alloy," *Metallurgical Transactions A,* Vol. 17A (1986), pp. 1043-1050.

21. McNelley, T.R., Lee, E.W. and Garg, A., "Superplasticity in Thermomechanically Processed High Mg, Al-Mg-X Alloys," *Aluminum Alloys–Their Physical and Mechanical Properties, Vol. II,* E.A. Starke and T.H. Sanders, eds., Chameleon Press, Ltd., London (1986), pp. 1269-1283.

22. Jones, A.R., "Grain Boundary Phenomena During the Nucleation of Recrystallization," Proceedings of the Seminar on *Grain Boundary Structure and Kinetics,* R.W. Balluffi, ed., American Society for Metals, Metals Park, OH (1980), pp. 379-426.

IDEA LAB

The Departments of Meteorology and Oceanography at the Naval Postgraduate School (NPS) have developed an interactive computer laboratory focused on using modern computer technology and real-time data bases to improve instruction in meteorology and oceanography. This facility, named the Interactive Digital Environmental Analysis Laboratory (IDEA/LAB), uses modern micro and mini-computers hosting twelve image analysis and graphics student work stations. The laboratory is designed so that complex data analysis and display tasks in environmental sciences, previously completed on main-frame computers, now can be executed on laboratory work stations. Digital satellite and synoptic data and numerical weather prediction model output can be processed and displayed on student work stations instead of using graphic maps or analog hard-copy photogaphy.

The facility, formally opened in June of 1987, makes a significant contribution to the school's instructional and research facilities, allowing NPS to remain at the forefront in educating its officer-students in oceanography and meteorology. Used in the analysis, forecasting, and remote sensing courses, it not only heightens student interest but provides greatly expanded capacity to combine and manipulate images and data from several sources. It permits examination of real-time and near real-time environmental data in the classroom and provides an excellent support facility for student and faculty research projects. The lab is an important asset in preparing students for the revolutionary changes occurring in the fields of oceanography and meteorology and will contribute directly to their performance in subsequent assignments.

Students at work stations

DEPARTMENT OF THE NAVY
OFFICE OF NAVAL RESEARCH
ARLINGTON, VA. 22217

OFFICIAL B
PENALTY FOR PRI

RESRV510ZC FEDLN54443

DIRECTOR
WEAPONS SYSTEMS
EVALUATION GP
ATTN LIBRARY
WASHINGTON DC
20305

**
**

NAVAL RESEARCH REVIEWS.
1987
V.39 I.1 C.3

6- 50 T+